STATISTICAL ADVANCEMENTS TO MODELLING ANIMAL MOVEMENT IN AQUATIC ENVIRONMENTS

by

Kim Whoriskey

Submitted in partial fulfillment of the requirements
for the degree of Doctor of Philosophy

at

Dalhousie University
Halifax, Nova Scotia
March 2021

to my family, old and new

Table of Contents

List of Tables

List of Figures

xiii

Abstract

Movement of animals provides information on ecological processes that influence individual survival and fitness like migration, foraging, and breeding. Over the past several decades, large-scale interest in the tracking of aquatic animals has sparked both technological and statistical innovation. Predicting accurate locations from noisy tracking data, as well as classifying different kinds of movement that can be used to infer animal behaviour, have emerged as prime objectives that can lead to better understanding of where animals go, and what processes might be driving their behaviour. These goals persist across taxa, such that ecologists wish to apply similar methods to data with varying structures. In tandem, coordinated efforts by international collaborative projects have generated massive datasets that require new solutions capable of answering increasingly complex ecological questions.

This thesis develops new methods that can concurrently account for measurement error in the tracking technology, and predict different kinds of movement using switching hierarchical models. Traditionally, switching hierarchical models have been fitted with techniques that sample from the likelihood or posterior distribution and which are computationally intensive. Instead, the workhorse of this research is the combination of the Laplace approximation and Automatic Differentiation, which is shown to enable the rapid fitting of hierarchical models with large numbers of random effects. Because switching hierarchical models have both continuous and discrete random effects, an iterative procedure is adopted to efficiently optimize the marginal negative log-likelihood.

The novel switching hierarchical model frameworks that are presented can accommodate different combinations of discrete and continuous space and time processes. Throughout, simulations are used to demonstrate a high level of accuracy under each of the contrasting scenarios. These methods are applied to animal tracking datasets collected using a variety of technology, including both satellite and acoustic telemetry. The general implementation developed here is versatile, and could be expanded to incorporate alternative mixed-scale random effects (e.g., individual or temporal effects). A groundwork is thereby laid for the statistical innovation that will be needed to accommodate the increasing size and complexity of contemporary animal telemetry research.

List of Abbreviations and Symbols Used

A   Transition probability matrix

γ Autocorrelation in step lengths and turning angle

Q   Generator matrix

Φ Behaviour equation parameters

Ψ Measurement equation parameters

Θ Movement equation parameters

θ Mean turning angle

x   True locations

y   Locations observed with error

b Behavioural state

L Likelihood

`swim`   SWItching Movement models

`TMB`   Template Model Builder

`YAPS`   Yet Another Positioning Solver

DCRWS   First-Difference Correlated Random Walk with Switching

GRF   Gaussian Random Field

HMM   Hidden Markov model

HMMM   Hidden Markov Movement Model

RMSE   Root mean squared error

SHM	Switching hierarchical model
SSM	State-space model
YAMS	Yet Another hidden Markov model Solver

Acknowledgements

There are many people without whom this thesis would never have been completed. In the following paragraphs I will attempt to do justice crediting their hard work and companionship, but I will undoubtedly fall short.

First and foremost, Joanna has been an absolutely incredible supervisor and mentor. Throughout these many years, she has offered relentless support and guidance both academically and emotionally, and within minutes of my asking for it. She has always encouraged my ideas, and allowed me to take advantage of opportunities that were not necessary for my studies, but that gave me invaluable experiences as a scientist. She is and will always remain the example of the statistician that I would like to be.

Following very closely, I must thank my supervisor Chris, not only for his statistical genius, but also for his constant provision of a kind ear and a calming smile. This thesis would not have been completed if not for the many stats coffees, turned into therapy sessions for my latest perceived research catastrophes, turned into supervisory meetings that resolved these crises (or determined that they never existed in the first place).

To the other members of my committee, you have my sincerest thanks for your constant guidance. I first entered Mike's office during my second year of Undergrad to inquire about the Honours program, and that moment undoubtedly started me along the path which has culminated in this thesis. Throughout my degrees, Sara's encouragement and inclusivity has given me a steady stream of support to draw on whenever I needed it. And Don has provided unceasing mentorship and patience as a researcher but especially in the field, where it took me a second to remember that in fact grey seals are mammals and as such do not have cloacas.

There are several mentors who have come (and some gone) which I will never forget. Robert has been the most stalwart friend throughout my entire time at Dalhousie. Without his encouragement I may never have gained confidence as a researcher, and this whole process would have been much less fun. I offer my gratitude to Marie, who excelled as a role model, and taught me how to think critically. To Nell, who's sharp intellect and wit have led to many stimulating conversations. To Greg Breed, who was the first famous scientist I ever met. To Shelley L, who is one of the hardest workers I have ever known, and who taught me the difference between a seagull and a helicopter. And to Chrissy, without whom I never would have realized the benefits of pretending to be a little bit insane.

There are countless companions who I have leaned on throughout these years. Benia, Janelle, and Xavier, have helped to create irreplaceable memories both in the field and as grad students in the office. More recently, the friendship of Claire R, Shannon, and Gabby has been enriching, and has bolstered me in some of my most stressful times. I will never forget the stats bros (Ethan, Jon, and Raph), our

Chapter 1

Introduction

Animals move to maximize their growth and to enhance their probability of survival and reproduction, and these individual animal movements have large-scale impacts on populations and ecosystems through the transportation of nutrients and energy (Hussey et al., 2015). For example, while movement of an individual directly influences abundance and diversity, it also facilitates the spread of pathogens or exotic species and ecological processes like herbivory and predation (Kays et al., 2015). As a result, understanding where, when, and why animal's move, or the study of movement ecology, can help to inform the management and conservation of both species and ecosystems (Nathan et al., 2008). In aquatic environments, where direct observation of animal movement is often impossible, researchers are rapidly expanding the use of electronic telemetry for documenting animal movement through space and time (Hussey et al., 2015; Lennox et al., 2017a).

A number of types of electronic telemetry technologies can be used to document animal movement. This thesis primarily concerns four types. The first is GPS technology, which generates location estimates via the Global Positioning System. The second is Argos technology, which estimates locations using an algorithm applied to measurements on the Doppler shift among multiple successive tag transmissions

registered by passing satellites of the ARGOS (Advanced Research and Global Observation Satellite) system (Hays et al. 2001; Jonsen et al. 2020; Fig 1.1). These first two technologies are typically used by surface-breathing taxa, or other animals that regularly break the surface, because the signals cannot be relayed through water (Teo et al., 2004; Lennox et al., 2017a). Fewer GPS locations can typically be obtained compared to Argos because relatively long transmission times (up to 30s) are required for GPS fixes, although this has improved since the advent of Fastloc GPS which significantly reduces transmission times (Witt et al., 2010). Alternatively, GPS locations may be archived and then downloaded if retrieval of the tag is possible (Lennox et al., 2017a,b). The third technology employs a geolocation algorithm to estimate locations based on light level measurements from a sensor in conjunction with sunrise and sunset times (Block et al., 2011). Because surface transmission is not required (except upon batch-download, e.g. pop-up archival tags) this technology is highly appropriate for aquatic animals that do not frequently surface (Teo et al., 2004; Lennox et al., 2017a). Finally, acoustic telemetry involves an acoustic tag that emits unique identifiers in the form of sonic signals - sound waves - that are registered and logged by receivers fixed to either stationary or mobile platforms, producing presence-only data of tagged animals at receiver locations (Whoriskey et al. 2019; Fig 1.1). These tags are also well-suited to non-surfacing animals, and can additionally be placed on animals of smaller size that are not capable of hosting the relatively large light-level tags, or can be manufactured with a larger battery size to significantly increase tag longevity

Figure 1.1: Left: satellite tagged grey seal pup on Sable island, Nova Scotia. Pink on the pup's coat is temporary dye used to more easily relocate the pup. Right: Acoustically tagged brown trout in Norway. Acoustic tags are surgically implanted. Right photo credit: Rob Lennox.

(Lennox et al., 2017a). Although GPS, Argos, and geolocation technology sample an animal wherever it travels, producing tracks in the form of paths over continuous space, the predefined receiver locations of acoustic telemetry generate spatially discrete locations of animal presence (Whoriskey et al., 2019). However, with enough receivers properly arranged in space, a path can be estimated by location averaging over temporal intervals (centers of activity; Simpfendorfer et al. 2002), triangulation via hyperbolic positioning of detections from three or more receivers (Smith, 2013), or hierarchical (state-space) modelling (Baktoft et al., 2017; Winton et al., 2018).

All of these kinds of technology produce error - noise - associated with the animal locations. GPS locations are typically highly accurate, usually producing errors < 100m (Frair et al., 2010; Ironside et al., 2017), but errors on the order of kms can still occur (Villepique et al., 2008). Argos technology (Fig 1.2) produces locations with considerably more error, regularly several to tens of km in magnitude (Vincent et al., 2002). Since CLS (Collecte Localisation Satellites; the company that processes the

data to produce location estimates) switched their location algorithm from a least squares method to a Kalman filter in 2011 (Jonsen et al., 2020), these errors have improved, although they can still occur on the order of kms (Lopez et al., 2014). Positions derived from archival light level technology contain significantly more error than either GPS or Argos, with mean errors occuring on the order of hundreds of km (Braun et al., 2015). Acoustic telemetry (Fig 1.2) data contain errors that are less straightforward to quantify. They have often been summarized as a detection range, i.e., the maximum distance from a receiver within which a tagged animal can be detected (Kessel et al., 2014b). However, representing them as the relationship between the distance from a receiver and the probability of detection is more precise and informative (Kessel et al., 2014b). Noting that they are inversely and exactly related, I will use the term detection range when the primary interest is in the distance as a function of the detection probability, and the term detection efficiency when the probability of detection as a function of distance is of more relevance. The probability of detecting an animal when it is within range depends on a variety of factors including distance, time, tag manufacturing specifications, habitat, and both anthropogenic and environmental noise (e.g., currents or boats; Kessel et al. 2014b; Baker et al. 2014; Brownscombe et al. 2019).

Accounting for error in aquatic telemetry data has become a primary interest over the last couple of decades because accurate estimates of animal location can improve the reliability of ecological inferences. Initially, various algorithms were developed that identify and discard erroneous locations based on comparing characteristics of
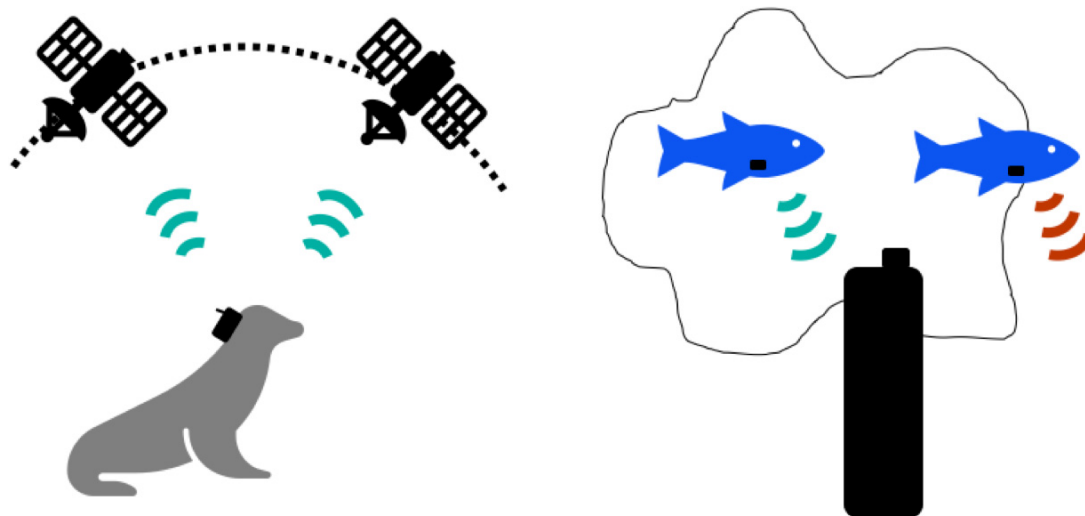
Figure 1.2: Illustration of two of the main tagging technologies discussed within this thesis. Left: Argos locations are generated by processing information on the Doppler shift in frequencies between multiple transmissions. Right: Acoustic telemetry logs the presence of tagged animals when they come within range of a receiver. This range varies with time, space, and extrinsic environmental (e.g., waves and currents) and anthropogenic (e.g., boat traffic) factors.

the data with prior knowledge of the ecology of the study animal, e.g., realistic swim speed vs. observed speed, or based on perceived behaviour of the measurement error distributions (Austin et al., 2003; Freitas et al., 2008; Meckley et al., 2014; Brownscombe et al., 2019). Inevitably, these filters can remove large parts of the data (up to 30%, Austin et al. 2003), an unfortunate consequence given the financial resources and animal welfare used to collect this information. Alternatively, state-space models (SSMs) have recently become a popular method used to account for telemetry error by predicting a true track from the noisy observations, while also quantifying the animal movement process (Auger-Méthé et al., 2020).

SSMs are hierarchical models of time series data that include at least two equations: a measurement equation that relates the observations to the true values that

we want to predict, and a process equation that stochastically models how the true values evolve through time (Auger-Méthé et al., 2020). The general structure of a simple SSM can be represented by

$$\text{Measurement Equation} \qquad \mathbf{y}_t = g(\mathbf{x}_t) + \boldsymbol{\eta}_t \tag{1.1}$$

$$\text{Process Equation} \qquad \mathbf{x}_t = h(\mathbf{x}_{t-1}) + \boldsymbol{\epsilon}_t \tag{1.2}$$

where $\mathbf{y}_t$ denotes the (possibly multidimensional) observations in time t, and they are related to the true values, $\mathbf{x}_t$ (also known as the states or random effects), through some function $g(\cdot)$. In turn, the $\mathbf{x}_t$ evolve through time according to some process $h(\cdot)$. The measurement and process errors here are represented by $\boldsymbol{\eta}_t$ and $\boldsymbol{\epsilon}_t$, respectively. The derivation of SSMs is typically attributed to Kalman (1960), who introduced the term "linear dynamic model" for an SSM where both the process and measurement equations are linear and the $\boldsymbol{\eta}_t$ and $\boldsymbol{\epsilon}_t$ are Gaussian random variables. In such a case the optimal solution of the resulting model is obtained with the Kalman filter (Kalman, 1960; Kalman and Bucy, 1961). The 1960s saw large-scale investment into research on SSMs and filtering techniques that was linked to development of navigation systems for submarines, aircraft, and spacecraft (Jazwinski, 1970). It is within this period that terminology like "state space approach/methods/techniques" came into play, and that extensions to SSMs like non-linearity (Jazwinski, 1970) were developed. Now, they have become a staple in marine ecology (Auger-Méthé et al., 2020), such that a wide variety of choices exist in both discrete and continuous

time (Jonsen et al., 2003, 2005; Johnson et al., 2008; Dowd and Joy, 2011; Breed et al., 2012; McClintock et al., 2012; Parton and Blackwell, 2017; Winton et al., 2018; Michelot and Blackwell, 2019; Jonsen et al., 2020).

Within the context of animal movement, I will denote the $\mathbf{y}_{1:T}$ to be the full set (from $t = 1, ..., T$) of noisy locations in two coordinates, while the $\mathbf{x}_{1:T}$ are the true and unknown locations. To fit an SSM, a researcher needs to calculate the marginal likelihood of the observations, i.e.,

$$\int_{\mathbf{x}_{1:T}} f(\mathbf{y}_{1:T} \mid \mathbf{x}_{1:T}, \Psi) f(\mathbf{x}_{1:T} \mid \Theta) d\mathbf{x}_{1:T}, \tag{1.3}$$

where Ψ and Θ denote the entire set of parameters associated with the measurement and process equations, respectively. In a maximum likelihood framework, Eqn 1.3 can be optimized directly with respect to the parameters, whereas within a Bayesian framework, Eqn 1.3 (with priors) becomes the quotient in a posterior likelihood calculation. If both $\boldsymbol{\eta}_t$ and $\boldsymbol{\epsilon}_t$ are Gaussian random variables, then an exact analytical solution exists in the Kalman filter; this has been applied to animal movement in Johnson et al. (2008). Although computationally efficient, Gaussian distributed measurement error does not frequently occur in animal telemetry (Jonsen et al., 2005; Breed et al., 2012; McClintock et al., 2015) unless pre-processing of the data to remove extreme outliers is employed (e.g., Johnson et al. 2008). In most other cases, this integral is typically analytically intractable. To address this, one option is to discretize the state-space and predict location on a grid, using the likelihood of a hidden

Markov model and turning this integral into a sum (e.g., Pedersen et al. 2011). Sampling methods like particle filters or Markov Chain Monte Carlo provide a means of approximating the likelihood or posterior distribution (e.g., Jonsen et al. 2005; Dowd and Joy 2011; Breed et al. 2012; Parton et al. 2017), but this can come at a significant computational cost. An alternative solution that has gained ground for fitting state-space models to ecological time series is the use of the Laplace approximation and Automatic Differentiation. Originally implemented through the software ADMB designed for fisheries modelling (Automatic Differentiation Model Builder, Fournier et al. 2012), a platform called Template Model Builder (TMB) now exists that makes this combination accessible through the popular R statistical software (Kristensen et al., 2016). As a result, Laplace's method can now be used to approximate complex integrals like that in Eqn 1.3, and the derivatives required to compute this approximation can be rapidly calculated via Automatic Differentiation (Skaug and Fournier, 2006). This combination has recently shown great promise and growth within the movement ecology paradigm, such that several implementations of SSMs exist and have been made available to movement ecologists through supplementary code or secondary packages (Albertsen et al., 2015; Auger-Méthé et al., 2017; Baktoft et al., 2017; Jonsen et al., 2020).

Although predicting the underlying true locations (location states) of an animal is important, this is frequently only the beginning of the statistical analysis. Further analyses vary based on the ecological question of interest, but can include studies

on home range or utilization distributions (Calenge, 2006; Hoenner et al., 2012; Wilson et al., 2015), network analysis to infer habitat and social connectivity (Jacoby et al., 2012; Scharf et al., 2016), resource selection functions to predict population distributions as related to habitat resource availability (Avgar et al., 2016), identifying migration pathways and diversity hotspots (Block et al., 2011), and investigating niche partitioning (Block et al., 2011; Dwyer et al., 2020). In particular, since the early 2000s there has been an increased interest in predicting the underlying motivations of animal movement. Because movement directly reflects an animal's response to its current physiological and biological needs and environmental characteristics (Hussey et al., 2015), understanding why an animal is moving can help to inform our knowledge of behaviours critical to survival such as foraging and reproductive performance. Inferring these underlying behaviours from animal tracks is possible by assuming that different types of movement can be discerned from changes in characteristics of an animal's path (Patterson et al., 2017). For example, while foraging is often assumed to be characterized by a tortuous track, a more directed path may suggest travelling between habitats (e.g., Jonsen et al. 2005). For these endeavours, the tool of choice is often the hidden Markov model (HMM), which is highly appropriate when the location data are accurate (Patterson et al., 2017; Auger-Méthé et al., 2020; McClintock et al., 2020).

HMMs are a large class of hierarchical models usually distinguished by a set of observations that depend on an unobserved Markov chain (Zucchini et al., 2016). Opinions on the relationship between HMMs and SSMs vary, with some researchers

using both names to refer to the same types of models (Cappé et al., 2005), others referring to HMMs as a special class of SSMs (McClintock et al., 2014), and still others claiming that SSMs are a special case of HMMs (Costa et al., 2012). This is probably partly fueled by the fact that early research and development of HMMs and SSMs were for the most part independent (Cappé et al., 2005). HMMs, or at least maximum likelihood theory and statistical inference for HMMs, were first introduced in 1966 by Baum and Petrie. They were initially described as probabilistic functions of "s-state Markov processes" (p.1554), because an HMM involves one stochastic process that is a function of a second, unobserved, Markov chain (Baum and Petrie, 1966). Much of their successive development was focused on automatic speech recognition (Baker, 1975; Rabiner, 1989). Despite their separate developmental histories, HMMs and SSMs are both hierarchical models wherein the observations are dependent upon a set of unobserved variables - random effects, or states - that follow a Markov process, and the literature appears to have converged around the viewpoint that HMMs are special cases of SSMs with discrete latent states (Auger-Méthé et al., 2020). Within the context of this thesis, I will adopt the term HMM when the unobserved random effects are discrete, and SSM when they are continuous. Furthermore, the SSMs that I will fit will all account for error associated with the technology, in one way or another.

The utility of HMMs for animal movement analysis was illustrated at least as early as 2004 (Morales et al., 2004). Within the context of animal movement, the set of observations follow a movement process, or one or more equations describing the

evolution of the animal movement through time, and these equations harbor multiple sets of parameters that are dependent upon the value of discrete random effects, or states. Using expert knowledge on a tagged animal's ecology, these sets of parameters and random effects can then be interpreted as underlying motivations driving the animal's movement (hereafter, behavioural states). Therefore, although the behavioural states correspond to mathematical distinctions between different kinds of movements, their interpretation is subject to human error, and they can only be interpreted as "apparent" behaviours (hereafter, the "apparent" will frequently be dropped, e.g., "apparent foraging" will be referred to as "foraging"). The observations can consist of either the location data (in latitude and longitude, e.g., Whoriskey et al. 2017) or metrics derived from the observed track, like turning angles and step lengths (e.g., Morales et al. 2004; Langrock et al. 2012; Michelot et al. 2016). When formulated within a maximum likelihood framework, several algorithms exist that enable rapid calculation of the likelihood (Zucchini et al., 2016) and relative ease of model fitting. Over the past two decades, significant resources have been poured into the development of HMMs, such that current implementations can include a variety of movement data streams (deRuiter et al., 2017; McClintock and Michelot, 2018), dependence of the switching probabilities or observation distributions on environmental covariates or temporal heterogeneity (Morales et al., 2004; Patterson et al., 2009; McKellar et al., 2015; Michelot et al., 2016; Li and Bolker, 2017), a choice of distributions for the state dwell-times (duration spent within a state before switching out; Langrock et al. 2012), multiple Markov chains to model movement simultaneously at different time

scales (Leos-Barajas et al., 2017; Adam et al., 2019), and individual or group-level heterogeneity through the use of discrete random effects (Schliehe-Diecks et al., 2012; McKellar et al., 2015; deRuiter et al., 2017).

Although both SSMs and HMMs can be fitted individually, often movement ecologists want to predict both location and behavioural states simultaneously from their data. Models that incorporate both sets of states are also commonly referred to as SSMs, but within this thesis for clarity I will largely refer to them as switching hierarchical models (SHMs), and reserve SSMs and HMMs for discussing models that predict solely location or behavioural states, respectively. SHMs have been well developed within Bayesian implementations (e.g., Jonsen et al. 2005; McClintock et al. 2012; Michelot and Blackwell 2019; Parton et al. 2017). Within a maximum likelihood framework, I am unaware of any current implementations that use a single model likelihood for fitting an SHM to predict continuous-space location states and discrete-valued behavioural states. Others have used SSM and HMM implementations in succession, i.e., first predicting location states using an SSM and then fitting HMMs to those predictions to predict behavioural states (e.g., Cote et al. 2020). Within these implementations, error from the SSM may not be accounted for during the behavioural state prediction. Alternatively, it is possible to account for this error by fitting a continuous-time SSM, imputing many random sets of location states in discrete-time from the SSM results, fitting a discrete-time HMM to each of those sets, and pooling the HMM results (McClintock and Michelot, 2018).

Within this thesis, I develop a method for fitting SHMs comprising a single model

likelihood within a maximum likelihood framework using the `TMB` platform that can be applied to both satellite and telemetry data. This implementation avoids: 1) the specification of priors, as are needed in a Bayesian analysis, 2) a large computational burden associated with sampling schemes, and 3) using the results of one model likelihood as the response in a second. With 1), the implementation removes subjective choices; with 2) it frees up computational resources such that model results and validation can be quickly reported, or resources can be reallocated to tackle larger datasets or further model complexity; and with 3) it simultaneously accounts for location and behavioural state error. Furthermore, by laying the foundation for fitting these models within `TMB`, I expand and test the utility of this package for fitting complex hierarchical models to animal movement data, and develop a method that could be applied to scenarios outside of movement ecology.

The remainder of this thesis constitutes four independent research articles (plus a Conclusion), each of which was a collaborative project led by me. That is, I largely led the study design, methodological development, data analysis, and writing of the manuscripts, with relevant advice and input from my supervisors and coauthors. The layout is as follows.

The second chapter employs current standard likelihood theory (Zucchini et al., 2016) to formulate the movement process of Jonsen et al. (2005) as an HMM in `TMB`, and demonstrates the model on GPS, acoustic, and filtered light level geolocation data. Although this model does not account for measurement error and can therefore only be fitted to highly accurate data, it was a necessary step towards the ultimate

goal of formulating a switching hierarchical model within `TMB`. Furthermore, this model made a significant contribution to the literature within its own right. The results of this chapter were published in *Ecology and Evolution* (Whoriskey et al., 2017), and the model was made available through an R package `swim` (SWItching Movement models), which was then used for an ecological study investigating the association of grey seal (*Halichoerus grypus*) foraging behaviour with oceanographic conditions (Nowak et al., 2020).

In the third chapter (which I have also published in *Methods in Ecology and Evolution*; Whoriskey et al. 2019), I pivot slightly to focus solely on acoustic telemetry, and review the current statistical methods available to movement ecologists for analyzing their (spatially discrete) detection data. These data are very versatile, and can be summarized into many different response variables to investigate a variety of different aspects of animal ecology. As a result, for several decades significant statistical advances have been made in the analysis of these data, without any clear guide on when/how to use the various available methods. The main goal of this chapter was to provide this guide, and to draw the reader's attention towards future directions by garnering inspiration from other fields. Specifically, I contend that the reader should look towards methods that could be applied to account for measurement error within the technology, as is achieved in the following (fourth and fifth) chapters.

The fourth chapter contains the formulation of the switching hierarchical model for spatially continuous data (specifically, satellite telemetry data) within `TMB`, and makes this implementation available through `swim`. I achieved this by utilizing the

key result that the maximum likelihood estimates of a subset of parameters can be found by optimizing the likelihood while holding the remaining parameters fixed at their maximum likelihood estimates (Patefield, 1977). Furthermore, I use this implementation to document intraspecific variability in 67 post-breeding grey seals on the East Coast of Canada. Thus, this chapter constitutes a significant contribution to both the statistical and ecological literature, in entirely separate yet complementary ways.

In the fifth chapter I use the basic tenets of my switching hierarchical model to develop an analogous model for analyzing acoustic telemetry data. This implementation capitalizes on the existing SSM available through `YAPS` (Baktoft et al., 2017), which produces spatially continuous location predictions from acoustic telemetry data, but advances it to additionally predict behavioural states. Although SSMs and HMMs have traditionally not been as popular for analyzing acoustic telemetry data as compared to satellite telemetry data, popularity is starting to increase (e.g., Whoriskey et al. 2017; Bacheler et al. 2019; Cote et al. 2020). This chapter therefore presents a timely contribution that synthesizes research from all of the previous chapters.

Throughout my research, I have learned and drawn from both statistical and ecological disciplines. I have made connections in both fields, profiting from integrative international collaborations like the Canadian Statistical Sciences Institute Project "Advancements to state-space models for fisheries science" and the Ocean Tracking Network. Finally, I have spent a significant amount of time in the field studying

marine fishes and mammals, attending conferences, and hosting and attending work-shops. The concluding chapter will synthesize the common themes throughout my work and offer thoughts on future directions in both disciplines that have not only been brought to light by my research, but also these additional enriching experiences.

Chapter 2

A Hidden Markov Movement Model for Rapidly Identifying behavioural States From Animal Tracks

2.1 Introduction

Animals move to enhance their probability of survival and reproduction. Movement is therefore a critical animal behaviour that reflects an animal's response to its current biological and physical needs and to its environment. Identifying these underlying drivers of animal movement (behavioural states) is required for understanding how and why animals use available space, and this knowledge informs the management and conservation of both species and ecosystems. In aquatic environments, where direct observation of animal movement and behavioural states is often impossible, researchers are rapidly expanding the use of electronic telemetry for documenting animal movement through time (Hussey et al., 2015).

Satellite telemetry and acoustic positioning systems are the most common types of telemetry technology for estimating an aquatic animal's location in continuous space, and yield time series of locations along an animal's path, usually referred to as tracks. Inferring behavioural states from animal tracks is possible by assuming that different types of movement, and therefore behavioural states, can be reflected by

changes in characteristics of an animal's path. For example, while foraging can often be characterized by a tortuous track, a more directed path may suggest travelling between habitats (Zollner and Lima, 1999; Jonsen et al., 2005).

Hidden Markov Models (HMMs) are a popular tool used to identify behavioural states from animal telemetry data with negligible error (e.g., Morales et al. 2004; Langrock et al. 2012). HMMs are a large class of models distinguished in the most general case by a set of observations that depend on an unobserved, underlying Markov process (Zucchini et al., 2016). In the context of animal movement, the latent Markov process is used to model the discrete behavioural states of interest, while the set of observations follow a movement process that can also be Markovian. The observations can consist of either location data (e.g., Jonsen et al. 2005) or metrics derived from the observed track, like turning angles and step lengths (e.g., Morales et al. 2004; Langrock et al. 2012). While current HMMs can be fitted rapidly using maximum likelihood (ML) methods, with the exception of the formulation of Pedersen et al. (2011), they are unable to account for measurement error associated with the technology used to obtain animal tracks. For those tracks measured with error, state-space models (SSMs) provide a more accurate and reliable method for identifying behavioural states, but are typically fitted using comparatively slow Bayesian methods like Markov Chain Monte Carlo (MCMC) sampling because of large numbers of random effects (e.g., Jonsen et al. 2005; McClintock et al. 2012; Jonsen 2016). Therefore, the ideal tool for identifying behavioural states from animal tracks should incorporate features of both HMM and SSM implementations, such that measurement error can

be accounted for within a ML framework that keeps the computational burden of estimation relatively small.

One particular SSM that has proven its utility through a wide range of applications on different species is the Bayesian SSM with a first-Difference Correlated Random Walk with Switching (DCRWS) process equation of Jonsen et al. (2005). This model has been previously used to quantify foraging behaviour in cetaceans (Bailey et al., 2009; Irvine et al., 2014), pinnipeds (Breed et al., 2009; Harwood et al., 2015), turtles (González Carman et al., 2012; Hart et al., 2012), sea birds (Reid et al., 2014), and manta rays (Graham et al., 2012). Furthermore, it has been used to determine migration corridors (Prieto et al., 2014), estimate intraspecific competition (Breed et al., 2013), predator-prey relationships (Fitzpatrick et al., 2012), site fidelity (Block et al. 2011), and to inform management and conservation of protected regions (Block et al., 2011; Maxwell et al., 2011; Graham et al., 2012).

Here we introduce a new HMM for estimating behavioural states from highly accurate animal tracks that is similar to the DCRWS SSM, but does not account for measurement error. We directly implement the DCRWS process equation as the basis for our HMM, but we adjust the model for fitting within a ML framework to allow for rapid estimation. Model fitting and parameter estimation are performed using the R-package TMB (Kristensen et al., 2016), which has previously shown great promise for analyzing animal tracking data (Albertsen et al., 2015; Auger-Méthé et al., 2017). We make this model, which we entitle the hidden Markov movement model (HMMM),

available through the R package `swim` (see supplementary material). To demonstrate the accuracy and applicability of the HMMM, we apply it to simulated animal tracks and to real tracks from multiple aquatic species. We additionally compare our HMMM results to those obtained using its Bayesian counterpart and to results from the `moveHMM` package (Michelot et al., 2016). We assess the advantages and disadvantages of each approach by comparing their computational efficiency, accuracy, and sequences of behavioural states.

2.2 Methods

2.2.1 The DCRWS Movement Process

The SSM of Jonsen et al. (2005) estimates the true locations, behavioural states, and parameters of a movement process from an Argos satellite system track. Given the true location $\mathbf{x}_t$ at time t, the DCRWS process equation is a correlated random walk on the first differences of the true locations, $\mathbf{d}_t = \mathbf{x}_t - \mathbf{x}_{t-1}$:

$$\mathbf{d}_t = \gamma_{b_{t-1}} \mathbf{T}(\theta_{b_{t-1}})\mathbf{d}_{t-1} + \mathrm{N}_2(\mathbf{0}, \boldsymbol{\Sigma}) \tag{2.1}$$

$$\mathbf{T}(\theta_{b_{t-1}}) = \begin{pmatrix} \cos(\theta_{b_{t-1}}) & -\sin(\theta_{b_{t-1}}) \\ \sin(\theta_{b_{t-1}}) & \cos(\theta_{b_{t-1}}) \end{pmatrix} \qquad \boldsymbol{\Sigma} = \begin{pmatrix} \sigma_{lon}^2 & \rho\sigma_{lon}\sigma_{lat} \\ \rho\sigma_{lon}\sigma_{lat} & \sigma_{lat}^2 \end{pmatrix}$$

The stochastic term in the movement process is a bivariate Gaussian (N_2) with mean $\mathbf{0}$ and covariance matrix $\boldsymbol{\Sigma}$, where σ_{lat} and σ_{lon} are the standard deviations in the latitude and longitude axes, respectively, and ρ is the correlation between the two axes. Like Breed et al. (2012), we assume here that $\rho = 0$, implying that stochasticity in the latitude and longitude directions are independent of each other. The parameter

$\gamma_{b_{t-1}}$ describes the autocorrelation in both direction and speed, and $\mathbf{T}(\theta_{b_{t-1}})$ is the rotational matrix through space given the turning angle $\theta_{b_{t-1}}$. Multiple values are possible for $\gamma_{b_{t-1}}$ and $\theta_{b_{t-1}}$, and these parameter values are dependent on the behavioural state at time $t-1$, i.e., b_{t-1}. This dependence provides the mechanism for distinguishing between multiple behavioural states at each location. Typically of interest are two states: the first is directed movement characterized by travelling in the same direction ($\theta \approx 0$) and at a similar, high speed ($\gamma > 0.5$), and the second is tortuous movement characterized by frequent course reversals ($\theta \approx \pi$) at dissimilar, slower speeds ($\gamma < 0.5$). Parameter sets for each state are identified with the appropriate subscript, either 1 or 2.

2.2.2 The HMMM

Our HMMM uses the movement process described by (2.1), but instead of using a Bayesian framework like Jonsen et al. (2005), we employ a ML framework and fit the process equation as a HMM via `TMB`, which requires that the likelihood function be coded in the C++ programming language. The probability distribution of the movement process is conditional on the assumed behavioural states b_t, and is given by

$$f(\mathbf{d}_t|b_{t-1}) \sim N_2(\gamma_{b_{t-1}}\mathbf{T}(\theta_{b_{t-1}})\mathbf{d}_{t-1}, \Sigma) \tag{2.2}$$

The likelihood of the HMMM is that of a HMM Zucchini et al. (2016):

$$\boldsymbol{\delta}'\mathbf{P}(\mathbf{d}_1)\mathbf{A}\mathbf{P}(\mathbf{d}_2)\mathbf{A}\cdots\mathbf{P}(\mathbf{d}_{t-1})\mathbf{A}\mathbf{P}(\mathbf{d}_t)\mathbf{1} \tag{2.3}$$

Assuming two behavioural states, the 2×1 vector $\boldsymbol{\delta}$ contains the initial probabilities of being in each state. $\mathbf{A}$ is a 2×2 transition probability matrix containing the switching probabilities $\alpha_{i,j}$ that describe the probability of switching from state i at time $t-1$ to state j at time t. Because the rows of $\mathbf{A}$ sum to 1, we need only estimate two switching probabilities instead of four; we choose to estimate $\alpha_{1,1}$ and $\alpha_{2,1}$. $\mathbf{P}$ is a 2×2 diagonal matrix with diagonal entries equal to $(f(\mathbf{d}_t|b_{t-1} = 1), f(\mathbf{d}_t|b_{t-1} = 2))$, i.e. the probabilities of being at the observed locations given each behavioural state as described by the movement process. $\mathbf{1}$ is a 2×1 vector of ones. We estimate the parameters of the movement process directly from the likelihood within `TMB`, and then use the Viterbi algorithm to estimate the unobserved behavioural states Zucchini et al. (2016).

2.2.3 Data Analysis and Simulation Study

To evaluate the performance of the HMMM, we compared it with two other approaches for estimating behavioural states from animal tracks with negligible measurement error. The first was the switching movement process described by (2.1) and (2.2), fitted using a Bayesian framework and Markov Chain Monte Carlo (MCMC) sampling via `rjags` (Plummer, 2015). This first model is the DCRWS process equation of Jonsen et al. (2005) without measurement error, and therefore differs from the HMMM solely in implementation (i.e., Bayesian vs. ML inference). Hereafter we refer to it as the DCRWS$_{NOME}$. Although the DCRWS$_{NOME}$ has not been fitted before,

implementations of the DCRWS for tracking data with minimal errors do exist (Jonsen, 2016), and the DCRWS$_{NOME}$ is the most direct implementation of the DCRWS when no measurement error is assumed. To fit the DCRWS$_{NOME}$, we used a burn-in period of 40,000 samples, then sampled 20,000 from the posterior distribution but only kept every 20th sample (thinning). We fitted and compared two MCMC chains to each track to check for convergence. All prior distributions were specified as in the R package `bsam` (Jonsen et al., 2005) that fits the original DCRWS SSM, with the exception of those for the error covariance matrix Σ. Instead, by setting $\rho = 0$, which we believe is more appropriate, we were able to specify separate vague uniform priors on σ_{lon} and σ_{lat} as opposed to using the original Wishart prior on the entire matrix (Jonsen et al., 2005). Parameters and behavioural states were estimated as the posterior medians of the samples from the two chains combined. We additionally fitted a HMM to the turning angles (rad) and step lengths (km) of the animal tracks with the R package `moveHMM` (Michelot et al., 2016), using a von Mises (mean μ and concentration parameter c) and Weibull (shape λ and scale parameter k) distribution, respectively. behavioural states were again identified via the Viterbi algorithm, using functions from `moveHMM`.

We fitted these three models to three animal tracks: 1) a GPS track collected by a Sea Mammal Research Unit head-mounted Satellite Relay Data Logger (accurate GPS positions acquired when the head surfaces) deployed on an adult male grey seal (*Halichoerus grypus*) at Kouchibouguac National Park, New Brunswick, in 2013;

2) an acoustic Vemco Positioning System (VPS; positions from triangulation of detections from multiple receivers in known locations; Smith 2013) track of an adult male lake trout (*Salvelinus namaycush*) in northern Lake Huron in 2014; and 3) a light-based geolocation track recorded by an immature female blue shark (*Prionace glauca*) tagged near Halifax, Nova Scotia, with a Wildlife Computers miniPAT tag in 2014. Because geolocation data can be error-prone, the track was processed with the Wildlife Computers (2015) GPE3 software (a SSM) to improve positioning accuracy by estimating the true blue shark locations, as suggested by the manufacturers. Although a SSM for geolocation data would have been the ideal approach for analyzing the blue shark data, our approach of fitting HMMs to true location SSM estimates has been previously adopted (e.g., Eckert et al. 2008). Because the data were collected in continuous-time but all three models assume underlying discrete-time Markov processes, we had to approximate the locations in discrete-time, and then assume that these were known. We linearly interpolated the datasets over time using a 6 hour, 15 minute, and 12 hour time step for the grey seal, lake trout, and blue shark data, respectively, yielding datasets with 1227, 2187, and 393 locations. Different time steps were required based on the different temporal resolutions of the tracks.

Additionally, using the parameter estimates from the grey seal HMMM and DCRWS$_{NOME}$ fits (Table 2.1), we conducted a simulation study to formally compare the accuracy of the HMMM and DCRWS$_{NOME}$, and compare their results with those obtained using `moveHMM`. We simulated 50 tracks corresponding to the HMMM from a known parameter set with turning angles $\theta_1 = 0, \theta_2 = \pi$, autocorrelation $\gamma_1 = 0.8, \gamma_2 = 0.05$,

process error standard deviations $\sigma_{lon} = 0.07, \sigma_{lat} = 0.05$, and switching probabilities $\alpha_{1,1} = 0.89, \alpha_{2,2} = 0.80$. These two behavioural states are often interpreted as transiting (θ_1, γ_1) and foraging (θ_2, γ_2). We then fitted the HMMM, `moveHMM`, and the DCRWS$_{NOME}$ to each simulated track and calculated the parameter estimates and interval measures of uncertainty for these estimates. For the HMMM and `moveHMM`, this consisted of the 95% confidence interval based on the standard error estimates. For the DCRWS$_{NOME}$, we determined the 95% credible interval as the 2.5% and 97.5% quantiles of the posterior samples. We found the behavioural state error rate, i.e. the proportion of states that were incorrectly identified, for each model, and additionally calculated the root mean squared error (RMSE) for each parameter estimate $\hat{\Theta}$ from the HMMM and DCRWS$_{NOME}$ fits as

$$RMSE_{\Theta} = \left(\frac{1}{n} \sum_{j=1}^{n} (\hat{\Theta} - \Theta)^2 \right)^{1/2}. \tag{2.4}$$

We were unable to calculate the RMSE for the `moveHMM` fits because the data were simulated according to the HMMM movement process and the `moveHMM` implementation does not involve the same parameters.

2.3 Results

2.3.1 Identifying behavioural States

We applied the HMMM, the DCRWS$_{NOME}$, and `moveHMM` to a grey seal, lake trout, and blue shark track estimated with negligible measurement error. All three models performed similarly and identified two clearly distinct behavioural states for the
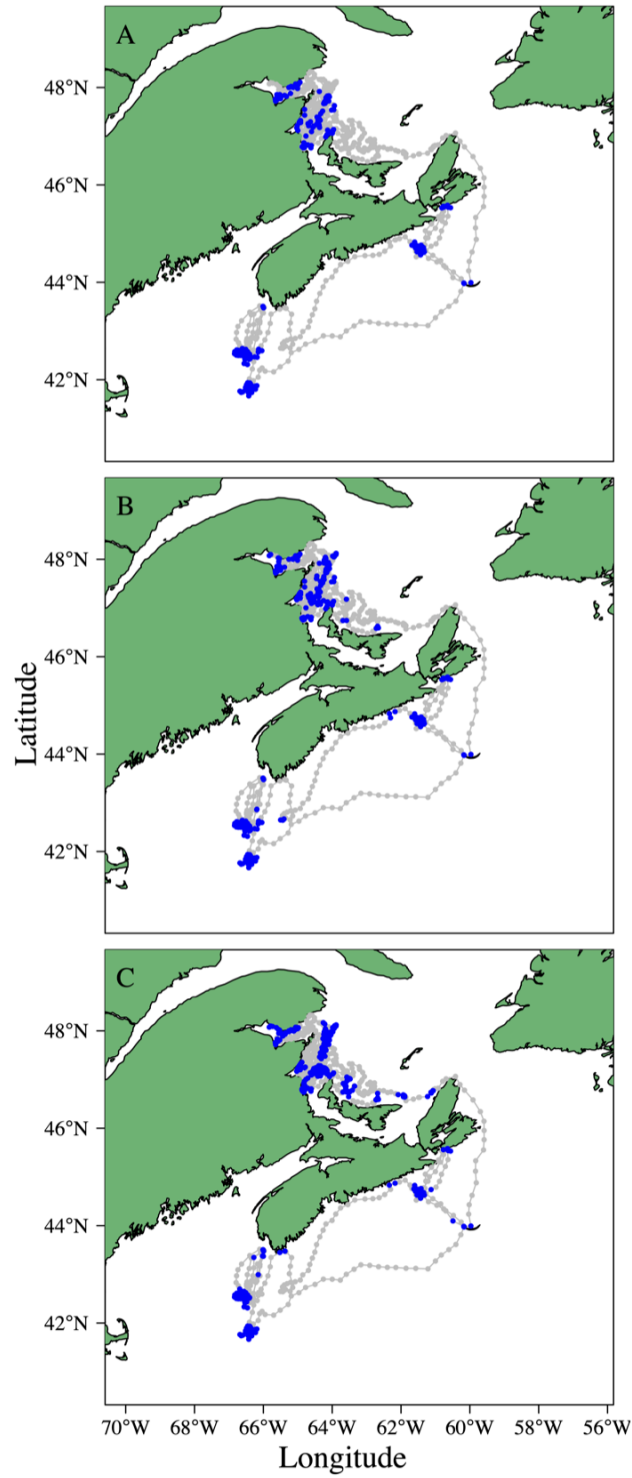
Figure 2.1: behavioural states as obtained by fitting the HMMM (panel A), DCRWS$_{NOME}$ (panel B), and moveHMM (panel C) models to the grey seal track. Different behavioural states are indicated by grey (state 1) and blue (state 2) colors.
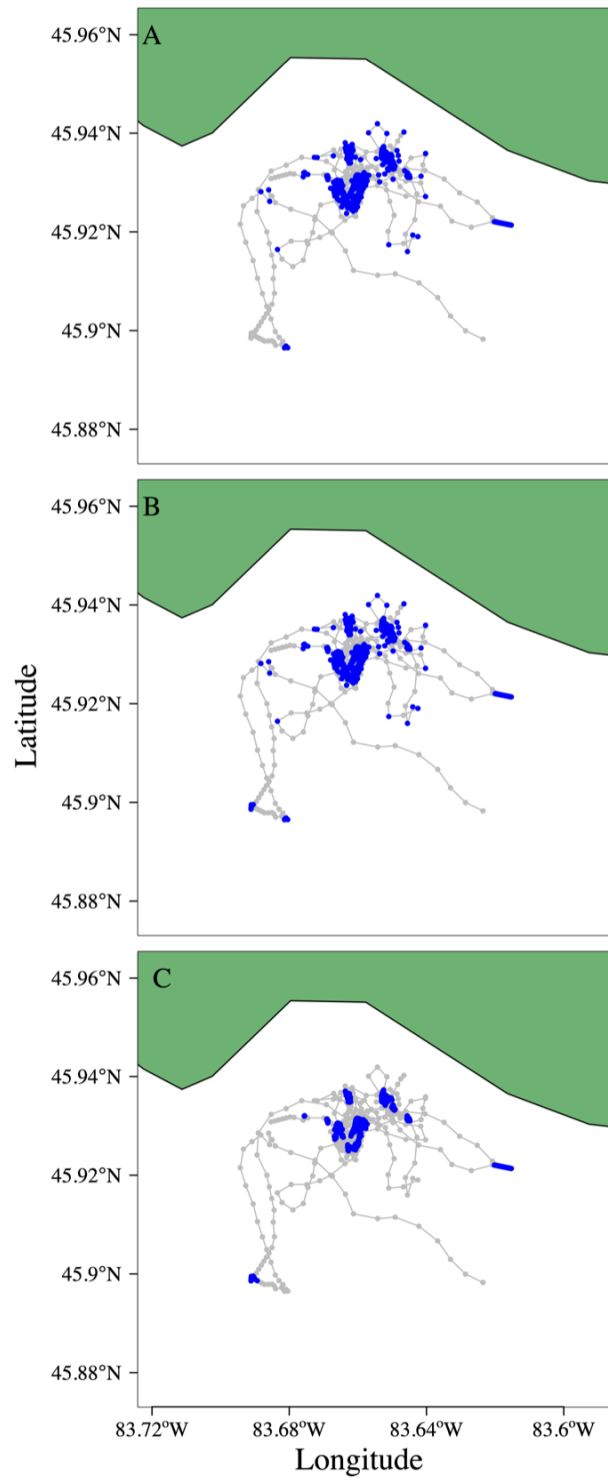
Figure 2.2: behavioural states as obtained by fitting the HMMM (panel A), DCRWS$_{NOME}$ (panel B), and `moveHMM` (panel C) models to the lake trout track. Different behavioural states are indicated by grey (state 1) and blue (state 2) colors.

grey seal and lake trout tracks (Figures 2.1,2.2). For both animals, HMMM and DCRWS$_{NOME}$ parameter estimates were similar except for the tortuous turning angle θ_2, which was estimated at a similar distance from the number π but in the opposite direction (i.e., while one was estimated turning slightly to the left, the other was estimated turning to the right; Tables 2.1, 2.2). This, along with the relatively large confidence intervals for θ_2, is not unusual because together with small γ_2, it suggests that the animal is exhibiting tortuous movement, in which case the mean turning angle does not have as much influence because the animal is more equally likely to travel in any direction. Switching probabilities ($\alpha_{1,1}$ and $\alpha_{2,1}$) were similar amongst all three models for the seal track. `moveHMM` estimated switching probabilities for the lake trout track different from the HMMM and DCRWS$_{NOME}$, although the estimated probabilities amongst all three models led to similar decoded behavioural state sequences. For the seal track, the DCRWS$_{NOME}$ took 6.4 hours to fit, `moveHMM` took 0.9 seconds, and the HMMM took 0.06 seconds. For the lake trout data, the DCRWS$_{NOME}$ took 9.4 hours to fit, `moveHMM` took 1.8 seconds, and the HMMM took 0.16 seconds.

Table 2.1: Parameter estimates from three models fitted to a grey seal track. Lower and upper columns are the lower and upper bound of 95% uncertainty intervals around the estimates. These correspond to 95% confidence intervals for the HMMM and `moveHMM`, and 95% credible intervals for the DCRWS$_{NOME}$. The only two parameters in common between all three models are the switching probabilities, $\alpha_{1,1}$ and $\alpha_{2,1}$.

Parameter	HMMM			DCRWS$_{NOME}$			Parameter	moveHMM		
	Estimate	Lower	Upper	Estimate	Lower	Upper		Estimate	Lower	Upper
θ_1	0.022	-0.023	0.066	-0.017	-0.060	0.027	μ_1	-0.010	-0.058	0.038
θ_2	4.662	2.441	5.835	1.831	0.275	5.980	μ_2	0.495	-0.358	1.348
γ_1	0.805	0.753	0.848	0.805	0.759	0.849	c_1	0.685	0.640	0.730
γ_2	0.055	0.013	0.201	0.048	0.003	0.128	c_2	0.069	0.002	0.135
σ_{lon}	0.071	0.068	0.074	0.071	0.068	0.074	λ_1	2.185	1.977	2.393
σ_{lat}	0.050	0.048	0.053	0.050	0.048	0.053	λ_2	0.816	0.757	0.875
							k_1	15.342	14.381	16.304
							k_2	3.487	2.878	4.097
$\alpha_{1,1}$	0.890	0.827	0.932	0.885	0.835	0.929		0.876	0.842	0.910
$\alpha_{2,1}$	0.198	0.133	0.285	0.204	0.141	0.292		0.111	0.090	0.158

Table 2.2: Parameter estimates from three models fitted to a lake trout track. Lower and upper columns are the lower and upper bound of 95% uncertainty intervals around the estimates. These correspond to 95% confidence intervals for the HMMM and `moveHMM`, and 95% credible intervals for the DCRWS$_{NOME}$. The only two parameters in common between all three models are the switching probabilities, $\alpha_{1,1}$ and $\alpha_{2,1}$.

Parameter	HMMM			DCRWS$_{NOME}$			Parameter	moveHMM		
	Estimate	Lower	Upper	Estimate	Lower	Upper		Estimate	Lower	Upper
θ_1	-0.118	-0.155	-0.082	0.119	0.084	0.155	μ_1	0.021	-0.041	0.083
θ_2	2.687	2.277	3.113	3.603	3.206	4.088	μ_2	-0.746	-2.042	0.447
γ_1	0.821	0.786	0.851	0.821	0.788	0.853	c_1	3.123	2.488	3.763
γ_2	0.128	0.083	0.191	0.123	0.075	0.177	c_2	0.113	0.033	0.238
σ_{lon}	0.001	0.001	0.001	0.001	0.001	0.001	λ_1	2.324	2.119	2.550
σ_{lat}	0.001	0.001	0.001	0.001	0.001	0.001	λ_2	0.838	0.786	0.894
							k_1	16.128	15.274	17.029
							k_2	4.084	3.621	4.606
$\alpha_{1,1}$	0.645	0.578	0.707	0.643	0.576	0.705		0.853	0.811	0.887
$\alpha_{2,1}$	0.288	0.212	0.377	0.289	0.214	0.384		0.102	0.077	0.132
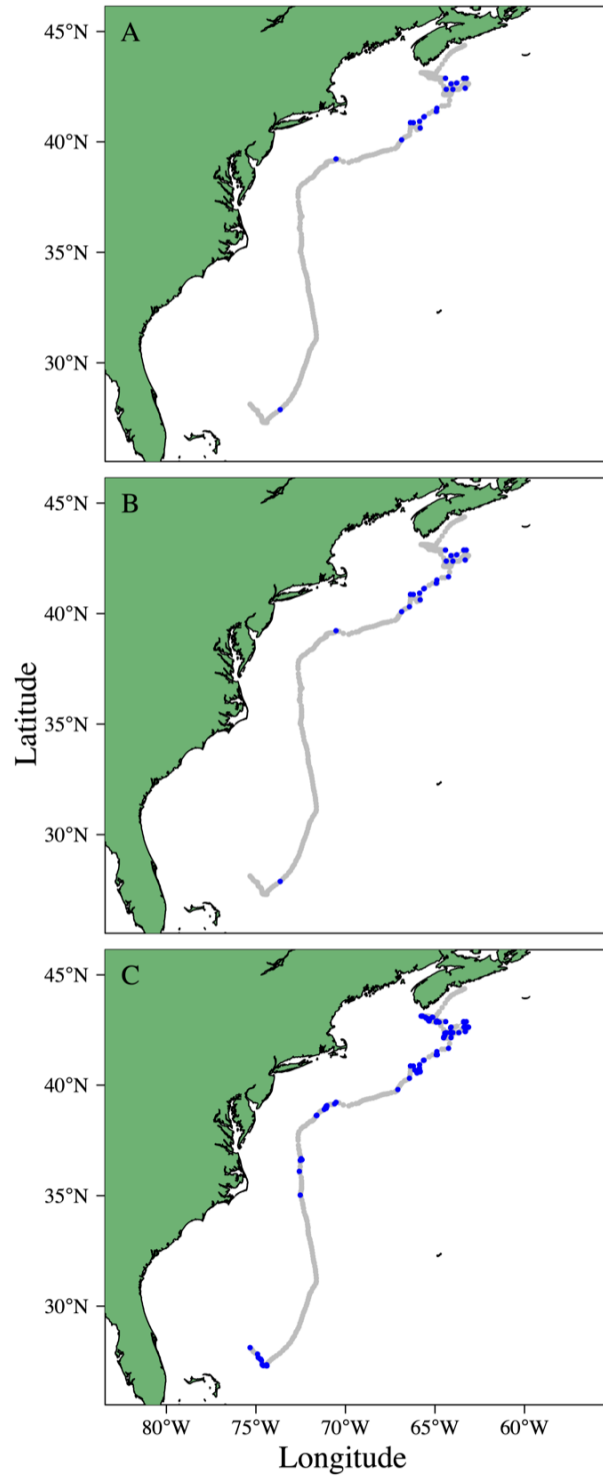
Figure 2.3: behavioural states as obtained by fitting the HMMM (panel A), DCRWS$_{NOME}$ (panel B), and `moveHMM` (panel C) models to the blue shark track. Different behavioural states are indicated by grey (state 1) and blue (state 2) colors.

All three models identified two states from the blue shark track, although half of the switching probabilities estimated by `moveHMM` differed greatly from those estimated by the HMMM and DCRWS$_{NOME}$ (Table 2.3), and this led to different state sequences (Figure 2.3). Specifically, all three models estimated a high probability of remaining in state 1, $\alpha_{1,1}$, but `moveHMM` estimated a low probability of switching from state 2 to state 1, $\alpha_{2,1}$, while the DCRWS$_{NOME}$ and HMMM estimated a high $\alpha_{2,1}$. The switching probabilities of the HMMM and DCRWS$_{NOME}$ therefore led to state sequences containing long stretches of state 1 interspersed with short (length 1 or 2) stretches of state 2. By contrast, `moveHMM` estimated a state sequence with longer stretches of both behavioural states. While the DCRWS$_{NOME}$ took 1.7 hours to fit to the blue shark track, `moveHMM` took 1.2 seconds, and the HMMM took 0.02 seconds.

Table 2.3: Parameter estimates from three models fitted to a blue shark track. Lower and upper columns are the lower and upper bound of 95% uncertainty intervals around the estimates. These correspond to 95% confidence intervals for the HMMM and `moveHMM`, and 95% credible intervals for the DCRWS$_{NOME}$. The only two parameters in common between all three models are the switching probabilities, $\alpha_{1,1}$ and $\alpha_{2,1}$. Because this track had some step lengths equal to zero, the two parameters ζ_1 and ζ_2 were used to estimate zero-inflation for each behaviour when using `moveHMM`.

Parameter	HMMM			DCRWS$_{NOME}$			Parameter	moveHMM		
	Estimate	Lower	Upper	Estimate	Lower	Upper		Estimate	Lower	Upper
θ_1	-0.021	-0.070	0.027	0.013	-0.040	0.062	μ_1	-0.003	-0.025	0.019
θ_2	0.528	0.232	1.131	-0.881	-0.006	0.157	μ_2	0.013	-0.273	0.300
γ_1	0.923	0.846	0.963	0.932	0.873	0.987	c_1	40.323	30.556	50.107
γ_2	0.289	0.199	0.400	0.303	0.188	0.423	c_2	0.949	0.616	1.302
σ_{lon}	0.045	0.042	0.049	0.046	0.043	0.049	λ_1	1.806	1.608	2.029
σ_{lat}	0.042	0.039	0.045	0.042	0.038	0.045	λ_2	1.069	0.927	1.232
							k_1	11.816	10.872	12.842
							k_2	6.610	5.255	8.314
							ζ_1	0.029	0.014	0.059
							ζ_2	0.035	0.013	0.091
$\alpha_{1,1}$	0.904	0.794	0.958	0.880	0.732	0.955		0.841	0.778	0.888
$\alpha_{2,1}$	0.722	0.385	0.915	0.742	0.437	0.925		0.320	0.211	0.454

2.3.2 Simulation Study

We simulated 50 tracks from the HMMM with a specific parameter set (representative of the grey seal track) to test the accuracy of the HMMM compared to the DCRWS$_{NOME}$ and `moveHMM`. The HMMM and DCRWS$_{NOME}$ provided accurate estimates of the model parameters (Figure 2.4), but the DCRWS$_{NOME}$ had a smaller average (over the parameters) RMSE (0.120 vs. 0.140; Table 2.4). The RMSE for individual parameters were similar (within 0.01) between the two models with the exception of θ_2, where the RMSE of the DCRWS$_{NOME}$ was smaller by 0.149 (Table 2.4). The DCRWS$_{NOME}$ additionally had the smallest behavioural state error rate (0.175) which differed from the HMMM and `moveHMM` by approximately 1.5% (0.189) and 18.7% (0.362), respectively. Finally, the average time needed to fit the DCRWS$_{NOME}$ was 5.10 hours, while `moveHMM` took 1.2 seconds and the HMMM took 0.08 seconds.
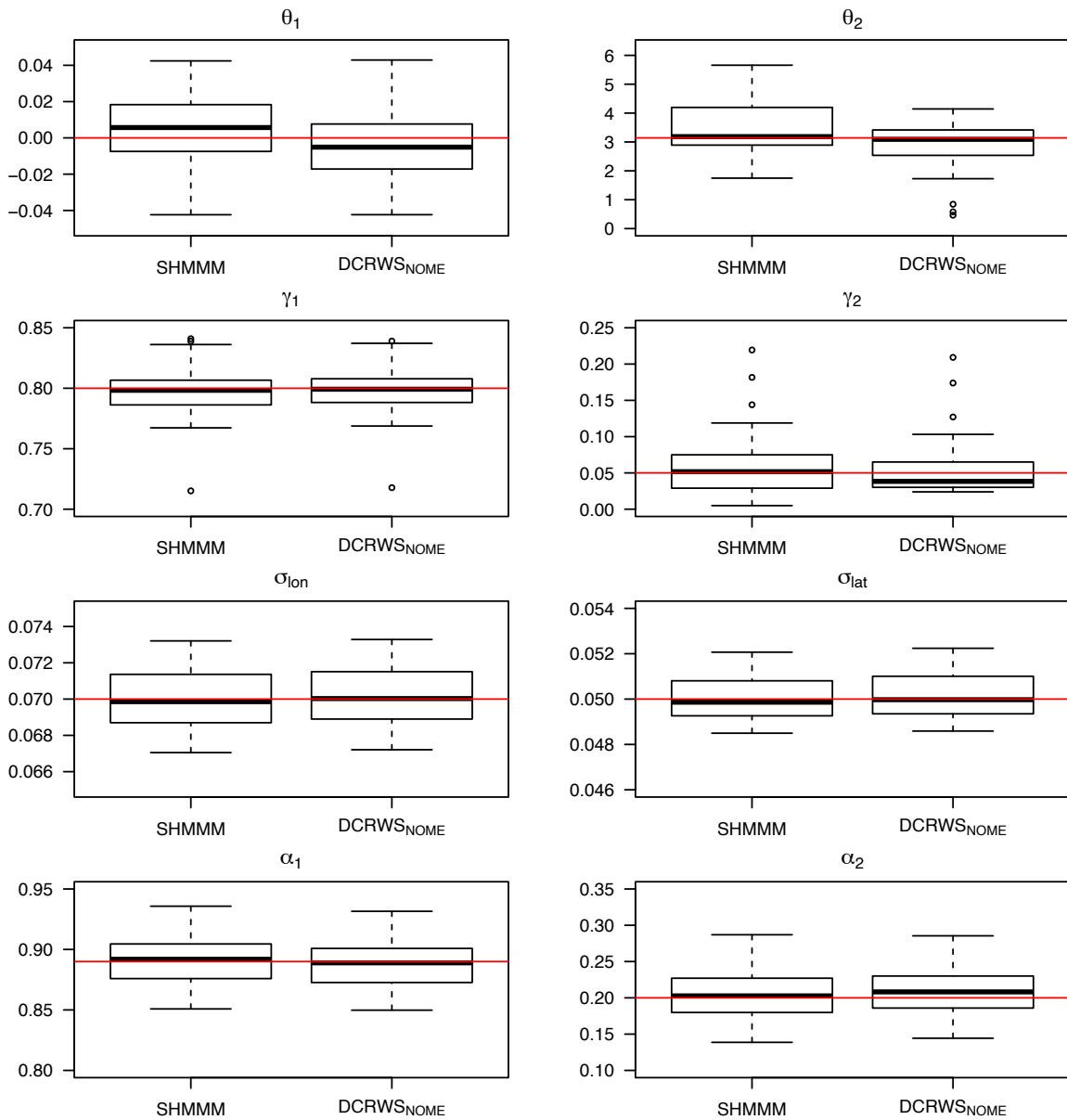
Figure 2.4: Boxplots of parameter estimates obtained from fitting the HMMM and the DCRWS$_{NOME}$ to 50 simulated tracks.

Table 2.4: Parameter results from the simulation study (n=50) comparing the HMMM to the DCRWS$_{NOME}$. The Lower and Upper columns correspond to the 95% confidence and credible intervals for the HMMM and the DCRWS$_{NOME}$, respectively. The Estimate, Lower, and Upper columns are averages taken over all simulations. The RMSE columns contain the root mean squared errors.

Parameter	True Value	HMMM				DCRWS$_{NOME}$			
		Estimate	Lower	Upper	RMSE	Estimate	Lower	Upper	RMSE
θ_1	0	0.004	-0.035	0.042	0.020	-0.004	-0.043	0.035	0.020
θ_2	π	3.433	1.599	4.730	0.978	2.931	0.483	5.400	0.829
γ_1	0.80	0.797	0.752	0.836	0.021	0.797	0.756	0.839	0.021
γ_2	0.05	0.060	0.018	0.321	0.044	0.052	0.007	0.138	0.037
σ_{lon}	0.07	0.070	0.067	0.073	0.002	0.070	0.067	0.073	0.002
σ_{lat}	0.05	0.050	0.048	0.052	0.001	0.050	0.048	0.052	0.001
$\alpha_{1,1}$	0.89	0.890	0.844	0.924	0.018	0.886	0.842	0.922	0.018
$\alpha_{2,1}$	0.20	0.205	0.140	0.290	0.034	0.208	0.143	0.293	0.033

2.4   Discussion

We have shown that the HMMM is a fast and reliable tool for estimating behavioural states from animal tracking data that contain negligible error. Our simulation study demonstrated the accuracy of the HMMM for estimating both the states and model parameters. Our use of data from different species and derived by different telemetry systems demonstrated the wide-ranging applicability of the HMMM. Coupled with the existing documentation of the DCRWS SSM (more than 45 papers using this model), we suspect that the HMMM will be an easily interpretable tool for ecologists who are interested in implementing the DCRWS SSM and have highly accurate data, which has an advantage over current methods with the DCRWS SSM of being fast to fit (on the order of seconds) and avoiding convergence issues with MCMC samplers.

HMMM implementation is available through the R package `swim`.

The HMMM, DCRWS$_{NOME}$, and `moveHMM` all identified two behavioural states from the grey seal track, consistent with previous analyses (Jonsen et al., 2005; Breed et al., 2009, 2011). Grey seal tracks from Atlantic Canada typically show clear bouts of directed and tortuous movement, and have been previously analyzed with the DCRWS SSM (e.g., Jonsen et al. 2005); therefore, an Atlantic Canada grey seal GPS track provided an ideal test for our study. For grey seals, tortuous movement is often assumed to represent apparent foraging, while directed movement is often regarded as travelling between foraging patches. The models identified several bouts of apparent foraging behaviour in the Northwest Atlantic and in the Gulf of Saint-Lawrence, specifically off the coasts of Nova Scotia, Prince Edward Island, New Brunswick, and Gaspésie, areas of high biological productivity that are consistent with those previously identified as grey seal foraging areas (Breed et al., 2009).

With the HMMM, DCRWS$_{NOME}$, and `moveHMM`, we identified two behavioural states within the lake trout track. The Drummond Island lake trout population spawn primarily at nighttime on rock rubble reefs in association with submerged drumlins (Riley et al., 2014; Binder et al., 2015). Lake trout show multiple behaviours characterized by tortuous movement, including spawning on the reefs. For example, lake trout (particularly males) often aggregate on the spawning reefs in the weeks leading up to spawning, a behaviour known as staging (Muir et al., 2012). Because egg surveys have verified that no spawning occurs in some locations where our models identified tortuous behaviour (T. Binder, unpublished observations), we

believe the models are distinguishing, more generally, reef and non-reef behaviours. Being able to mathematically distinguish between reef and non-reef behaviours can allow for identification of key lake trout habitats for conservation like spawning sites in places where direct observation is difficult. Furthermore, by building a dependence of the HMMM on one or more covariates, it may be possible to more acutely identify spawning behaviour. For example, because the Drummond Island lake trout tend to spawn at night close to the substrate, time of day and lake trout depth (which is often recorded by positioning systems like the VPS) may provide sufficient additional information for the HMMM to distinguish spawning behaviour from other reef-associated behaviours. One possible way to achieve this is by allowing the switching probabilities of the HMMM to depend on these covariates in a linear fashion (as in e.g., Bestley et al. 2013; Michelot et al. 2016). Additionally, an extension to the HMMM which could estimate more than two behavioural states may be able to distinguish reef from spawning behaviour. We chose to model only two states so that we could more directly compare results of the HMMM to our implementation of the original DCRWS SSM (the DCRWS$_{NOME}$); however, the HMMM should be directly extendible.

When fitted to the blue shark track, `moveHMM` produced different state sequences than the HMMM and DCRWS$_{NOME}$, as `moveHMM` estimated longer stretches of behavioural state 2 than either of the other models. This is likely because `moveHMM` models the distributions of the turning angles and step lengths calculated from an animal path, which is fundamentally different from the movement process of the HMMM and DCRWS$_{NOME}$. Furthermore, (McClintock et al., 2014) showed that the

continuous-time analog to the movement process introduced by Jonsen et al. (2005) and modeled by the HMMM has step lengths and bearings (turning angles) that are correlated, whereas the step lengths and bearings of the process modeled by McClintock et al. (2012) (close to that of `moveHMM`) are uncorrelated. `moveHMM` identified two behaviours that were distinguished primarily by different step lengths, and therefore travelling speeds, with state 1 characterized by longer step lengths and faster speeds, and state 2 characterized by slower movement. The HMMM and DCRWS$_{NOME}$ identified two behaviours that were distinguished by high (state 1) and low (state 2) autocorrelations, or how related the speed at time t was to the speed at time $t - 1$. By modelling autocorrelation, the HMMM and DCRWS$_{NOME}$ were able to directly estimate persistence in animal movement. It is possible that the shorter sequences of state 2 identified by the HMMM and DCRWS$_{NOME}$ resulted because the behaviours they were trying to estimate occured on a finer time scale than was modelled, which could make biological interpretation of these states difficult.

Our simulation study results suggested that while the DCRWS$_{NOME}$ was slightly more accurate than the HMMM, the difference was marginal. The two models performed similarly while estimating model parameters with the exception of θ_2, which the DCRWS$_{NOME}$ more accurately estimated. This result is likely explained by the rather informative priors on θ_1 and γ_1 when fitting the DCRWS$_{NOME}$. The DCRWS$_{NOME}$ also more accurately estimated the behavioural states, which may have resulted from the fact that the DCRWS$_{NOME}$ directly samples each of these random

effects from the posterior likelihood, while the HMMM uses a post hoc global decoding algorithm (the Viterbi algorithm) to identify the most likely sequence of states. Predictably, `moveHMM` had the highest behavioural state error rate of the three approaches, likely because it was fitted to simulated data from a movement process not equivalent to its own. Finally, the HMMM was the fastest model to fit, with `moveHMM` and the DCRWS$_{NOME}$ taking on average 15 times and 229,500 times longer to fit than the HMMM, respectively. Quicker fits of the DCRWS$_{NOME}$ may be achieved by reducing burn-in and sampling sizes of the MCMC, but they would still take orders of magnitude longer and may be less accurate. We chose these sizes based on prior experience with fitting the DCRWS SSM, and to try to ensure convergence of the MCMC chains during the simulation study.

Our HMMM is a major advance in using `TMB` to solve animal movement problems. Highly accurate data are becoming more common in the marine realm, and the HMMM, as implemented through the R package `swim`, provides a fast and reliable tool for making meaningful inference from animal movement data. Fast methods for analyzing data will become more important as larger datasets are collected. The HMMM therefore additionally provides a baseline method for movement modelling in `TMB` that can be further developed for more specific and nontrivial animal movement problems like determining relationships between movement and environmental covariates, or accounting for measurement error.

Chapter 3

Current and Emerging Statistical Techniques for Aquatic Telemetry Data: A Guide to Analysing Spatially Discrete Animal Detections

3.1 Introduction

Aquatic animals live in habitats that create inherent challenges for those attempting to study their ecology, behaviour and physiology. Telemetry enables the remote monitoring of free-living animals, whereby a signal emanating from a device (i.e., transmitter or tag) carried by an animal transfers information to a receiver. The advent of telemetry tools has provided researchers with effective means of studying aquatic animals in the streams, rivers, lakes, estuaries, and oceans of the world (Lucas and Baras, 2000; Hussey et al., 2015).

Three common telemetry technologies used with aquatic animals are radio and acoustic telemetry, and passive integrated transponders (PIT). Radio telemetry uses radio signals that are detected by an antenna affixed to a receiver, whereas acoustic telemetry uses sound waves to transmit tag information to a hydrophone on a receiver. The transmitters of both technologies are dependent on internal batteries that, along with the tag-animal size ratio and tag settings, limit the duration of data

collection. PIT tags rely on external energy derived from an electromagnetic field emitted by receiver antennas, which prolongs the tag lifespan but requires close proximity (Lucas and Baras, 2000). Despite design differences (Lucas and Baras, 2000; Cooke et al., 2012), these three telemetry technologies all record one specific kind of data: detection data that consist of time-stamped, tag-specific records registered and stored by receivers when tagged animals are within range.

Recently, a shift from mobile tracking towards using fixed receiving stations that automatically log detections has led to a large number of tagged animals and extensive receiver coverage crossing geopolitical boundaries (Donaldson et al., 2014). The collection and aggregation of large aquatic detection datasets has created both challenges and opportunities for the study of wild aquatic animals (Lennox et al., 2017a). Although there have been substantial developments in the statistical analysis of aquatic detection data, to our knowledge, there have been no attempts to synthesize the existing and emerging methods. Our goal is to provide this synthesis. Although the methods we review are the most ubiquitous (today), they are not exhaustive. In particular, because detection data are limited to collection at discrete locations, we do not review methods for spatially continuous data (e.g. movement paths collected by satellite telemetry devices). It is possible to obtain estimates of spatially continuous data from detection data using positioning systems (Niezgoda et al., 2002; Smith, 2013) or by calculating centers of activity (Simpfendorfer et al., 2002), in which case other statistical methods not reviewed herein may be used, for example, home range analysis (Marshell et al., 2011), state-space models (Marins

et al., 2014), or hidden Markov models (Whoriskey et al., 2017). We also do not discuss software designed primarily for the data management and visualization of aquatic detection data. These developments, e.g. the Ocean Tracking Network Toolbox (otndc@dal.ca), ZoaTrack (Dwyer et al., 2015), the Integrated Marine Observing System's Animal Tracking Facility detection database and quality control procedures (Hoenner et al., 2018), and the R (R Core Team, 2018) packages `glatos` (Holbrook et al., 2017), and `VTrack` (Campbell et al., 2012), provide high-quality standardized methods for handling detection data; however, they typically do not incorporate a stochastic component.

First, we review statistical methods for detection data derived from fixed telemetry arrays in aquatic environments. To illustrate the differences between statistical methods, throughout the review, we analyse a portion of a dataset collected on acoustically tagged bull trout *Salvelinus confluentus*. Then, we comment on potential future directions that could help advance our understanding of how aquatic animals interact with each other, their environment, and humans in a rapidly changing world. To close, we present a decision tree to summarize the differences among the statistical methods and to help guide researchers on how to analyse their detection data given the scientific questions of interest and sampling design.

3.2 Illustrative Dataset

Between 2010 and 2012, 187 bull trout were acoustically tagged and monitored by an array of 42 receivers deployed in the Kinbasket Reservoir of British Columbia,

Canada (Fig 3.1). The full dataset was previously analysed in Martins et al. (2013) and Gutowsky et al. (2016); for simplicity, we chose to analyse data collected only during January 2011. The resulting dataset comprised three files: receiver metadata, that includes the identities and locations of the deployed receivers, along with environmental information; tag metadata, that consists of the unique tag ID codes and other animal characteristics (e.g. length/ weight/sex); and detection data, i.e. the records of tags registered by receivers at a specific date and time. Together, these data (hereafter 'detection data') provide a comprehensive view on individual movements.

For any telemetry study, the question of interest and the spatiotemporal design of the receiver deployments will influence the applicability of various statistical methods. Once a method has been chosen, the detection data will need to be summarized into an appropriate response variable (y). Examples include: counts of detections (Zhang et al., 2015), counts or proportions of receivers visited within a specific time scale (Udyawer et al., 2015), presence/absence data (Dudgeon et al., 2013; Kessel et al., 2014a), time spent in particular areas or residency indices (Kessel et al., 2014a; Ketchum et al., 2014), and movement rates (Stich et al., 2015). We discuss the form of the response variable for each method reviewed below, and use the Kinbasket dataset to illustrate the versatility of detection data.
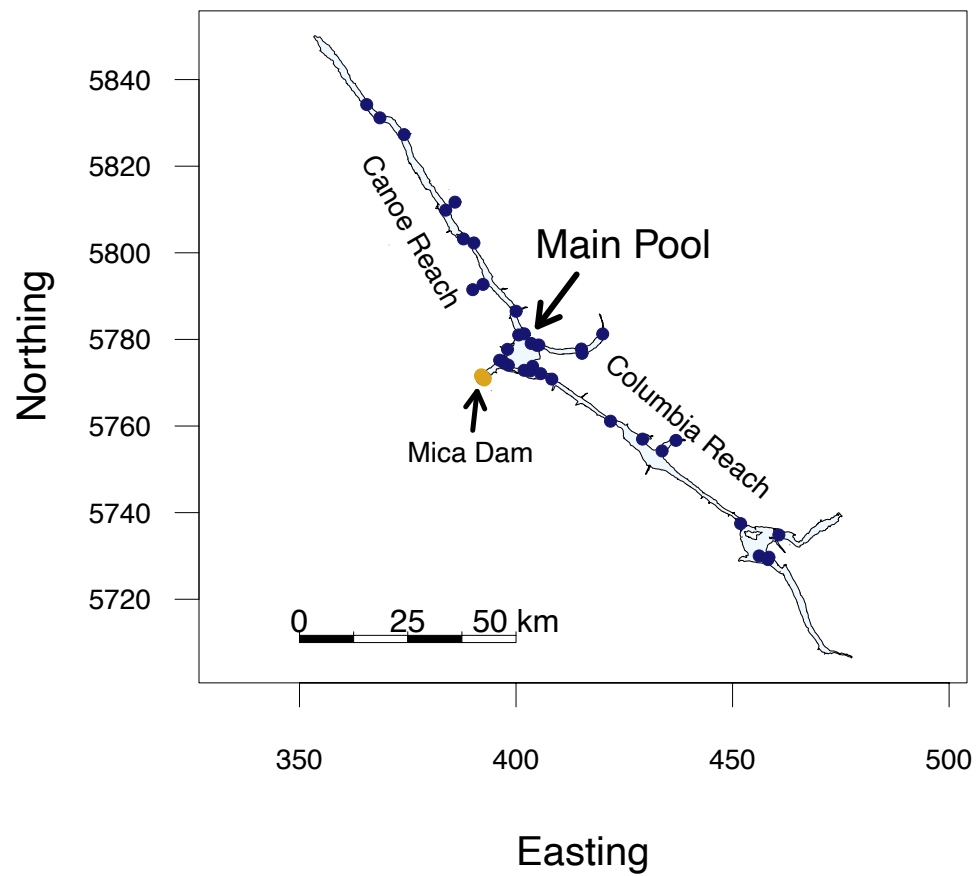
Figure 3.1: Study location of the illustrative dataset, i.e. the Kinbasket reservoir in British Columbia, Canada, with the location of the dam in yellow, and the receiver locations in dark blue. Detection range was assumed to be 500 m, a distance shorter than the width of either Reach in most places.

3.3 Review of Current Statistical Methods

3.3.1 Generalized Modelling Framework

Researchers who use telemetry are often interested in determining whether there is a relationship between animal movement patterns and a set of putative explanatory variables or covariates. Because many of the possible response variables are non-Gaussian, traditional statistical methods like analysis of variance and linear regression are not directly applicable. Generalized linear models (GLMs) enable the modelling of non-Gaussian response variables provided they follow a distribution belonging to the exponential family (Wood, 2006). A GLM links an observation y_i to a set of covariates $\mathbf{X}_i$:

$$\mu_i \equiv \mathrm{E}[y_i] \tag{3.1}$$

$$g(\mu_i) = \mathbf{X}_i \boldsymbol{\beta} = \beta_0 + \beta_1 x_{i,1} + \beta_2 x_{i,2} + \cdots + \beta_k x_{i,k}, \tag{3.2}$$

where $\mathrm{E}[\cdot]$ denotes the expectation of a random variable, $g(\cdot)$ is a monotonic link function, and the vector β contains $k+1$ entries that describe the relationship between μ_i and the k covariates (plus an intercept) contained in each row vector $\mathbf{X}_i$ (Wood, 2006).

Because telemetry does not directly measure animal absence, researchers must decide whether to interpret a lack of detections as absence and encode them as zeros within a dataset. The temporal resolution of the study directly affects the number of zeros in the response, whereby many zeros will be included if animals are rarely

detected over numerous short time intervals. Furthermore, environmental features like topography, weather, and biological noise, as well as collisions with other telemetry transmissions, can lead to false absences (Cagua et al., 2013). A dataset will be more difficult to accurately model when the number of observed zeros is substantially greater than the number predicted; such models may show evidence of overdispersion (when the response variance is larger than expected) or lack of fit (Zuur et al., 2009). In these cases, zero-inflated models may provide more accurate results (Zuur et al., 2009).

Both discrete and continuous covariates can be included in GLMs if they are linearly related to the response. For nonlinear relationships, generalized additive models (GAMs) relate the response and covariates using a sum of smooth functions $f(\cdot)$ of the variables (Wood, 2006), e.g.

$$g(\mu_i) = f_1(x_{i,1}) + f_2(x_{i,2}, x_{i,3}) + \cdots \qquad (3.3)$$

Detection data have been related to covariates like lunar phase and tidal stage (Dudgeon et al., 2013), water temperature (Kessel et al., 2014a; Udyawer et al., 2015), discharge (Richard et al., 2014; Stich et al., 2015), and diel period (Ketchum et al., 2014; Zhang et al., 2015). Temporal data can also be used, often by summarizing the response into temporal blocks and including the blocks as a covariate. Blocks can be defined based on species ecology (e.g. reproductive timing), or anthropogenically (e.g. by monthly intervals; Matich and Heithaus 2014). When investigating a temporal trend in the response, temporal autocorrelation should be checked and accounted for

if the assumption of independence is violated, e.g. by incorporating lagged temporal variables (Kessel et al., 2014a) or including a correlation structure (Börger et al., 2006).

Because most detection data are collected under the largely uncontrolled conditions of the natural environment, some responses may only be independent when conditioned upon other variables. These variables, also known as random effects, can be accounted for by incorporating a second stochastic term into GLMs and GAMs to form generalized linear mixed models (GLMMs) and generalized additive mixed models (GAMMs; Wood 2006). In practice, random effects are often included to account for variation within and among sampling units. For example, detection data are usually collected on a random subset of individuals from a population. To conduct population-level inference, individual ID can be included as a random effect with either, or both, an intercept and slope (Bolker et al., 2009). Random effects can also be associated with space or time, e.g. receiver location (Ketchum et al., 2014) or age and sampling year (Börger et al., 2006).

Generalized models were used to assess the factors affecting spatial distribution and movement of bull trout in the full complement of the illustrative dataset (Gutowsky et al., 2016). Using a GLMM, Gutowsky et al. (2016) assessed the effects of year, season, sex, and body size (covariates in $\mathbf{X}$) on home range size (response $\mathbf{y}$; 95% minimum convex polygon). A GAMM was used to quantify the relationship between total displacement (response $\mathbf{y}$; sum of distances between receivers) and sex, body size, and smoothed month. Larger β coefficient values for spring and fall

suggested that bull trout home ranges were larger in those seasons than in winter and summer. Additionally, a positive sex-size interaction term suggested that larger females moved farther than smaller females.

3.3.2 Survival (Time-to-Event) Analysis

Telemetry measures animal positions over time and changes in position can be related to important ecological events. For example, tagged animals may disperse or migrate (Kawabata et al., 2010), interact with humans (Thorley et al., 2007), pass an obstacle (Castro-Santos and Haro, 2003; Naughton et al., 2005; Martins et al., 2013), be depredated (Danylchuk et al., 2007; Lennox et al., 2017b), or die (Curtis et al., 2015). These events can be analysed with GLMs using a binomial response, where study animals are grouped into those that experience an event and those that do not. Survival analysis extends the response by incorporating the time it takes for the event to occur (e.g. $y = 2$ days) and estimates the survival function, $S(t)$,

$$S(t) = \Pr(T > t), \tag{3.4}$$

which describes the probability, $\Pr(\,\cdot\,)$, that an event will occur at some random time T after the set time t (Pollock et al., 1989a; Klein and Moeschberger, 2003). Two common survival function estimators include the non-parametric Kaplan–Meier and Nelson-Aalen estimators (Klein and Moeschberger, 2003). A log-rank test can be used to compare the estimated survival curves of different groups (e.g. sex and reproductive state or moult stage; Pollock et al. 1989b; Huserbråten et al. 2013).

Further inference is possible with the hazard function $h(t)$, which describes the conditional rate of an event occurring during a period of time $\{t, t + \Delta t\}$ given that it has not already been experienced (Klein and Moeschberger, 2003):

$$h(t) = \lim_{\Delta t \to 0} \frac{P[t \leq T < t + \Delta t \mid T \geq t]}{\Delta t}. \tag{3.5}$$

When the shape of the hazard or survival function is assumed, parametric survival analysis can be performed with error distributions (e.g., the Weibull) and this allows for predictive extrapolation (Benoît et al., 2015). However, selecting a parametric hazard function requires accurate knowledge of the true shape, which is not often known (White and Garrott, 1990; Murray, 2006). Consequently, using semi-parametric Cox proportional hazards regression can be advantageous because there is no assumption about the hazard shape, yet the response can still be compared to a set of covariates $\mathbf{X}$ (Murray, 2006; Harrell, 2015),

$$h(t_i) = h_0(t_i)c(\mathbf{X}_i\boldsymbol{\beta}). \tag{3.6}$$

The hazard $h(\cdot)$ is related to an arbitrary baseline hazard $h_0(\cdot)$ that is treated non-parametrically, and a known parametric function $c(\cdot)$ of the covariates and their coefficients (Klein and Moeschberger, 2003). The Cox proportional hazards model is also less sensitive to outlying observations than parametric models, but does require hazard proportionality which can be verified graphically or by testing for independence between Schoenfeld residuals and time (Harrell, 2015). Violations of this assumption

may be compensated for by fitting stratified models (Harrell, 2015).

In telemetry studies, animals often go undetected for extended periods, either because they leave the detection range of the array or because they are inactive. The resulting monitoring gaps can cause discontinuity in the hazard function (Murray, 2006) and bias survival estimates (Bunck et al., 1995). The Andersen–Gill estimator (Andersen and Gill, 2005) is a variation of the Cox proportional hazards model that uses a counting process to account for discontinuous monitoring (Murray 2006; see e.g. Johnson et al. 2004). In addition, individuals that fully drop out of the study before the event occurs can be censored from survival analysis techniques without having to be removed entirely (Pollock et al., 1989b). For example, Topping and Szedlmayer (2011) used survival analysis to study the residency time (event = emigration) of red snapper (*Lutjanus campechanus*), and censored fish that either died before emigration or did not emigrate in order to retain them in the analysis.

An example of survival analysis using detection data can be found in Martins et al. (2013), where the Kaplan–Meier estimator was used to compute the risk of bull trout unintentionally passing through hydro-electric dam turbines (the event of interest) from the full Kinbasket dataset. The Kaplan–Meier estimator exhibits larger jumps in the survival curve for the fall and winter, suggesting that the risk of passing through the dam was higher during those seasons.

3.3.3 Mark-Recapture Models

Mark-recapture models are used for estimating movement or demographic attributes, e.g. abundance or survival. These models are fitted to data collected by capturing and marking a sample of animals from a population, subsequent release, and resampling such that additional samples can include both marked and unmarked animals (Amstrup et al., 2005). When using telemetry, mark-recapture models are applicable if the tagging procedure is considered the marking process, and detections are the recaptures. Few telemetry studies record the presence of untagged animals (but see Dudgeon et al. 2015), therefore the most applicable mark-recapture models incorporate data collected on tagged animals only, which include known-fate, live-recapture, and recovery models (Lindberg, 2012).

Known fate models (related to survival analysis) assume perfect detection probabilities, which rarely occur in telemetry. Alternatively, live-recapture models are highly applicable for analyzing detection data because they enable the joint estimation of detection probability and demographic quantities. Among live-recapture models, the Cormack–Jolly–Seber model is frequently used, often to estimate survival along migratory routes (e.g. Welch et al. 2009; Moore et al. 2015). The Cormack–Jolly–Seber model is fitted using a product of probabilities with two basic parameters: ϕ is the probability that an individual survives between detections, and p is the probability that an individual is detected if alive and marked (Amstrup et al., 2005). The response variable consists of a binary encounter history (absence $= 0$ and presence $= 1$) for every marked animal that is recorded on a discrete temporal scale

chosen by the researcher. If a single animal's encounter history is encoded as 1101, where the first digit is the initial capture and tagging, then the associated encounter probability would be

$$\phi p \phi (1 - p) \phi p, \tag{3.7}$$

if ϕ and p are assumed constant through time, or

$$\phi_1 p_2 \phi_2 (1 - p_3) \phi_3 p_4, \tag{3.8}$$

if these probabilities are allowed to vary. Because the Cormack–Jolly–Seber model cannot distinguish between mortality and emigration, survival estimates are more appropriately termed apparent survival (Williams et al., 2001).

A useful extension of the Cormack–Jolly–Seber model is the multi-state Arnason–Schwarz model, which estimates survival and detection probabilities as a function of an observed animal state (Schwarz et al., 1993; Amstrup et al., 2005). The states are assumed to follow a first-order Markov process governed by transition probabilities (Amstrup et al., 2005). It has been applied to detection data to estimate daily probabilities of horseshoe crab spawning (*Limulus polyphemus*; reproductive state; Brousseau et al. 2004), survival of downstream migrating Atlantic salmon (*Salmo salar*; location state; Holbrook et al. 2011), and movement probabilities along walleye (*Sander vitreus*) migratory routes (location state; Hayden et al. 2014).

Recovery mark-recapture models are useful when the recapture process is terminal

(Lindberg, 2012). Information on deceased individuals can be jointly modeled with live detection data using the Burnham model (Burnham, 1993), which has been used to provide more precise survival estimates (Sollmann et al., 2010) and to estimate the joint probability that tagged individuals were caught and reported (Martins et al., 2011). The Barker model is an extension of the Burnham model useful for analysing temporally continuous detection data (Barker, 1997), and has been used to estimate the effects of gastric lavage on common snook survival (*Centropomus undecimalis*; Barbour et al. 2012). Finally, Fouchet et al. (2016) proposed an approach for temporally continuous data that combines survival analysis with an inhomogenous Poisson process for modelling detection probability.

We fitted several Cormack–Jolly–Seber models using MARK (White and Burnham, 1999) and `RMark` Laake (2013) to test whether sex or length were associated with weekly bull trout survival, and whether the receiver array detection probability changed over time. We compared candidate models using corrected Akaike's information criterion (AICc), and found that the best model estimated intercepts only for both survival and the detection probability (Table 3.1). The apparent weekly survival probability was estimated at 0.91. In addition, the detection probability was estimated at 0.69, which suggests that a combination of receiver coverage/efficiency, environmental conditions, and fish behaviour limited the array's ability to detect bull trout.

Table 3.1: Model fits with corrected AIC (AICc) values from the mark recapture analysis of the illustrative bull trout dataset. Construction of the model is given by the Model formula, where $\phi(\cdot)$ denotes the effects related to the apparent survival probability and $p(\cdot)$ denotes those related to the probability of detection. 1 denotes an intercept only model. ΔAICc is the difference in AICc from the best model.

Model formula	No. parameters	AICc	Δ AICc
$\phi(\sim 1)p(\sim 1)$	2	258.0	0.00
$\phi(\sim \text{length})p(\sim 1)$	3	259.4	1.41
$\phi(\sim \text{sex})p(\sim 1)$	3	260.0	2.02
$\phi(\sim \text{sex} \times \text{length})p(\sim 1)$	5	260.6	2.59
$\phi(\sim \text{sex} + \text{length})p(\sim 1)$	4	261.5	3.42
$\phi(\sim 1)p(\sim \text{time})$	4	261.5	3.50
$\phi(\sim \text{length})p(\sim \text{time})$	5	263.3	5.29
$\phi(\sim \text{sex})p(\sim \text{time})$	5	263.6	5.58
$\phi(\sim \text{sex} \times \text{length})p(\sim \text{time})$	7	264.6	6.57
$\phi(\sim \text{sex} + \text{length})p(\sim \text{time})$	6	265.4	7.39

3.3.4   Network Analysis

Networks are mathematical objects consisting of nodes connected by edges (Dale and Fortin, 2010). They can be used to study animal movement by analysing the relationships between nodes, which can represent receivers or tagged animals separately (unipartite graphs; e.g. Jacoby et al. 2012) or simultaneously in the same graph (bipartite graphs; e.g. Finn et al. 2014). To study movement, nodes are often specified as the stationary receivers and edges represent either the directed or undirected movements of animals between receivers. Social aggregations can also be studied when the animals are treated as nodes, e.g. by testing whether there exist preferred associations among individuals (Stehfast et al., 2013). A network's response variable is an adjacency matrix, which describes the connections between pairs of nodes (Farine and Whitehead, 2015). For example, the adjacency matrix

$$
\begin{array}{c c c c}
 & R1 & R2 & R3 \\
R1 & \begin{pmatrix} 0 & 0 & 0 \\ R2 & 0 & 0 & 3 \\ R3 & 0 & 0 & 4 \end{pmatrix}
\end{array}
\tag{3.9}
$$

describes a system of three receivers ($R1$, $R2$, and $R3$), where three movements were recorded from $R2$ to $R3$ and four records indicate animals staying at $R3$. Adjacency matrices for null networks can also be of interest, e.g. to document potential direct routes among receivers. For the above example, the following null network

$$
\begin{array}{c c c c}
 & R1 & R2 & R3 \\
R1 & \begin{pmatrix} 1 & 1 & 0 \\ R2 & 1 & 1 & 1 \\ R3 & 0 & 1 & 1 \end{pmatrix}
\end{array}
\tag{3.10}
$$

indicates that movements are possible between all pairs of receivers except from $R1$ to $R3$ in either direction. Once the adjacency matrix is defined, visuals and metrics can be calculated that describe the network connectivity (Dale and Fortin, 2010). For example, the node degree is the number of incoming and outgoing edges of a node, which describes the amount of traffic through a receiver and therefore may indicate areas of importance (Jacoby et al., 2012; Farine and Whitehead, 2015), whereas edge density is the fraction of observed edges to all theoretically possible edges, and can help indicate the amount of random/non-random movement (Jacoby et al., 2012).

Network metrics can be compared amongst groups, e.g. to determine sex-specific differences in movement (Jacoby et al., 2012) or preferred areas (Stehfast et al., 2015). When the groups are not necessarily known *a priori*, community detection algorithms can be used to identify groups of receivers or animals that are closely related, for example to identify home ranges (Finn et al., 2014). If an observed network can be classified as a theoretical network pattern, then known properties can be interpreted (e.g. Fox and Bellwood 2014). Finally, disrupting the networks by removing nodes and studying the subsequent network fragmentation can help to assess the effects of habitat disruption (Jacoby et al., 2012) and the protective capabilities of potential marine reserves (Espinoza et al., 2015).

Direct hypothesis testing on network measures is possible using GLMMs, but the assumption of independence may be violated (Farine and Whitehead, 2015). Permutation and randomization techniques provide non-parametric methods for hypothesis testing by comparing an observed statistic to those calculated from randomly generated networks (Dale and Fortin, 2010), and have been used to assess whether animals are moving randomly (Espinoza et al., 2015). In addition, networks can be compared to each other or other dyadic variables using a Mantel test which assesses the correlation between two matrices (Urban et al., 2009; Farine and Whitehead, 2015), e.g. to test whether yellowfin tuna (*Thunnus albacares*) social associations are related to pre-defined cohorts (Stehfast et al., 2013). Relationships between networks and more than one covariate can be evaluated using the multiple regression quadratic assignment procedure (Farine and Whitehead, 2015), which has been used to assess the
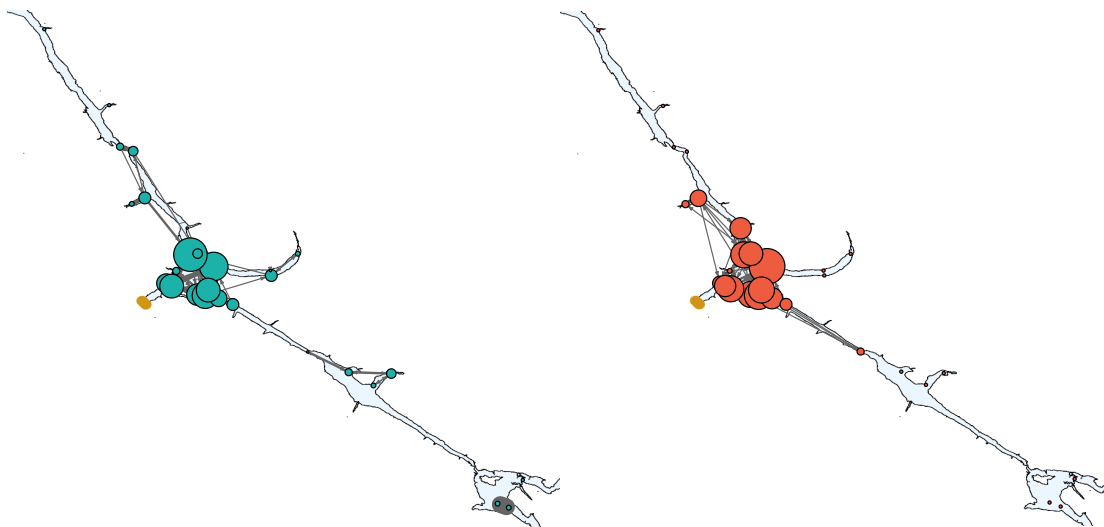
Figure 3.2: Sex-specific results from applying network analysis to the illustrative dataset. Yellow represents the position of the dam. Circles denote the receiver positions, and are weighted based on their node degree, i.e. the number of incoming and outgoing edges of a node. Edges are weighted based on the number of directed bull trout movements between receivers. Males are on the left (green), and females are on the right (orange).

effect of environmental variables on small-spotted catshark (*Scyliorhinus canicula*) movements (Jacoby et al., 2012).

We applied network analysis to the bull trout dataset (Figure 3.2) after summarizing detection data into directed movements between pairs of receivers. Using the R package `igraph` (Csárdi and Nepusz, 2006) and treating the receivers as nodes, we plotted a network for each sex making the size of each node proportional to its degree and using weighted edges to represent the number of directed movements between nodes. These networks suggest that the main pool of the reservoir experiences more fish traffic compared to either of the reaches, and therefore likely contains important bull trout overwintering habitat. In addition, a Mantel test between the two networks suggested a weak but statistically significant (r = 0.17, p < 0.05) correlation

in movement patterns between the males and females.

3.4 Future Directions

3.4.1 Gaussian Random Fields

Gaussian random fields (GRFs) are a promising approach for analyzing detection data within a spatial context. Specifically, GRFs estimate the residual spatial correlation remaining after accounting for measured explanatory variables (Thorson and Minto, 2015). In fisheries, they have been used to model the spatial dependence of population processes and to understand the relationship between fish distribution and habitat (Thorson and Minto, 2015; Thorson et al., 2015; Carson et al., 2017). With telemetry data, GRFs have been used to show how the number of at-sea seal encounters co-varied with bathymetry and distance to the seal haul-out site (Carson and Mills Flemming, 2014). In that study, the receiver locations changed through time; here, we demonstrate the potential of GRFs for detection data collected at fixed locations by investigating whether the presence of the dam affects bull trout distribution using the illustrative dataset. Because the GRF is a flexible hierarchical model, these data could have been modeled in several different ways. For example, we could have: modeled the duration or number of detections (e.g. Carson and Mills Flemming 2014); accounted for false absences by using a zero-inflated distribution (e.g. Cosandey-Godin et al. 2015); or used a state-space model to account for technological error (e.g. Thorson et al. 2015).

We assumed that the number of individuals y_s detected at a given receiver location

s (of which there are n) was Poisson distributed:

$$y_s \sim \text{Poisson}(\lambda_s). \tag{3.11}$$

We linked the mean of the distribution, λ_s, to the linear predictor, η_s, through a log-link function:

$$\log(\lambda_s) = \eta_s. \tag{3.12}$$

In turn, η_s was related to the distance between the receiver and the dam through the linear equation:

$$\eta_s = \beta_0 + \beta_1 x_s + \xi_s, \tag{3.13}$$

where β_0 represents the log of the number of detections expected when the distance to the dam (x_s) and the spatial random effect (ξ_s) both have no effect, and β_1 is the regression coefficient for x_s. The random effect ξ_s accounts for the effect of unknown spatial factors influencing the response and we model it as a GRF, meaning that for any $\xi_s \in D \subset \mathbb{R}^2$, where D is the domain, we let $\boldsymbol{\xi} = (\xi_1, ..., \xi_n)^T$ be distributed as a multivariate normal:

$$\boldsymbol{\xi} \sim \text{MVN}(0, \boldsymbol{\Sigma}). \tag{3.14}$$

Here, $\boldsymbol{\Sigma}$ is a $n \times n$ covariance matrix where the (i, j)th element of $\boldsymbol{\Sigma}$ is defined by the

Matérn covariance structure, which for $i \neq j$ is defined as:

$$\mathrm{Cov}[\xi_i, \xi_j] = \frac{\sigma^2}{\Gamma(\nu)2^{\nu-1}}(\kappa h_{i,j})^\nu K_\nu(\kappa h_{i,j}) \tag{3.15}$$

where K_ν is a modified Bessel function of the second kind, $h_{i,j}$ is the Euclidean distance between receiver locations s_i and s_j, the smoothness parameter ν is set equal to 1, and the spatial scale κ and marginal variance σ^2 are both estimated. As in (Thorson et al., 2015), we used `R-INLA` (Illian et al., 2012) to simplify model implementation with stochastic partial differential equations (SPDEs) and we used `TMB` (Kristensen et al., 2016) to estimate the model parameters.

Model fitting resulted in parameter estimates of $\beta_0 = 2.42$ (95% CI: 1.73-3.12) and $\beta_1 = -0.042$ (95% CI: -0.063 to -0.022), indicating that as distance to the dam increased the number of individuals detected decreased. This may result in part because the distance from the dam increases proportional to the distance from the main lacustrine habitat for most locations within the reservoir. In addition, the spatial correlation of the GRF accounts for some of the bull trout distribution not explained by distance from the dam (Figure 3.3).

3.4.2 Accounting for Spatial Correlation and Measurement Error

We expect that methods for estimating spatial correlation associated with animal movement will grow in popularity as receiver coverage and method documentation continue to expand. While we proposed the GRF as a flexible method for modelling animal movement data with a spatial component, other spatial methods exist that
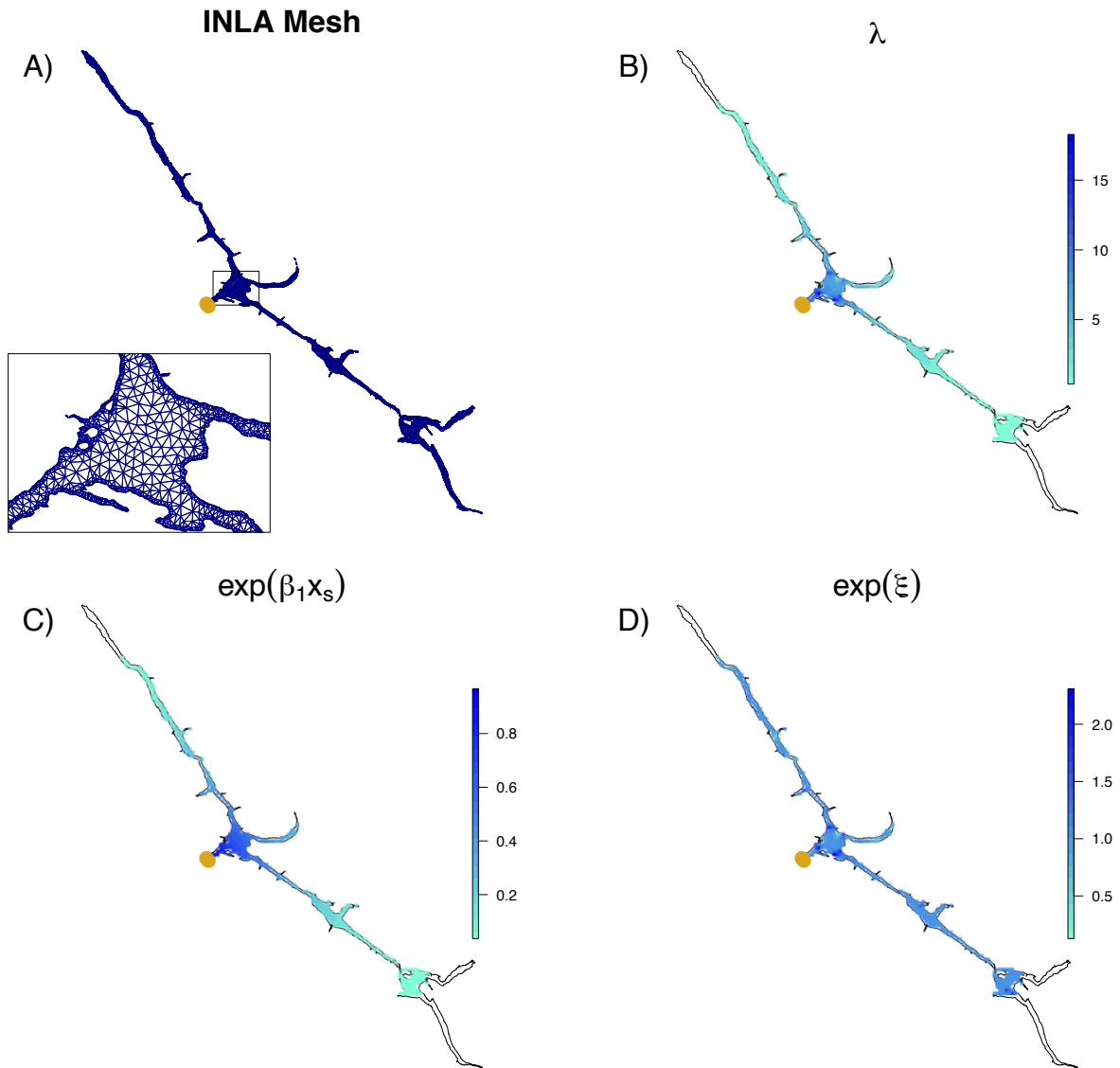
Figure 3.3: Results from the GRF analysis on the illustrative dataset. (a) shows the mesh calculated by the INLA SPDE; (b) represents the expected number of bull trout across the reservoir returned by the full model; (c) represents the expected number of fish as influenced by distance from the dam; and (d) represents the expected number of fish based on the effect of the GRF only. Yellow represents the position of the dam.

could be applied to detection data. For example, one terrestrial study used a spatial (and temporal) correlation structure within a GLMM to assess the factors affecting home range size of radio-tracked roe deer (*Capreolus capreolus*; although home range in this case was calculated from spatially continuous detection data, similar principles would apply to responses calculated from discrete detection data; (Börger et al., 2006)). Network autocorrelation models (Leenders, 2002) could be used to estimate the correlation between network attributes caused by receiver location. In addition, spatial capture–recapture models are a spatial extension of mark-recapture models, and are well established in terrestrial studies with encounter data like those generated by camera trapping (Royle et al., 2014). These models involve hierarchical modelling of a spatial point process of unobserved animal activity centres and a detection probability function depending on distance from the activity centres (Efford and Fewster, 2013). Despite similarities with terrestrial encounter data, we have seen few studies that apply spatial capture–recapture methods to aquatic detection data, but see Raabe et al. (2014), who studied the survival and movement of PIT-tagged American shad (*Alosa sapidissima*) using these methods.

Many studies have investigated the measurement error of aquatic tracking technology by estimating the detection efficiency (the frequency with which a receiver will detect a fish within its given range; Simpfendorfer et al. 2008), detection range (the probability of detection given distance from a receiver; Kessel et al. 2014b), or the frequency of false detections (when a receiver logs a false ID or detects an absent animal; Heupel et al. 2006). However, few studies incorporate this information into

their biological inferences. Those that do may use it to pre-process their data (e.g. Hoenner et al. 2018; Kessel et al. 2014a), or directly incorporate measurement error into the statistical method (Pedersen and Weng, 2013; Simpfendorfer et al., 2008; Winton et al., 2018). Measurement error can additionally be used to help numerically optimize the spatiotemporal design of a receiver array before deployment, resulting in a study design with enhanced ability to acquire high-quality data (Pedersen et al., 2014).

State-space models are hierarchical models that can pair a measurement equation with a model for animal movement, and simultaneously estimate both processes (Auger-Méthé et al., 2017). Two notable examples with detection data include: (a) a non-parametric function for detection probability paired with an Ornstein–Uhlenbeck movement process to estimate the home range of a humphead wrasse (*Cheilinus undulatus*; Pedersen and Weng 2013); and (b) a Gaussian decay measurement equation coupled with a binomial spatial point process to estimate centres of activity of a black sea bass (*Centropristis striata*; Winton et al. 2018). State-space models have gained popularity for analyzing spatially continuous animal movement data, likely because of their flexibility — multiple measurement error distributions can be included and matched specifically to the tracking technology (e.g. Winship et al. 2012), and the movement process can range from individual models of movement (e.g. Auger-Méthé et al. 2017) to GRFs (e.g. Thorson et al. 2015). We believe that state-space models could provide a framework that improves the reliability of statistical analyses of detection data.

3.5 Broadening the Scope of Animal Movement Analyses

Telemetry technology will continue to improve technically in ways that will increase study longevity, target more species or life stages, and expand the scope of data collection (Lennox et al., 2017a). Study designs will also evolve, as auxiliary biological and environmental variables are collected during sampling or independently, and as telemetry networks facilitate the sharing of resources and multi-species data (Lennox et al., 2017a). As a result, telemetry studies will have the potential to generate massive, interdisciplinary datasets, and statistical methods for analysing such complex data will have to adapt appropriately. In the future, movement ecologists may look to the burgeoning research field of human mobility, which has exploded since the advent of the smartphone with GPS tracking and geolocated social media postings (Thums et al., 2018). Because humans and non-human animals appear to conform to similar ecological principles, e.g. site fidelity, aggregation, and sociality (Meekan et al., 2017), movement ecologists will have the opportunity to readily appropriate big data approaches from human mobility studies (Thums et al., 2018).

3.6 Discussion

To aid researchers in matching a statistical method to their data and study objective, we devised a decision tree which we present in Figure 3.4. We recognize that accounting for every possible study design would be unrealistic, therefore we suggest that researchers utilize our decision tree as a first general guide through some of the possible statistical methods, not an exhaustive instruction catalog. We hope
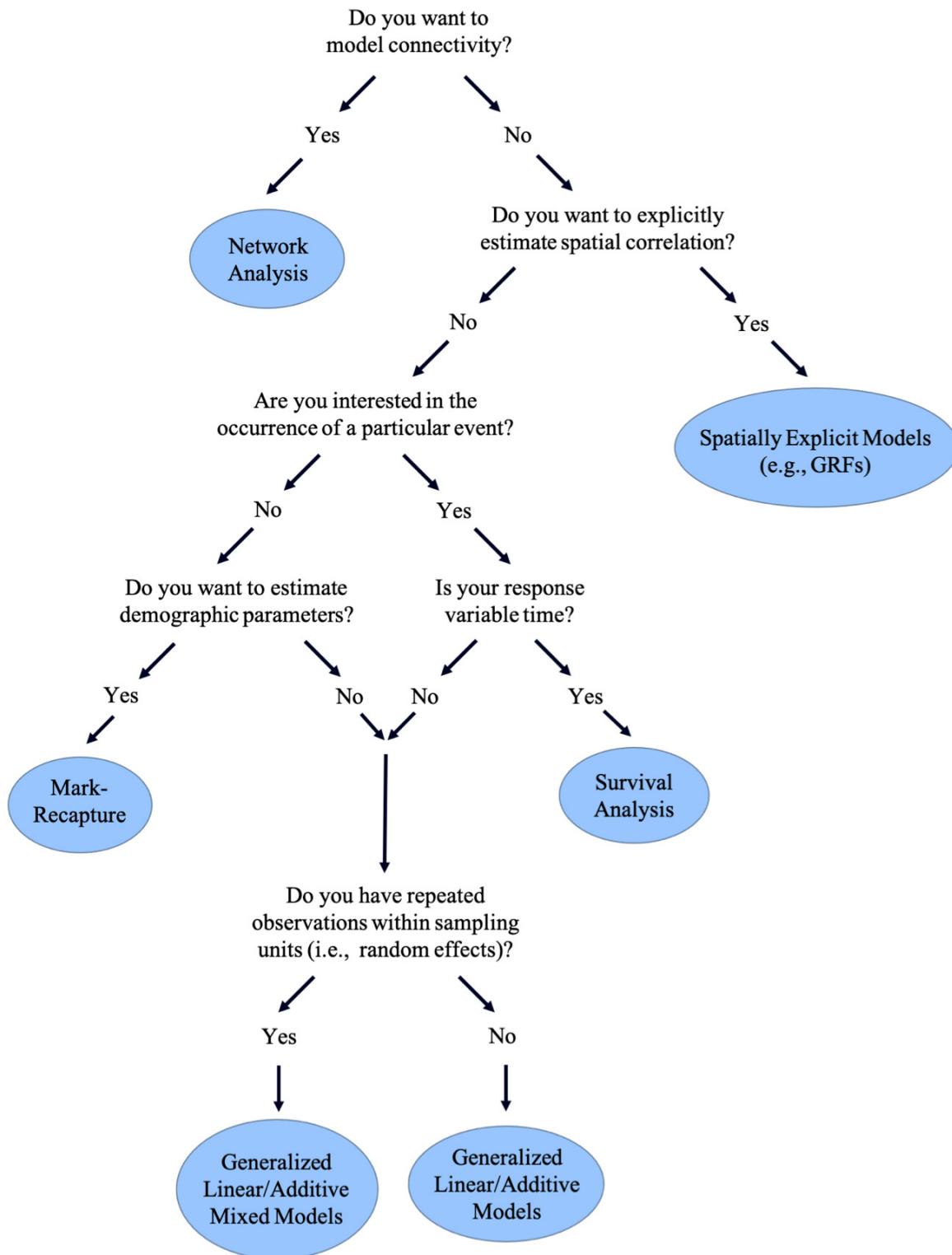
Figure 3.4: Decision tree for identifying appropriate statistical methodologies for analyzing detection data collected by acoustic, radio, or PIT telemetry

that a tree will help researchers narrow their selection, but then we strongly suggest that this is followed by comprehensive study of the chosen method(s), and its(their) accompanying assumptions. To that end, we summarize our guide below.

We suggest using mark-recapture methods when studying population dynamics, especially when the detection ability of the array is suspect. However, note that the most commonly used mark-recapture method, the Cormack–Jolly–Seber model, is dependent upon the following assumptions: (a) tags are not lost and do not fail; (b) survival is not influenced by the tag or tagging procedure; and (c) survival and detection probability do not vary among tagged animals. Preliminary laboratory studies assessing tag attachment and retention can help to determine the risk of tag loss or failure (Holbrook et al., 2013). Holding studies can be used to assess whether tagging influences survival (Furey et al., 2016); however, tagging may negatively affect multiple traits in a cumulative way such that the full influence is not understood by assessing the effect on survival alone (Bodey et al., 2018). In fact, tagging can affect traits like growth, swimming performance, and social interactions (Jepsen et al., 2015), and these potential effects should be carefully considered in any analysis. Finally, some of the factors affecting individual variation in survival and detection (e.g. sex, age) can be incorporated into the Cormack–Jolly–Seber model through stratification or regression analysis (Williams et al., 2001).

To understand the occurrence of an event when temporal records for the event exist, consider using survival analysis. Survival analysis can be used to understand the survival of tagged animals; however, it is distinguishable from mark-recapture via

their response variables. Survival analysis requires a temporal value for the response (e.g. $y = 12$ hr), whereas mark-recapture uses a discrete time series (e.g. 1001101), and time is often incorporated by allowing probabilities to be dynamic. Although a temporal response can also be modelled using GLMs/GLMMs/GAMs/GAMMs, survival analysis can account for the fact that for some study animals it may not be possible to determine whether they experience the event (censoring). Censoring is appropriate as long as the probability of being censored is independent of the probability of the event (Harrell, 2015).

To describe the connectivity among receiver locations or tagged animals, we encourage the use of network analysis which provides easily interpretable visualizations of this connectivity. However, network analysis does assume that all of the nodes of a system are represented in the graph (Dale and Fortin, 2010) and is therefore more useful for datasets collected by many receivers/individuals. Nodes and edges must be carefully defined in order to accurately represent the study system; any deviations from the true network, for example through data transformation, inclusion of false absences, or exclusion of individuals, can significantly impact network measures and the overall network structure (Farine and Whitehead, 2015).

If spatial correlation is of interest then researchers should use spatially explicit methods like GRFs. It is possible to incorporate spatial information into some of the other statistical methods we have described. For example, with network analysis

a receiver node can include a location, and with regression-type analyses (e.g. Cormack–Jolly–Seber models or GLMs) spatial references can be incorporated as covariates. However, spatial models are distinguishable from these methods because they estimate spatial correlation, which when ignored can invalidate analyses by violating the assumption of independence (Thorson and Minto, 2015). In addition, estimating spatial correlation can show how unobserved/unmeasured variables correlated in space affect the response variable (Carson and Mills Flemming, 2014; Thorson et al., 2015). Network autocorrelation models, spatial capture–recapture, or spatial generalized models (not reviewed here; see Zuur et al. 2009) can also be used to estimate spatial correlation.

Finally, for most other scenarios, we recommend using GLMs/ GLMMs or GAMs/ GAMMs. Generalized modelling is arguably the most accessible statistical method presented in this paper in terms of documentation and application. It is also flexible, as several different response variables can be used, both linear and nonlinear covariate relationships are possible, and random effects and correlative structures can be included (Zuur et al., 2017). However, these methods come with their own assumptions (e.g. distribution assumptions of the residuals) and complexities, therefore we would encourage readers to consult more specific guides (e.g. Bolker et al. 2009) before implementation.

3.7 Conclusion

Telemetry is increasingly used to track aquatic animals. This has led to a massive expansion in the volume and detail of ensuing movement data, and significant growth in the availability of suitable statistical methods. It is often no longer sufficient to rely on relatively simple descriptive analytical techniques, yet choosing from among available methods can be daunting. We reviewed advanced statistical methods useful for detection data in order to introduce them to aquatic telemetry users and provide researchers with the tools necessary for more comprehensive detection data analysis. We focused specifically on detection data recorded in aquatic environments, which can differ in small but substantial ways from those collected in terrestrial studies. For example, the camera traps often used in terrestrial studies can detect previously unknown/unmarked individuals, whereas acoustic, radio, and PIT receivers can only identify tagged individuals, thus hindering our ability to estimate population size from these data using mark-recapture methods. However, some of the methods mentioned here (e.g. spatially explicit capture-recapture) have been established in terrestrial studies for 10+ years, and minor modifications could significantly enhance the analysis of aquatic detection data. Going forward, we recommend that aquatic ecologists look towards terrestrial studies and other fields like human mobility to help motivate the statistical advances that will be needed to analyse detection datasets that are rapidly growing in both size and complexity.

Chapter 4

Concurrent Prediction of Location and Behavioural States Reveals Colony-Specific Foraging Tactics of Adult Female Grey Seals

4.1 Introduction

Telemetry and archival data-logging devices are frequently used to record the movements of free-ranging animals through time. However, data collected from marine environments are often imperfect because of measurement errors associated with the telemetry technology. As a result, early telemetry studies often used filters to remove erroneous locations and then the corrected data were used to describe where the study individuals went and for how long. Now, advanced statistical modelling can account for some of the technological error, and the corrected location data can be combined with other information to study complex ecological processes like sociality (Scharf et al., 2016), niche partitioning (Dwyer et al., 2020), species distribution shifts (Hazen et al., 2013), and foraging behaviour (Breed et al., 2009). To this end, inferring the underlying motivations that manifest in movement is often of great interest and can better inform our understanding of life history strategies and behaviours critical to survival such as foraging and reproductive performance.

69

How foraging behaviour impacts fitness is frequently explored within movement ecology frameworks (e.g., Arthur et al. 2015). In pinnipeds, intraspecific variability in foraging can result from a variety of factors or processes, including geographic distribution and niche partitioning (Breed et al., 2013; Wilson et al., 2015; Dmitrieva et al., 2016). Geography often plays a key role in the decision of where to forage because locations will have different characteristics, e.g., oceanographic conditions and biological productivity, that will influence prey species composition and abundance (Nowak et al., 2020) and the presence of predators (Moxley et al., 2020). Intraspecific niche partitioning may also play a role by reducing competition for local resources. This kind of competition is likely exacerbated in pinnipeds because many species are central-place foragers that compete for resources within the vicinity of the breeding colony (Breed et al., 2013; Wilson et al., 2015). Niche partitioning may manifest when individuals spatially segregate within geographic locations, as is seen in the Caspian seal (*Pusa caspica*; Dmitrieva et al. 2016) and the grey seal (*Halichoerus grypus*; Breed et al. 2006), or by depth in the water column, as has been documented in the Galapagos sea lion (*Zalophus wollebaeki*; Villegas-Amtmann et al. 2013) and the harbour seal (*Phoca vitulina*; Wilson et al. 2015). It may also be expressed by differential prey selection (Beck et al., 2007), temporal segregation over a shared space (Field et al., 2005), or a combination of the above factors (Field et al., 2005; Newland et al., 2009). Discriminating among the factors that drive intraspecific variability in foraging behaviour can be difficult. One approach is to test the differences in foraging

distribution and behaviour of geographically separated breeding colonies under the assumption that differences arise in response to variability in the nature and availability of resources (Robson et al., 2004; Heerah et al., 2017). To achieve this, accurate estimates of location are necessary.

State-space models (SSMs) and hidden Markov models (HMMs) are two statistical tools commonly used to account for measurement error associated with locations derived from telemetry tags and to infer underlying motivators (e.g., foraging) of animal movement. Both methods are hierarchical models for a time series of observations (here, two-dimensional locations) that are dependent upon a set of unobserved random variables (also known as random effects). The term "SSM" is frequently used when measurement error from the data-collection process is stochastically modelled such that the random effects constitute true locations (Auger-Méthé et al., 2020). The term "HMM" is typically used when the data are measured with negligible error, but are assumed to be dependent on a set of discrete random effects that can be predicted for each observation and used to infer animal behaviour (hereafter: behavioural states; Langrock et al. 2012). A model that incorporates both levels of random effects, i.e., one that predicts both true locations and behavioural states, has been referred to as a SSM or switching SSM (Jonsen et al., 2005; Auger-Méthé et al., 2020). Here for clarity (see Section 4.3.2), we refer to such a movement model as a switching hierarchical model (SHM), and reserve the terms SSM and HMM for models that predict only one set of random effects, either location states or behavioural states, respectively.

Although separately fitting either SSMs or HMMs to animal tracks can be achieved via closed form solutions, e.g., the Kalman filter (Johnson et al., 2008) or the forward algorithm (Zucchini et al., 2016), or via accurate approximation methods (Albertsen et al., 2015), simultaneously predicting real-valued location states and integer-valued behavioural states is a non-trivial problem for which solutions are desired because many researchers collect error-prone movement data. Bayesian statistics can be used (Jonsen et al., 2005; Michelot and Blackwell, 2019), as well as multiple imputation and pooling of results (McClintock and Michelot, 2018). Alternatively, the combination of Laplace's method to approximate marginal likelihoods and Automatic Differentiation to calculate numerical derivatives as implemented through the R package Template Model Builder (`TMB`) has proven to be a useful tool for analyzing animal movement data (e.g., Albertsen et al. 2015; Lawler et al. 2019; Jonsen et al. 2020) that can produce accurate results comparable to well-established Bayesian methods while using a fraction of the computing time (Auger-Méthé et al., 2017; Whoriskey et al., 2017). Although both SSMs and HMMs are individually well developed within the `TMB` platform, a combined hierarchical model is not. Such a model would provide ecologists with a highly efficient tool to study movement based on error-prone tracking data that 1) avoids the specification of priors, thus removing subjective choices; 2) frees up computational resources for reallocation towards analyzing larger datasets or incorporation of additional model complexity; and 3) utilizes a single likelihood function such that errors in both the location and behavioural state processes can be simultaneously estimated.

In this paper, we provide this tool by developing a framework for fitting switching hierarchical models to animal movement data within the TMB platform. Our framework relies on the key result that the maximum likelihood estimates of a set of parameters of interest can be found by optimizing the likelihood while holding the remaining parameters fixed at their maximum likelihood estimates (Patefield, 1977). We demonstrate the efficacy of our framework by analyzing 67 satellite tracks from grey seals of multiple colonies in the Northwest Atlantic to infer foraging behaviour, and illustrate its accuracy through parametric bootstrap simulation studies. Previous research on this population suggests among-colony variability in diet. For example, stomach samples analyzed from inshore and offshore grey seals in Eastern Canada by Bowen et al. (1993) indicated that although the types of prey species present overlapped, their relative compositions varied. Other research suggests similarities in foraging decisions, e.g., Harvey et al. (2012) documented some geographic overlap in foraging areas among Sable Island and Gulf of St. Lawrence seals. Although the factors underlying variability in grey seal foraging tactics have been studied within colonies, among-colony differences have not been broadly examined.

4.2 Study System and Data Collection

Grey seals are generalist predators that exploit a broad foraging range of coastal and offshore habitats from Nantucket sound, Massachusetts, to the southern coast of Labrador in the Northwest Atlantic (Bowen and Harrison, 2006; Breed et al., 2006). The total population size in Eastern Canada has been increasing for more than 50
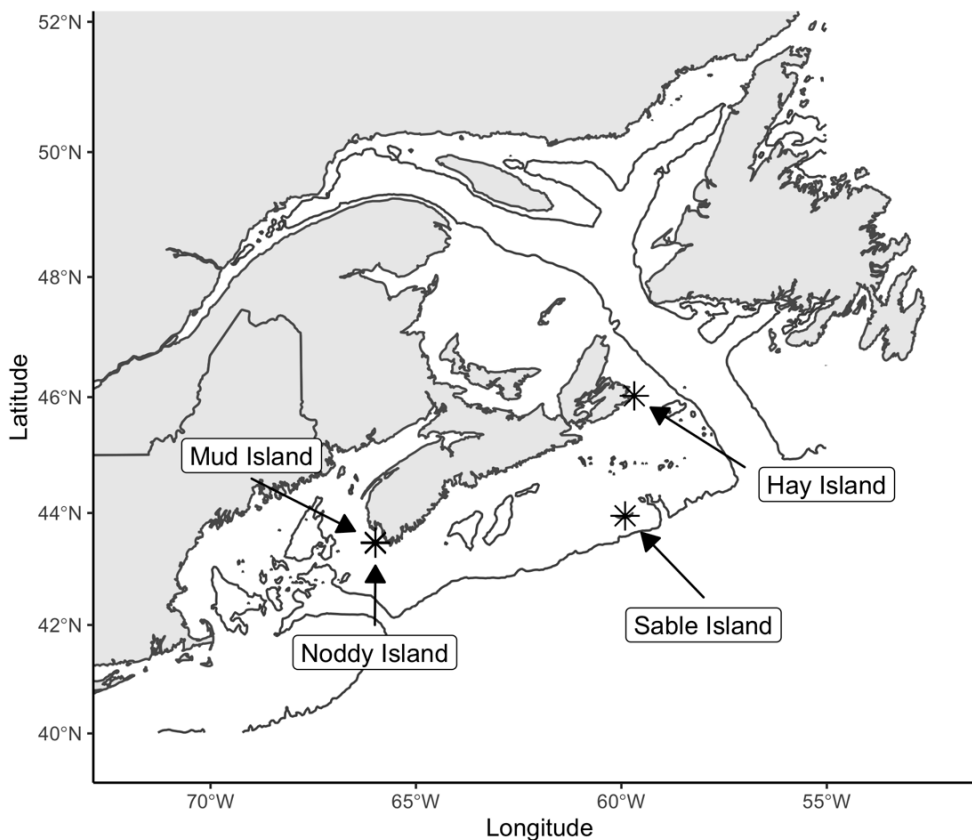
Figure 4.1: Study area where grey seals from four breeding colonies were tagged in Nova Scotia, Canada. Solid black lines denote the 200m isobath.

years and was estimated in 2016 to be 424,300 (Hammill et al., 2017). It includes three breeding components located in the southern Gulf of St. Lawrence (10 breeding colonies), on coastal Nova Scotia (7 breeding colonies), or at Sable Island, Nova Scotia (a single and the largest breeding colony; Hammill et al. 2017; den Heyer et al. 2020). Females give birth from December to the end of January. They are considered capital breeders because they fast during lactation and rely on body energy stores accumulated during the months prior to parturition to fuel their metabolism and milk production (Iverson et al., 1993). Lactation lasts 16-18 days and results in a dramatic transfer of energy, with pups nearly tripling in size and females losing up

to 40% of their body mass (Mellish et al., 1999). As a result, foraging is critically important for females during the post-breeding season, when energy stores of the adult female are severely depleted and she must prepare for delayed implantation and foetal development (Beck et al., 2003a, 2007).

Betweeen 2003 and 2018, adult female grey seals were captured, anaesthetized with Telazol, and tagged with satellite trackers (a combination of Wildlife Computers Mk10, SPOT, and SPLASH tags, as well as Sea Mammal Research Unit SRDL 7000 tags and Telonics ST-18 tags) that were affixed to the top of the individuals' heads with 5 min epoxy and programmed to transmit every 15 mins. Further details on the standard tagging procedures used can be found in Breed et al. (2009) and Nowak et al. (2020). Individuals were tagged near the end of lactation (mid to end of January), and these tags were expected to remain with the seal until the spring moult (approximately May-June). Study individuals were randomly selected from females who had successfully raised a stage three pup (the stage immediately preceding weaning). Females varied in age from newly matured to older individuals (Table 4.1). The tagging sites consisted of four breeding colonies (Fig 4.1): Sable Island (43 tagged individuals), Hay Island (14 individuals) and two colonies Mud (one individual) and Noddy Island (nine individuals) grouped into one referred to as the Southwest colony. The Sable Island colony is 493 and 231 km (great circle distance) from the Southwest and Hay colonies, respectively, whereas the Southwest and Hay colonies are themselves separated by 573 km. The distances among these colonies are well within the observed foraging range of adult female grey seals (e.g., Fig 3 of

Table 4.1: Tagging metadata for the 67 post-breeding female grey seals analyzed with a switching hierarchical model

Year	Island	Age < 15	$15 \leq$ Age < 30	$30 \leq$ Age	Total Tagged
2003	Sable	1	3	3	7
2004	Sable	1	2	0	3
2007	Sable	1	1	1	3
2011	Hay	2	2	0	4
2012	Hay	1	8	1	10
2016	Mud	7	1	1	9
2017	Noddy	1	0	0	1
2018	Sable	0	18	12	30

Breed et al. 2009 and Fig 2 of Nowak et al. 2020).

4.3 Methodological Development

4.3.1 The Movement Model

Our model is adapted from the DCRWS first presented in Jonsen et al. (2005). It is a hierarchical model defined by three conditional distributions that we refer to as the measurement, movement, and behaviour processes:

$$\text{Measurement Process} \quad \mathbf{y}_t = (1 - j_t)\mathbf{x}_{i-1} + j_t\mathbf{x}_i + \boldsymbol{\eta}_t \tag{4.1}$$

$$\text{Movement Process} \quad \mathbf{x}_i = \mathbf{x}_{i-1} + \gamma_{b_i}\mathbf{T}(\theta_{b_i})(\mathbf{x}_{i-1} - \mathbf{x}_{i-2}) + \boldsymbol{\epsilon}_i \tag{4.2}$$

$$\text{Behaviour Process} \quad b_i \sim cat(\boldsymbol{\phi}_{b_{i-1}}) \tag{4.3}$$

We observe a set of T multidimensional, irregularly sampled, locations $\mathbf{y}_{1:T}$ from a stochastic process $\mathbf{Y}_{1:T}$ ordered in time t. These observations are measured with error, here denoted by $\boldsymbol{\eta}_t$, which can take on one of two distributions. If the data are

derived from Argos technology, we model them with a generalized t-distribution that has a unique scale and degrees of freedom for each Argos class that are assumed to be known, and an unknown and estimated inflation parameter ψ multiplied by the scale that is kept constant across all classes (Auger-Méthé et al., 2017). If the data are GPS, then $\boldsymbol{\eta}_t$ becomes a zero-mean Gaussian distribution with a diagonal covariance matrix with entries ω_{lon} and ω_{lat}. We let $\mathbf{x}_{1:N}$ be the N unobserved true locations (location states) that we wish to predict from the observed $\mathbf{y}_{1:T}$. It is not necessary for $N = T$; the observed locations are related to the unobserved through a linear interpolation according to the j_t, which is the proportion of time elapsed between the observation $\mathbf{y}_t$ and the true (interpolated) locations $\mathbf{x}_{i-1}$ and $\mathbf{x}_i$. We assume that the $\mathbf{x}_{1:N}$, ordered in regular time i, follow a second order Markov process $\mathbf{X}_{1:T}$, governed by a turning angle θ_{b_i}, autocorrelation parameter γ_{b_i}, and zero-mean Gaussian error term $\boldsymbol{\epsilon}_i$. The covariance matrix of $\boldsymbol{\epsilon}_i$ is diagonal, with elements $\sigma_{lon}, \sigma_{lat} > 0$ that represent the process error in longitude and latitude. The parameters θ_{b_i} and γ_{b_i} are dependent on a set of discrete random effects $b_{1:N}$ that can be interpreted as representative of different behaviours that drive the movement process (behavioural states). The $b_{1:N}$ are assumed to follow a Markov process $B_{1:N}$ with parameters $\boldsymbol{\phi}_{b_{i-1}}$. Collectively, we denote all parameters associated with the measurement $\{\psi, \ \omega_{lon}, \ \omega_{lat}\}$, movement $\{\theta_{b_i}, \ \gamma_{b_i}, \ \sigma_{lon}, \ \sigma_{lat}\}$, and behaviour $\{\phi_{b_{i-1}}\}$ processes as Ψ, Θ, and Φ, respectively.

4.3.2　The Iteration

The joint likelihood L in this scenario is:

$$L_{\mathbf{y}_{1:T},\mathbf{x}_{1:N},b_{1:N}}(\Psi,\Theta,\Phi) = f(\mathbf{y}_{1:T},\mathbf{x}_{1:N},b_{1:N} \mid \Psi,\Theta,\Phi). \qquad (4.4)$$

We need to optimize the marginal likelihood,

$$L_{\mathbf{y}_{1:T}}(\Psi,\Theta,\Phi) = \int_{\mathbf{x}_{1:N}} \sum_{b_{1:N}} L_{\mathbf{y}_{1:T},\mathbf{x}_{1:N},b_{1:N}}(\Psi,\Theta,\Phi)\, \mathrm{d}\mathbf{x}_{1:N}. \qquad (4.5)$$

Taking advantage of the hierarchy, we can re-express the marginal as a product of its conditionals

$$L_{\mathbf{y}_{1:T}}(\Psi,\Theta,\Phi) = \int_{\mathbf{x}_{1:N}} \sum_{b_{1:N}} f(\mathbf{y}_{1:T}|\mathbf{x}_{1:N},\Psi) f(\mathbf{x}_{1:N}|b_{1:N},\Theta) f(b_{1:N}|\Phi)\, \mathrm{d}\mathbf{x}_{1:N} \qquad (4.6)$$

$$= \int_{\mathbf{x}_{1:N}} f(\mathbf{y}_{1:T}|\mathbf{x}_{1:N},\Psi) \left(\sum_{b_{1:N}} f(\mathbf{x}_{1:N}|b_{1:N},\Theta) f(b_{1:N}|\Phi) \right) \mathrm{d}\mathbf{x}_{1:N}. \qquad (4.7)$$

In theory we could calculate this marginal by approximating the integral over $\mathbf{x}_{1:N}$ with Laplace's method. In practice, numerical optimization of models with large numbers of both discrete and continuous-valued random effects is infeasible (Altman, 2007; McKellar et al., 2015).

Instead, we choose to optimize this function iteratively. Patefield (1977) notes that for parameters of interest $\{\Theta,\Phi\}$ and nuisance parameters Ψ, the curvature of the full likelihood is preserved by the maximized likelihood function $MaxL(\cdot)$. Denoting all

maximum likelihood estimates with a circumflex (hat), the $MaxL(\cdot)$ for our scenario
might look like:

$$MaxL(\Theta, \Phi) = \sup_{\Psi} L(\Psi, \Theta, \Phi) = L(\hat{\Psi}(\Theta, \Phi), \Theta, \Phi). \tag{4.8}$$

This means that, if we can find the maximum likelihood estimates of Ψ (the measure-
ment error parameters), say $\hat{\Psi}$, then we can find the maximum likelihood estimates
of $\{\Theta, \Phi\}$ (the movement and behaviour parameters), as well as their standard errors
from the Hessian matrix, by holding Ψ fixed at $\hat{\Psi}$. Furthermore, by strategically fixing
sets of parameters and random effects such that certain terms reduce to constants,
we can take advantage of well-established HMM and SSM likelihood frameworks.

First, by fixing $\mathbf{x} = \hat{\mathbf{x}}$ and $\Psi = \hat{\Psi}$, the likelihood reduces to an HMM (Zucchini
et al., 2016):

$$L_{HMM}(\hat{\Psi}, \Theta, \Phi) = \sum_{b_{1:N}} f(\mathbf{y}_{1:T}|\hat{\mathbf{x}}_{1:N}, \hat{\Psi}) f(\hat{\mathbf{x}}_{1:N}|b_{1:N}, \Theta) f(b_{1:N}|\Phi) \tag{4.9}$$

$$= c \sum_{b_{1:N}} f(\hat{\mathbf{x}}_{1:N}|b_{1:N}, \Theta) f(b_{1:N}|\Phi) \tag{4.10}$$

$$= c\boldsymbol{\delta}'\mathbf{P}(\hat{\mathbf{x}}_2)\mathbf{A}\mathbf{P}(\hat{\mathbf{x}}_3)\cdots\mathbf{A}\mathbf{P}(\hat{\mathbf{x}}_N)\mathbf{1}, \tag{4.11}$$

where $\mathbf{A}$ is a matrix of switching probabilities, $\boldsymbol{\delta}$ is a column vector of the initial
behavioural state probabilities which we set equal to the stationary distribution, $\mathbf{P}(\hat{\mathbf{x}}_i)$
is a diagonal matrix of the state-dependent distributions $f(\hat{\mathbf{x}}_i|b_i, \Theta)$, and c denotes
a constant resulting from treating all of the measurement process components as

known. Second, by fixing $b = \hat{b}$ and $\Phi = \hat{\Phi}$ (and optionally $\Theta = \hat{\Theta}$), the marginal

likelihood reduces to that of an SSM:

$$L_{SSM}(\Psi, \Theta, \hat{\Phi}) = \int\limits_{\mathbf{x}_{1:N}} f(\mathbf{y}_{1:T}|\mathbf{x}_{1:N}, \Psi)f(\mathbf{x}_{1:N}|\hat{b}_{1:N}, \Theta)f(\hat{b}_{1:N}|\hat{\Phi}) \, d\mathbf{x}_{1:N}, \qquad (4.12)$$

$$= \int\limits_{\mathbf{x}_{1:N}} f(\mathbf{y}_{1:T}|\mathbf{x}_{1:N}, \Psi)f(\mathbf{x}_{1:N}|\hat{b}_{1:N}, \Theta)c \, d\mathbf{x}_{1:N}, \qquad (4.13)$$

where c now represents a constant from fixing all of the behaviour components. This

lays the groundwork for fitting Eqns 4.1-4.3 by iteratively fitting a series of HMMs

and SSMs. We carry out the procedure for K iterations as follows:

1. **Set $\mathbf{x}_{1:N} = g(\mathbf{y}_{1:T})$ and assume $\Psi = 0 \rightarrow$ fit HMM $\rightarrow$ estimate $\left\{\hat{\Theta}^{(1)}, \hat{\Phi}^{(1)}, \hat{b}_{1:N}^{(1)}\right\}$**

2. **Set $\Theta = \hat{\Theta}^{(1)}$, $\Phi = \hat{\Phi}^{(1)}$, and $b_{1:N} = \hat{b}_{1:N}^{(1)} \rightarrow$ fit SSM $\rightarrow$ estimate $\left\{\hat{\mathbf{x}}_{1:N}^{(1)}, \hat{\Psi}^{(1)}\right\}$**

3. **for $k = 2$ to K**

   - **Set $\mathbf{x}_{1:N} = \hat{\mathbf{x}}_{1:N}^{(k-1)}$ and assume $\Psi = \hat{\Psi}^{(k-1)} \rightarrow$ fit HMM $\rightarrow$ estimate $\left\{\hat{\Theta}^{(k)}, \hat{\Phi}^{(k)}, \hat{b}_{1:N}^{(k)}\right\}$**

   - **Set $\Theta = \hat{\Theta}^{(k)}$, $\Phi = \hat{\Phi}^{(k)}$, and $b_{1:N} = \hat{b}_{1:N}^{(k)} \rightarrow$ fit SSM $\rightarrow$ estimate $\left\{\hat{\mathbf{x}}_{1:N}^{(k)}, \hat{\Psi}^{(k)}\right\}$**

4. **Choose $\left\{\hat{\Theta}, \hat{\Phi}, \hat{b}_{1:N}, \hat{\mathbf{x}}_{1:N}, \hat{\Psi}\right\}_{MLE} = \left\{\hat{\Theta}^{(k)}, \hat{\Phi}^{(k)}, \hat{b}_{1:N}^{(k)}, \hat{\mathbf{x}}_{1:N}^{(k)}, \hat{\Psi}^{(k)}\right\} \ni$**

$$k = \text{argmax} \, L_{SSM}(\hat{\Psi}^{(k)}, \hat{\Theta}^{(k)}, \hat{\Phi}^{(k)})$$

In effect we first linearly interpolate the observations via the function $g(\cdot)$ to

produce locations with error on a regularized time scale. Then, we assume that the

measurement error is negligible and fit an HMM to the regularized observations to estimate $\{\hat{\Theta}, \hat{\Phi}\}$ and predict $\hat{b}_{1:N}$. Next, fixing $\{\Theta, \Phi, b_{1:n}\}$ at $\{\hat{\Theta}, \hat{\Phi}, \hat{b}_{1:n}\}$, we fit a SSM to the original (un-regularized) observations to estimate $\hat{\Psi}$ and predict $\hat{\mathbf{x}}_{1:N}$. This combination of fitting an HMM followed by an SSM constitutes a single iteration. The initial iteration is unique because the HMM is fitted to the regularized observations; the rest of the iterations are identical to the first except that the HMM is fitted to the location states predicted during the previous iteration's SSM. After carrying out K iterations, we contend that the true maximum likelihood estimates of our parameters and random effects, $\left\{\hat{\Theta}, \hat{\Phi}, \hat{b}_{1:N}, \hat{\mathbf{x}}_{1:N}, \hat{\Psi}\right\}_{MLE}$, can be well represented by the iteration that achieved the highest value of the SSM likelihood at the parameter estimates, $L_{SSM}(\hat{\Psi}^{(k)}, \hat{\Theta}^{(k)}, \hat{\Phi}^{(k)})$. In practice, we calculate negative log likelihoods rather than likelihoods. In addition, although we calculate the constant c in Eqn 4.13 so that we can accurately evaluate $L_{SSM}(\hat{\Psi}^{(k)}, \hat{\Theta}^{(k)}, \hat{\Phi}^{(k)})$ and therefore identify the best parameter estimates, we do not calculate the constant in Eqn 4.11 because it is redundant.

4.3.3   Model Checking and Standard Errors

For model checking, we rely on one step ahead residual calculations during the HMM step, also known as pseudoresiduals (Zucchini et al., 2016). These residuals assess the goodness of fit of the HMM assuming that the true location predictions $\hat{\mathbf{x}}_{1:T}$ are accurate.

Standard errors are calculated in two ways. First, `TMB` uses the delta method and

the observed information matrix to approximate the standard errors of the parameters and location states in their observed spaces (Auger-Méthé et al., 2015). Patefield (1977) outlines the theory that enables us to use these standard errors with our iterative optimization scheme: that is, assuming that one of the HMM or SSM steps finds the maximum likelihood estimates, the curvature (and therefore the Hessian) will be preserved in the other step. We additionally use a parametric bootstrap to quantify the standard errors, and compare these bootstrap estimates to those calculated from the observed information. The bootstrap serves two purposes: 1) it provides alternative estimates of the parameter standard errors to the asymptotic estimates which might not be reliable; and 2) it provides a convenient framework for evaluating the accuracy of the model akin to a simulation study. We simulate R (indexed by r) random draws of the random effects $\{b^*_{r,1:N}, \mathbf{x}^*_{r,1:N}\}$ and observations, $\mathbf{y}^*_{r,1:T}$ from $\left\{ \hat{\Theta}, \hat{\Phi}, \hat{b}_{1:N}, \hat{\mathbf{x}}_{1:N}, \hat{\Psi} \right\}_{MLE}$, and re-fit our model to obtain R estimates of the parameters and random effect predictions, $\left\{ \hat{\Theta}^*_r, \hat{\Phi}^*_r, \hat{b}^*_{r,1:N}, \hat{\mathbf{x}}^*_{r,1:N}, \hat{\Psi}^*_r \right\}_{MLE}$. We then calculate the bias and variance of an individual parameter p by

$$bias_p = R^{-1} \sum_{r=1}^{R} (\hat{p}^*_r - \hat{p}) \qquad V_p = \frac{1}{R-1} \sum_{r=1}^{R} (\hat{p}^*_r - \hat{p})^2 \qquad (4.14)$$

(Davison and Hinkley, 1997). For the random effects, we calculate the behavioural state error rate err_r and the root mean squared error $RMSE_{r,c}$ in longitude and

latitude within each track (c denotes coordinate axis):

$$err_r = N^{-1} \sum_{i=1}^{N} \mathbf{1}(\hat{b}^*_{r,i} = b^*_{r,i}) \qquad RMSE_{r,c} = N^{-1} \sum_{i=1}^{N} (\hat{x}^*_{r,c,i} - x^*_{r,c,i})^2 \qquad (4.15)$$

Here, $\mathbf{1}(\cdot)$ now denotes an indicator function equal to 1 when the behavioural state prediction $\hat{b}^*_{r,i}$ is correct and 0 otherwise.

4.4   Data Analysis

4.4.1   Fitting Switching Hierarchical Models

Although satellite tracks were irregularly sampled in time, Eqn 4.2 evolves over regular intervals, prompting the choice of a time step. We considered a 3 hour, 6 hour, and 12 hour time step between successive location states. These time intervals are similar to the lengths of time steps chosen in previous grey seal foraging studies (e.g., 3 hours in Nowak et al. 2020 and 8 hours in Breed et al. 2013). We chose a 3 hour time step based on inspection of QQ plots from the HMM iteration, and model results. Observations collected after May 31 were removed, because the start of the moulting season (May-June; Goulet et al. 2001) signifies the end of post-breeding. Subsequently, the data were examined for temporal gaps, and following Lawler et al. (2019), split into track segments when gaps longer than a specified group cutoff were detected. Any segments with fewer than three observations and where the duration of the segment lasted less than 3× the chosen time step for the model were removed. This ensured that there would be at least three unobserved locations per segment

to make a meaningful negative log-likelihood contribution for the movement process (Eqn. 4.2), and at least one observed location per location random effect. For most tracks, we used a cutoff of 6 hours ($2\times$ the time step). However, seal tracks collected in 2003 and 2004 required a longer cutoff of 24 hours to satisfy these criteria. All data were projected using the Mercator projection.

Significant outlying locations occurred. In order to reduce instances of NaN likelihood evaluations, we winsorized (Tukey, 1962) the data rather than removing these locations entirely. First, we identified outliers based on the Freitas et al. (2008) filter using the **prefilter** function of the R package `foieGras` (Jonsen et al., 2020), with the following criteria: 1) a max speed of $10ms^{-1}$ (the actual max sustained speed of a grey seal is approximately $3ms^{-1}$; Gallon et al. 2007); 2) internal angles of 15 degrees coinciding with step lengths of 10,000m; and 3) internal angles of 25 degrees coinciding with a step length of 50,000m. Once we identified the outliers, we scaled the observations based on the empirical distribution of the observed swim speeds. We calculated the observed swim speed s_t as $s_t = d_t/\Delta_t$, where d_t is the step length between $\mathbf{y}_{t-1}$ and $\mathbf{y}_t$, and Δ_t is the observed time difference. Then, for each Argos class ac, we calculated the 25th and 75th percentiles of $s_{2:T}$, $q_{ac,0.25}$ and $q_{ac,0.75}$, the interquartile range, $IQR_{ac} = q_{ac,0.75} - q_{ac,0.25}$, and the upper outlier bound $q_{ac}^w = 1.5 * IQR_{ac}$. Finally, we calculated the winsorized observation $\mathbf{y}_t^w$ by scaling the observed displacement $(\mathbf{y}_t - \mathbf{y}_{t-1})$ by a ratio of the upper outlier bound corresponding

to the Argos class of $\mathbf{y}_t$ to the observed speed, i.e.,

$$\mathbf{y}_t^w = \mathbf{y}_{t-1} + \frac{q_{ac}^w}{s_t}(\mathbf{y}_t - \mathbf{y}_{t-1}) \tag{4.16}$$

Traditional winsorization replaces an outlier with the nearest unaffected value (Tukey, 1962). By using the upper outlier bound, and by calculating q_{ac} for each Argos location class, we aim to preserve the relative structure of the errors modelled in Eqn 4.1.

Finally, we fitted the switching hierarchical model to each track allowing for twenty iterations. Throughout the analysis, we interpreted the first state ($\gamma_1 > 0.5$ and $\theta_1 \sim 0$) as travelling behaviour and the second state ($\gamma_2 > 0.5$ and $0 < \theta_2 < 2\pi$ with a wide variance) as a composite of apparent foraging and haulout (Whoriskey et al., 2017; Nowak et al., 2020). Further analyses were used to filter state 2 for foraging behaviour (see Section 4.4.3).

4.4.2 Bootstrapping

Based on the model results, we ran bootstrap simulations for nine randomly selected tracks (three from each of the colonies) to provide alternative estimates of standard errors and to assess model accuracy. For each track, we ran 100 simulations that maintained the observed time series of data gaps and error classes. We then calculated the accuracy of the location and behavioural states and the parameters as stated above. Furthermore, we calculated the bootstrap efficiency as V_p^{tmb}/V_p, where V_p^{tmb} is the variance calculated by `TMB`.

To quantify differences in model performance among colonies, we tested for significant differences in mean bias, RMSE, and error rates of the switching hierarchical model using the R package `npmv`. This package provides nonparametric tests for multivariate responses based on rank values (Ellis et al., 2017). It additionally provides subset algorithms to determine which variables displayed the significant differences, and which factor levels contributed to their significance, using a Ryan adjustment to an overall Type 1 error rate of $\alpha = 0.05$.

4.4.3   Colony-Based Comparison

By fitting the switching hierarchical model, we obtained predictions of both location and behavioural states along each female's track, which we used to infer foraging behaviour (and therefore is actually apparent foraging). One individual did not exhibit apparent foraging; this individual was excluded from further analysis on the foraging state. With these states, we compared the spatial distribution of the full tracks and of the foraging patches for our three grey seal colonies. For the full tracks, we fitted a Gaussian kernel as implemented in the `adehabitatHR` package (Calenge, 2006) to estimate the 95% utilization distribution (KUD) of each individually predicted track. We denote this the "ranging" distribution. To avoid oversmoothing and a large overlap with land, we multiplied the smoothing parameter h for each track by 0.5, and then removed any remaining parts of the distribution that overlapped with land.

To compare the distributions of foraging patches, we first identified a foraging patch as a series of locations where a sequence of at least five successive foraging

states occurred. If one track segment ended in a foraging patch and the next segment began with one, these patches were considered to be part of the same patch if the gap separating the two segments was < 24 hrs. For each patch we calculated the minimum convex polygon (also using `adehabitatHR`), and its centroid. Patches where the centroid occurred within 2 km (Breed et al., 2011) of land were assumed to be haulout behaviour, and were removed from subsequent analysis. This then yielded the (apparent) "foraging" distribution. For each of the full and foraging distributions, we calculated the union of the polygons within each colony to estimate a spatial distribution, and then we compared these distributions among colonies by quantifying their overlap.

To quantify differences in movement and foraging tactics among colonies, we applied the non-parametric multivariate tests of `npmv` to the sets of movement parameters. We additionally calculated distance from the centroid of each foraging patch to the colony as the least cost path around land, using the `gdistance` package (van Etten, 2018). Then, we combined the mean distance per individual with the number, mean duration, and mean area of each foraging patch, as well as the proportion of overall time spent within foraging patches. We treated these five variables as a multivariate response and also tested for differences among colonies using `npmv`. Although generalized linear mixed models are frequently used to test for differences among derived metrics of movement paths, we opted to utilize `npmv` for two reasons. First, it avoids distributional assumptions on metrics derived from random variable predictions (the location and behavioural states). Second, it accounts for the fact

that these metrics are likely inherently dependent, despite the fact that they may not

be correlated.

4.5   Results

Overall, a total of 126,578 locations were collected from the 67 females between the

individual-specific tagging dates and May 31 of the same year. On average, 1889

locations were collected per individual (range=241-4544) over an average of 78 days

(range=35-138).

4.5.1   Bootstrap Studies

The switching hierarchical model accurately predicted both behaviour and location

states (Fig 4.2). Mean accuracy for the behavioural states ranged between 0.69 and

0.91 (proportion of correctly identified states), while the mean RMSE ranged between

990-2487 m and 802-2416 m in the longitude and latitude directions, respectively. The

magnitude of the RMSE can be interpreted in Fig 4.3. A multivariate non-parametric

test with `npmv` suggested no significant difference among colonies in the mean accuracy

and RMSE (p= 0.45).

Bias did not appear to significantly differ among colonies (Figs 4.4, 4.5). We

conducted both univariate and multivariate nonparametric tests on the mean bias

using Kruskal-Wallis tests and `npmv`, respectively. The multivariate test on the bias

of the movement parameters and switching probabilities was insignificant (p=0.417),

as was a multivariate test on the bias in the variance parameters ($\sigma_{lon}, \sigma_{lat}$, and
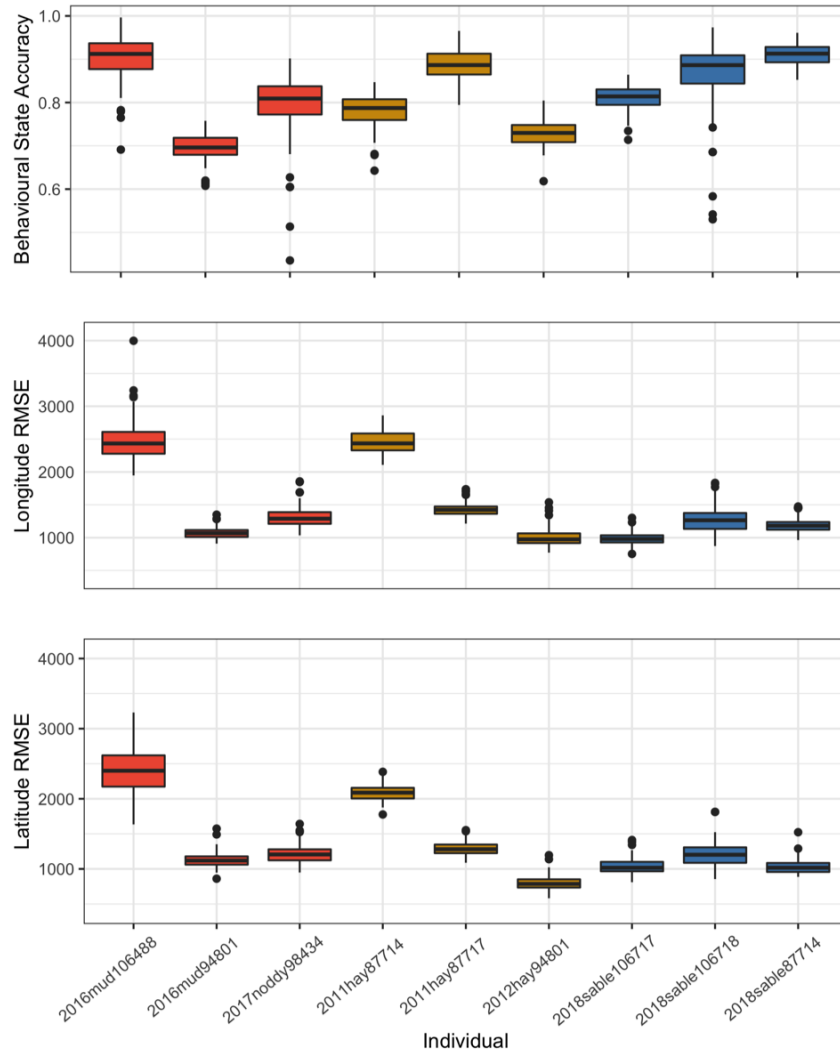
Figure 4.2: Accuracy of the switching hierarchical model as determined by a parametric bootstrap on nine randomly selected grey seal tracks. Top: the proportion of behavioural states correctly identified. Middle and bottom: RMSE in the longitude (middle) and latitude (bottom) axes, with units in metres under the Mercator projection. For all plots, orange, yellow, and red denote tracks selected from the SW, Hay, and Sable colonies, respectively. Individual names on the x axis denote a unique alphanumeric describing the sampling year, the island of tagging, and the PTT used for the tag.
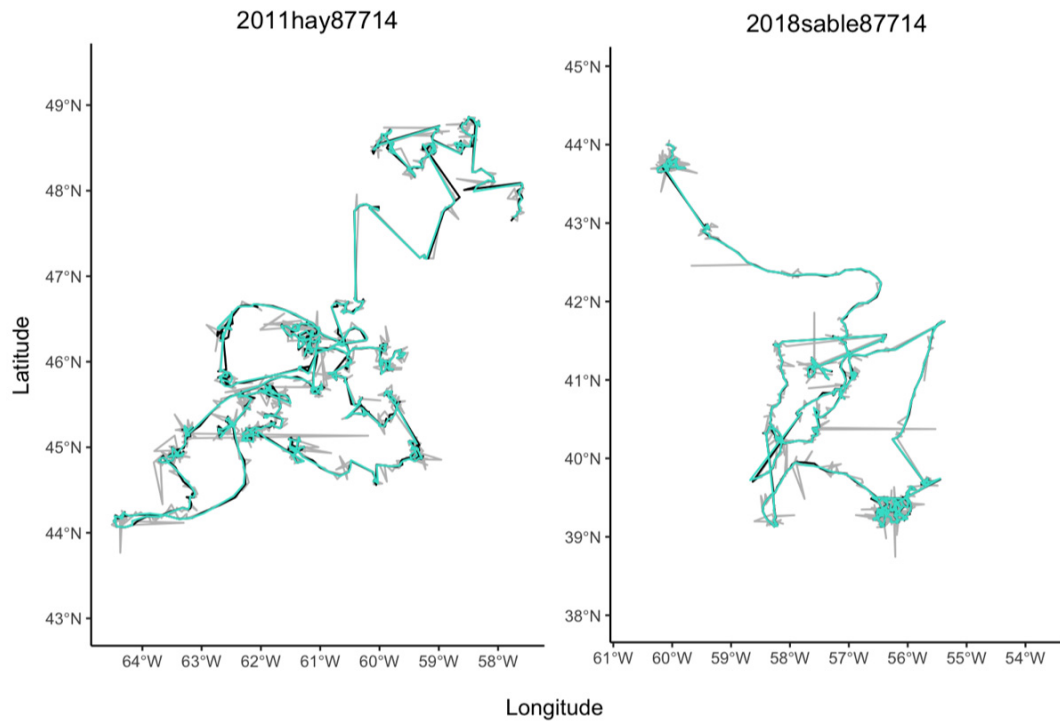
Figure 4.3: An example of two simulated tracks from the bootstrap studies. Grey is the simulated track observed with error, while black is the simulated true track, and green is the predicted track from the switching hierarchical model. The RMSE for the track on the left was 2,623 and 2,225 m in the longitude and latitude directions, while the RMSE of the track on the right was 1,138 and 999 m. Headings denote a unique alphanumeric describing the sampling year, the island of tagging, and the PTT used for the tag of the grey seal that the bootstrap was based on.

ψ; p=0.957). All Kruskal-Wallis tests on single parameters were also insignificant ($p > 0.4$ in all cases). In general, bias was low, although some parameters, appeared more prone to bias than others (σ_{lon}, σ_{lat}, and ψ). Additionally, the bias in θ_2 for the Hay seal bootstraps does encompass the entire parameter range for all three tracks (Fig 4.4). This unusually large bias corresponded with extreme values of bootstrap efficiency ($< 50^{-1}$; Table 4.2). Otherwise, bootstrap efficiency ranged from 0.14 to 2.24. Most often ($\sim 73\%$ of the time), bootstrap standard errors were larger than those calculated by TMB, although over half of those that were larger ($\sim 54\%$) were less than twice as large.

Although bias in the GPS variance parameters was low (Fig 4.5), estimates of the process variance σ_{lon} and σ_{lat} and measurement error ψ were consistently biased negative among all colonies. Appendix A shows evidence that in some cases this bias was correlated, i.e., that when an estimate of either σ_{lon} or σ_{lat} was biased negative, so was the estimate of ψ (Figs A.1,A.2).

4.5.2 Switching Hierarchical Models and Intraspecific Variability in Foraging

We obtained parameter estimates and random effect predictions for 67 seal tracks (Fig 4.6, Fig 4.7). The individual tracks and the colony-based 95% kernel utilization distribution show that although the spatial distribution of Sable seals overlapped with both the Hay and Southwest colonies, the Hay and Southwest colonies did not overlap (Fig 4.8, Table 4.3). The Southwest seals largely travelled south of Nova
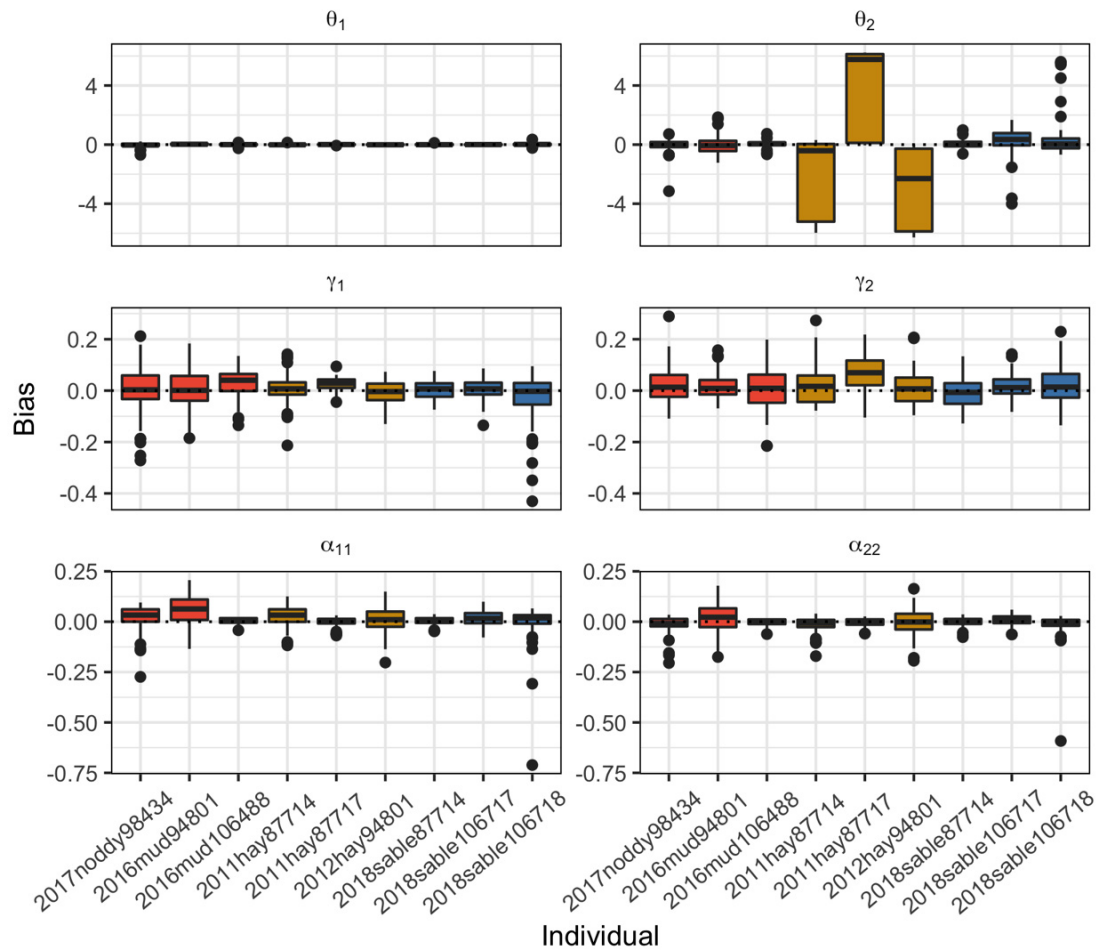
Figure 4.4: Bias in the movement parameters from fitting the switching hierarchical model to 100 simulated tracks parametrically bootstrapped from nine randomly selected grey seal tracks. Note the different y-axis scales because different facets indicate different parameters. For all plots, orange, yellow, and red denote tracks selected from the SW, Hay, and Sable colonies, respectively. Individual names on the x axis denote a unique alphanumeric describing the sampling year, the island of tagging, and the PTT used for the tag.
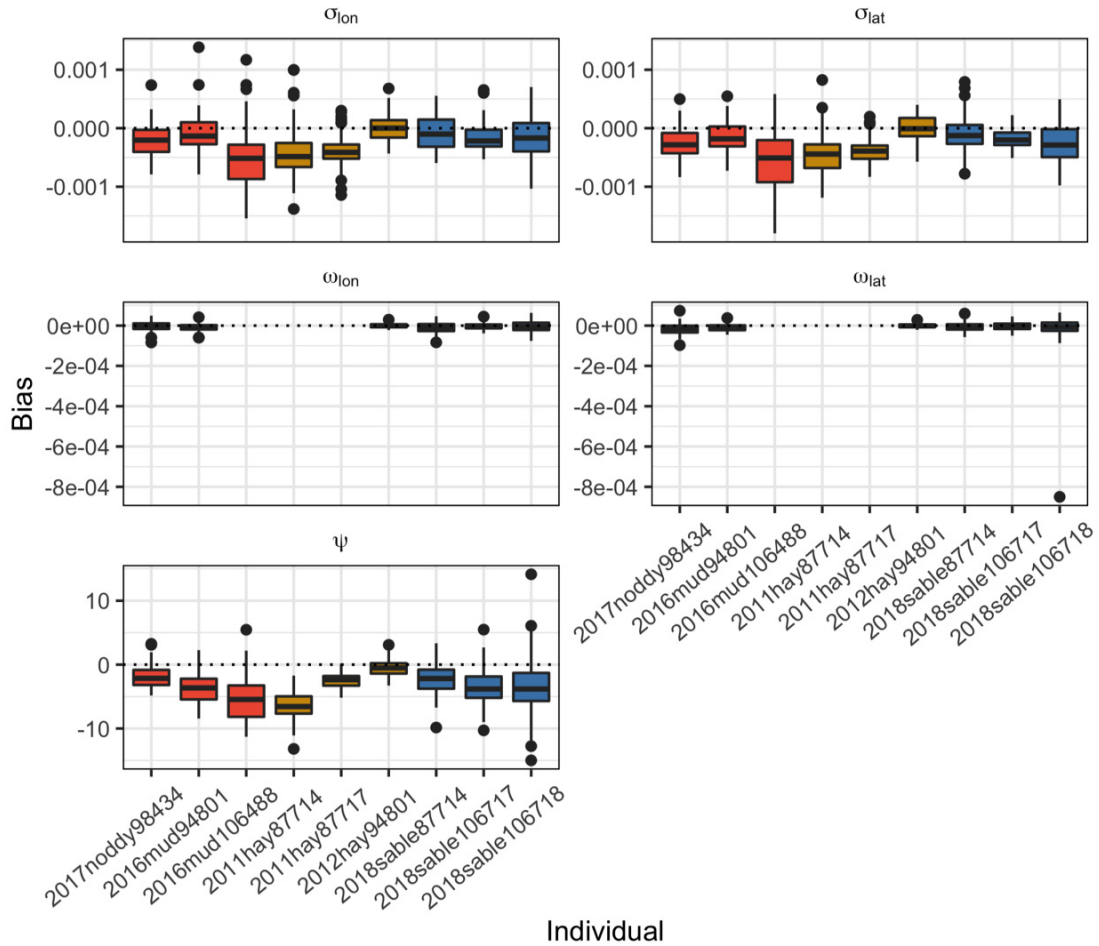
Figure 4.5: Bias in the variance parameters from fitting the switching hierarchical model to 100 simulated tracks parametrically bootstrapped from nine randomly selected grey seal tracks. Note the different y-axis scales because different facets indicate different parameters. Absent boxplots result because not all of the grey seal tracks used for the bootstrap included GPS locations. For all plots, orange, yellow, and red denote tracks selected from the SW, Hay, and Sable colonies, respectively. Individual names on the x axis denote a unique alphanumeric describing the sampling year, the island of tagging, and the PTT used for the tag.

Table 4.2: Bootstrap and TMB standard errors for each of the nine bootstraps. ID is a unique alphanumeric that describes the sampling year, tagging place, and tag PTT of the seal that the bootstrap was based off. TMB errors are calculated via the Delta method using the observed information (Hessian) matrix. Occasionally these return NA. Bootstrap errors are calculated as the standard deviation of the 100 parameter estimates obtained from a bootstrap. Missing values are denoted with '-', and occurred when the simulated tracks included no simulated GPS locations.

ID	Type	θ_1	θ_2	γ_1	γ_2	a_{11}	a_{22}	σ_{lon}	σ_{lat}	ω_{lon}	ω_{lat}	ψ
2017noddy98434	TMB	0.0738	0.180	0.0641	0.0464	0.0609	0.0176	0.000233	0.000254	2.47e-05	2.87e-05	2.12
	Bootstrap	0.129	0.430	0.0835	0.0619	0.0584	0.0393	0.000270	0.000249	2.19e-05	2.61e-05	1.72
	Efficiency	0.324	0.175	0.591	0.563	1.09	0.201	0.743	1.04	1.27	1.21	1.51
2016mud94801	TMB	0.0525	0.432	0.0490	0.0385	0.0715	0.0600	0.000128	0.000171	1.67e-05	1.45e-06	NA
	Bootstrap	0.0506	0.581	0.0736	0.0448	0.0829	0.0712	0.000300	0.000243	1.79e-05	1.78e-05	2.25
	Efficiency	1.07	0.552	0.443	0.737	0.744	0.708	0.184	0.495	0.865	0.00667	NA
2016mud106488	TMB	0.0493	0.102	0.0423	0.0557	0.0137	0.0100	0.000275	0.000331	-	-	3.71
	Bootstrap	0.0605	0.188	0.0511	0.0772	0.0159	0.0151	0.000488	0.000530			3.17
	Efficiency	0.662	0.296	0.685	0.521	0.747	0.442	0.317	0.390			1.37
2011hay87714	TMB	0.0365	0.343	0.0385	0.0435	0.0424	0.0221	0.000170	0.000173	-	-	2.56
	Bootstrap	0.0435	2.52	0.0530	0.0715	0.0478	0.0355	0.000411	0.000335			2.17
	Efficiency	0.706	0.0184	0.526	0.370	0.786	0.389	0.171	0.268			1.39
2011hay87717	TMB	0.0220	0.259	0.0211	0.0532	0.0185	0.0176	0.000114	0.000130	-	-	1.38
	Bootstrap	0.0238	2.97	0.0235	0.0688	0.0195	0.0191	0.000246	0.000198			1.09
	Efficiency	0.855	0.00764	0.805	0.597	0.895	0.853	0.217	0.432			1.61
2012hay94801	TMB	0.0308	0.00213	0.0381	0.0698	0.0537	0.0942	0.000171	0.000131	NA	1.07e-05	NA
	Bootstrap	0.0325	2.68	0.0433	0.0629	0.0605	0.0630	0.000222	0.000193	1.05e-05	9.59e-06	1.07
	Efficiency	0.899	6.28e-07	0.773	1.23	0.788	2.24	0.597	0.459	NA	1.25	NA
2018sable87714	TMB	0.0284	0.182	0.0254	0.0520	0.0196	0.0177	0.000171	0.000166	2.91e-05	2.58e-05	2.73
	Bootstrap	0.0390	0.233	0.0360	0.0550	0.0192	0.0207	0.000285	0.000279	2.69e-05	2.10e-05	2.46
	Efficiency	0.533	0.610	0.500	0.894	1.05	0.737	0.361	0.353	1.17	1.51	1.23
2018sable106717	TMB	0.0242	0.539	0.0249	0.0382	0.0316	0.0277	0.000113	0.000146	1.88e-05	2.02e-05	3.25
	Bootstrap	0.0333	0.873	0.0366	0.0435	0.0359	0.0273	0.000231	0.000165	1.59e-05	1.96e-05	2.75
	Efficiency	0.527	0.381	0.462	0.770	0.774	1.03	0.240	0.783	1.41	1.06	1.40
2018sable106718	TMB	0.0507	0.501	0.0496	0.0661	0.0519	0.0241	0.000285	0.000248	3.09e-05	4.39e-05	4.95
	Bootstrap	0.0686	1.26	0.0886	0.0718	0.0863	0.0635	0.000323	0.000328	2.66e-05	9.02e-05	4.40
	Efficiency	0.545	0.158	0.314	0.846	0.361	0.144	0.779	0.571	1.35	0.237	1.27
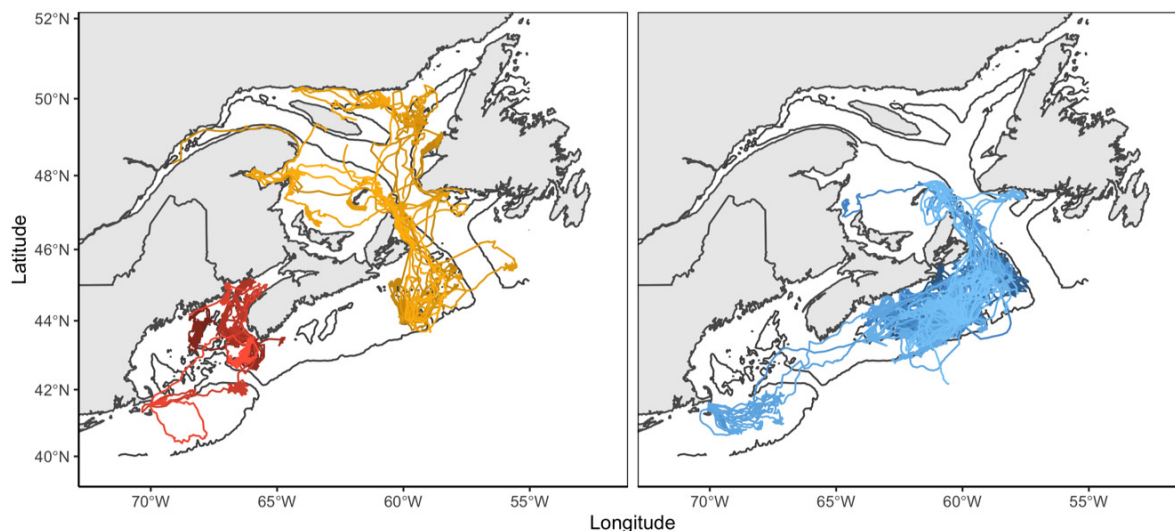
Figure 4.6: Predictions of 67 individual tracks for female grey seals from three colonies on the East Coast of Canada, obtained by fitting an iterative switching hierarchical model to data collected between the individual-specific tagging date at the end of January to May 31 of the same year. Shades of red, yellow, and blue designate individuals from the Southwest (10), Hay (14), and Sable (43) colonies, respectively. Solid black lines denote the 200m isobath.

Scotia into the Bay of Fundy and Gulf of Maine, with some dispersal as far as Cape Cod, Massachusetts. The Hay Island female ranged from the northern part of the Eastern Scotian Shelf and throughout the Gulf of St. Lawrence. The Sable females mostly travelled throughout the Eastern Scotian Shelf, but ranged as far south as Cape Cod, and into the south-eastern Gulf of St. Lawrence. The estimated total area traversed by females from the three breeding components differed with the Southwest seals using 89,166 km^2, the Hay seals using 279,551 km^2, and the Sable seals using 319,145 km^2. Movements of females from the Sable Island colony overlapped with those of females from the Southwest and Hay Island colonies by 57,534 and 126,189 km^2, respectively. Overall, the Sable colony shared 58% of its ranging distribution with the Southwest and Hay colonies, while the Southwest and Hay colonies shared

Table 4.3: Proportion of distribution (ranging on the left and foraging on the right) that colonies share with each other. An entry was calculated by taking the overlap between the colonies denoted by the row and column and dividing by the total area of the colony denoted by the column.

	Ranging Distribution			Foraging Distribution		
	Southwest	Hay	Sable	Southwest	Hay	Sable
Southwest	-	0	0.18	-	0	0
Hay	0	-	0.40	0	-	0.08
Sable	0.65	0.45	-	0	0.20	-

approximately 65% and 45%, respectively (Table 4.3).

The estimated model parameters demonstrated variability among the colonies (Fig 4.7). We tested for differences among colonies in the parameters that govern the individual movements of the animals $\{\theta_1, \theta_2, \gamma_1, \gamma_2\}$ by treating these as a multivariate response using the nonparametric tests of `npmv` Ellis et al. (2017), and found significance (p=0.003). Subset testing suggested that although the Hay and Sable colonies share similar movement characteristics, the Southwest seals differ from both of the other colonies (overall type I error rate controlled at α=0.05). Specifically, the Southwest colony exhibited significant differences from the Hay and Sable colonies, and these differences were largely driven by γ_1 (the movement persistence of the inferred travelling state; overall type I error rate controlled at α=0.05). For the Hay and Sable seals, behavioural state-dependent distributions were frequently defined by differences in the γ parameters (i.e., $\gamma_1 \neq \gamma_2$), while for the Southwest seals, there was a higher incidence of the θs (mean turning angles) driving the state classification ($\theta_1 \neq \theta_2$; Fig 4.7).

We detected 600 foraging patches among the 67 tracks (Fig 4.8). Of these, 88, 155,
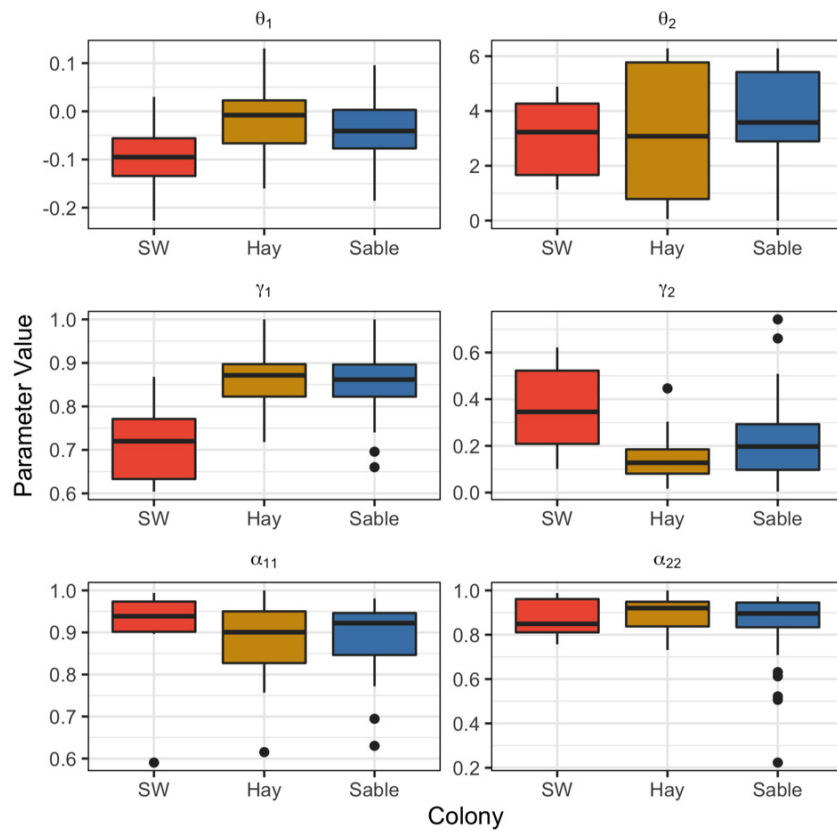
Figure 4.7: Boxplots of the estimated parameters from the movement process (except the process error) for the 67 grey seal tracks. The θs denote the mean turning angle of the tracks for each state, while the γs can be interpreted as the persistence within a track for each state. In all plots, red, yellow, and blue depict parameters for the Southwest, Hay, and Sable colonies, respectively.
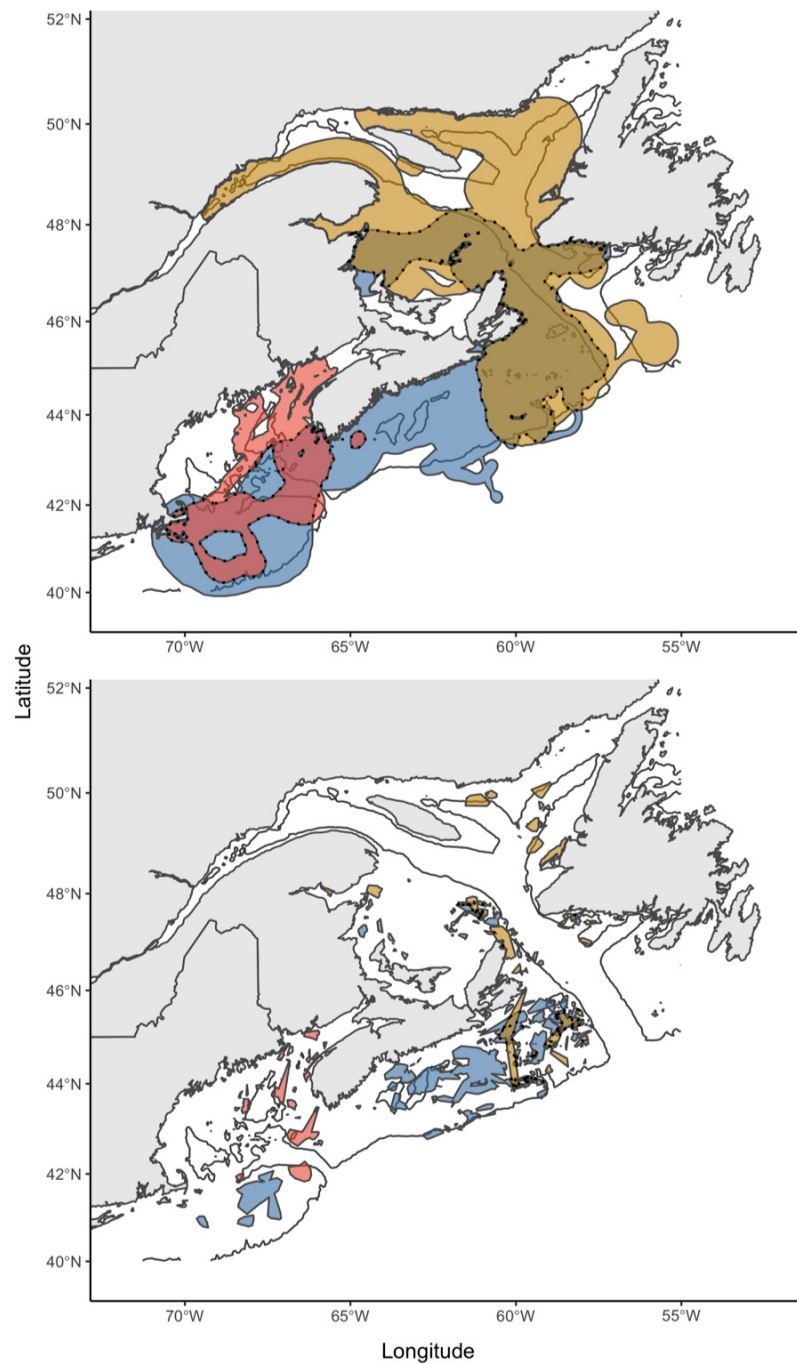
Figure 4.8: Top: Ranging distribution over all of the predicted locations for each colony, as estimated by 95% kernel utilization distributions. Bottom: Foraging patches as estimated by minimum convex polygons for behavioural state predictions. In both plots, red, yellow, and blue depict the Southwest, Hay, and Sable colonies, respectively. Dotted black lines depict areas of overlap between colonies, and solid black lines denote the 200m isobath.

and 357 patches were found for the Southwest, Hay, and Sable colonies, respectively, which totaled to an area of 8,595, 18,603, and 45,254 km^2. Of the roughly 63,957 km^2 of foraging patch area used by females from Sable and Hay islands, only 3,743 km^2 overlapped in space. This equated to approximately 20% and 8% of the total Hay and Sable colony foraging distributions, respectively (Table 4.3). No other overlap was observed (Fig 4.8; Table 4.3).

We observed variability among colonies in several foraging metrics that we calculated (Fig 4.9). Means and standard deviations are formally reported in Table 4.4. First, Southwest seals exploited on average 8.8 patches, while Hay and Sable seals exploited 11.1 and 8.5, respectively. Second, Southwest seals exploited patches of medial average size (0.037 km^2) compared to Hay (0.034 km^2) and Sable (0.050 km^2) seals. Third, the Southwest females spent the least amount of time within a patch on average (59.5 hrs) compared to the Hay (68.7 hrs) and Sable (89.6 hrs) seals. When standardized for the total duration of the track by dividing the time spent foraging by the total time tracked, Southwest seals were observed to be foraging on average 35.5% of the time, while Hay and Sable seals foraged 44.4% and 45.7% of the time, respectively. Finally, the Southwest seals foraged on average the closest to their colony (mean = 256 km), while the Hay seals exploited patches furthest from their colony (mean = 428 km), (Fig 4.9). Although the Sable seals typically foraged at distances in between the averages of the Southwest and Hay seals (mean = 280 km), they documented the maximum average distance among all females (730 km) (Fig 4.9). A multivariate non-parametric test with npmv of the colonial differences in

Table 4.4: Average count, area (km^2), duration (hrs), proportion of time spent within, and distance (km) from the colony of foraging patches. Entries are calculated from the averages per individual within each colony. Standard deviations are in brackets.

Colony	Count	Area	Duration	Proportion	Distance
Southwest	8.8 (5.9)	0.037 (0.054)	59.5 (43)	0.36 (0.24)	256.4 (122.6)
Hay	11.1 (6.2)	0.034 (0.03)	68.7 (42.1)	0.44 (0.23)	428.3 (152.9)
Sable	8.5 (4.3)	0.05 (0.08)	89.6 (53.7)	0.46 (0.2)	280.2 (145.7)

the number, mean area, mean distance, and mean duration of foraging patches per individual, as well as the overall proportion of time spent foraging by individual was significant (p=0.008). Subsequent subset testing suggested that the Hay seals were significantly different from the Southwest and Sable seals, but that the Southwest and Sable seals were similar, and that the mean area, mean distance and mean duration drove the differences (overall type I error rate controlled at α).

4.6 Discussion

4.6.1 Iteratively Predicting Location and Behavioural States

Computationally efficient methods for fitting switching hierarchical models have remained elusive. We develop such a method using maximum likelihood estimation that provides quick and reliable inference. Our use of `TMB` and an iterative optimization procedure reduced computation to minutes down from the hours that we have previously used to fit the Bayesian model from which it was based on (the DCRWS of Jonsen et al. 2005). Another popular method for predicting location and behavioural states from tracking data is the R package `momentuHMM` (McClintock and Michelot,
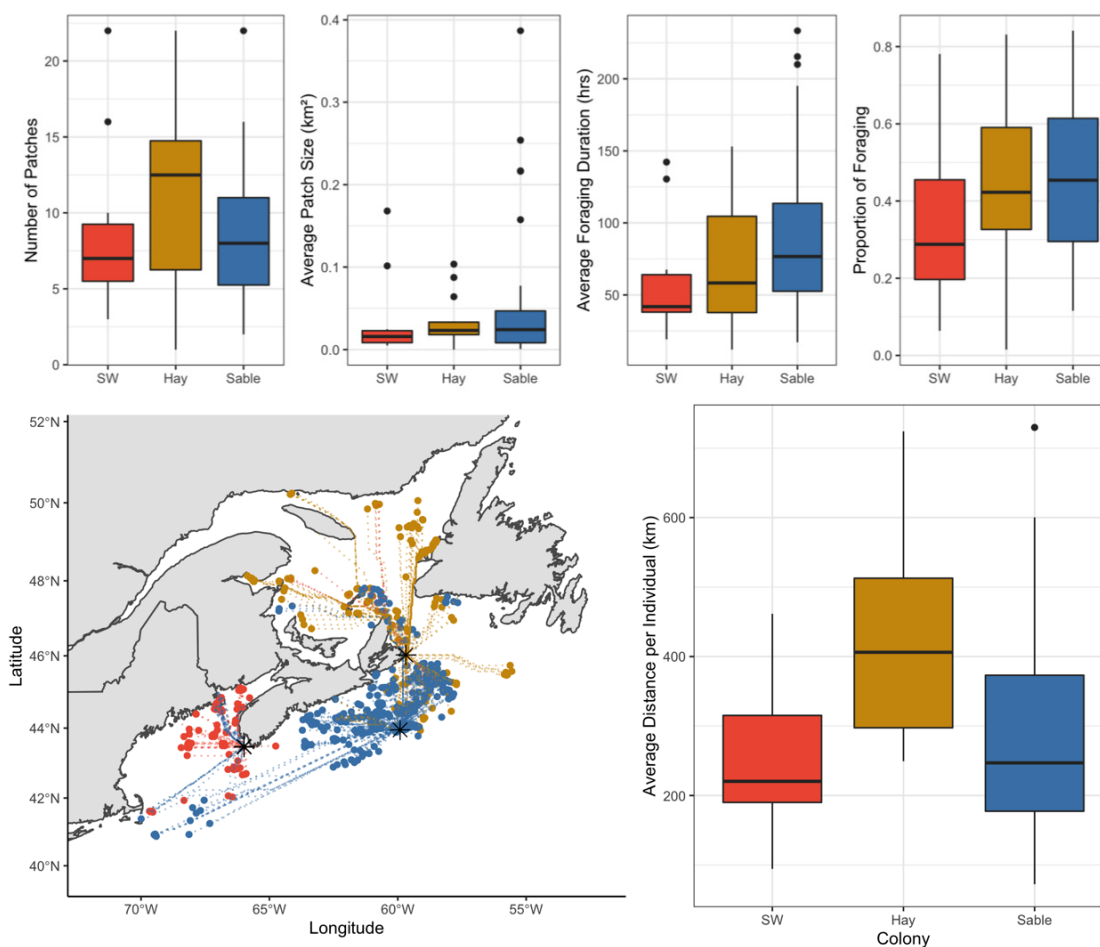
Figure 4.9: Foraging patch metrics per colony. Top row from left to right: 1) number of patches per individual; 2) average patch size per individual; 3) average foraging duration within a patch per individual; and 4) overall proportion of time spent foraging compared to full duration tracked. Bottom row: on the left, least cost paths (dotted lines) from the colony location (black stars) to the centroid of each foraging patch (solid dots); on the right, average distance of the least cost paths per individual. In all plots, colours depict each of the different colonies, with red, yellow, and blue for the Southwest, Hay, and Sable colonies, respectively.

2018). This modelling framework differs from ours in that McClintock and Michelot (2018) make use of two separate likelihoods, while we use only one. Specifically, McClintock and Michelot (2018) predict the location states using a continuous-time model, and predict the behavioural states using the discrete-time step length and turning angle model of moveHMM (Michelot et al., 2016). Our modelling framework is faster than Bayesian implementations (e.g., Jonsen et al. 2005). Furthermore, our general implementation could be applied to other modelling scenarios with large numbers of mixed-scale random effects (e.g., year, individual, etc.) that otherwise may not have been possible in a maximum likelihood framework. As a result, this research outlines an effective framework for rapidly analyzing larger datasets that are becoming increasingly available in both aquatic and terrestrial ecosystems.

As with all movement models, some subjective decisions were involved in model fitting, including the choice of projection, the number of behavioural states, the time step between successive location predictions, the group cutoff factor, and the starting values. We chose the Mercator projection because it is widely used, and it preserves local directions and shapes. We decided to model two behavioural states for consistency with previous foraging studies on grey seals (Breed et al., 2009, 2011, 2013; Nowak et al., 2020), but we recognize that it may be possible to infer additional behaviours if further information are collected (e.g., dive data; Carter et al. 2020). It is possible that we overestimated foraging by classifying time resting at sea as foraging, as these two behaviours can look similar from two dimensional location data (McClintock et al., 2017). Incorporating depth can help distinguish these behaviours;

however, depth data were not available. We selected a three hour time-step based on results from previous studies using the same movement process (Nowak et al., 2020), and qualitative analysis of QQ plots and parameter values. For most seals we chose the group cutoff to be twice our time step to prevent more than one linearly interpolated location state to occur between observations. However, we had to increase this group cutoff for 10 individuals, in which case we chose the smallest value that enabled model fitting. Finally, although we subjectively chose sets of starting values based on previous knowledge and model results, we objectively chose the best model fit by selecting the one with the optimal negative log likelihood value for further analysis.

Although these models provide useful information on the movement of individuals, fitting them can be challenging. We encountered NaN likelihood evaluations, lack of convergence, false convergence, and parameter boundary issues. These challenges are commonly encountered when maximizing likelihood functions. We combatted them by winsorizing, by adjusting convergence criteria based on the evaluations of the negative log likelihood and its gradient, by using multiple sets of starting values for the parameters, by reducing the number of steps used in the iteration, and by heuristically adjusting the time step and group cutoff factors.

4.6.2 Bootstrapping

The bootstrapping results indicate that our iterative modelling framework is accurate (Figs 4.2, 4.3, 4.4, 4.5). Behavioural state accuracy, location RMSE, and parameter bias were comparable across nine different seal tracks, suggesting that this method is

accurate across varying parameter sets. Furthermore, the behavioural state accuracy appears similar to that reported by Whoriskey et al. (2017), who fitted the HMM equivalent of this model under the scenario where no measurement error is assumed (see Chapter 2). In that paper, animal locations were simulated for a single track's parameter set, and the behavioural state accuracy of the HMM was 81.1%. Here, our median behavioural state accuracy ranged from approximately 70% to 96%. Furthermore, our average coordinate-wise RMSE (800 and 2500 m) coincides with those of previously reported SSM techniques. Albertsen et al. (2015) evaluated the performance of five SSMs and reported an average RMSE of ∼900 and ∼1,400 m in longitude and latitude, respectively, although performance ranged by approximately ±500 m. Jonsen et al. (2020) compared their location predictions to GPS tracks and showed that root mean squared distances (RMSDs) of 3-6 km can frequently occur. These results are encouraging because they suggest that 1) our implementation often performs just as well predicting behavioural states as its analogue under a no-measurement-error scenario, and 2) the accuracy of our location state prediction is comparable to other frequently used methods.

Consistent bias occurred with the measurement and process errors, and we found some evidence that the estimates of these parameters were inversely correlated (Figs A.1, A.2). Noting that larger values of ψ reflect smaller measurement errors, this suggests that if the measurement error is overestimated, then the process error will frequently be underestimated. This relationship could suggest an identifiability or estimability issue between these parameters. We are not the first to document such

problems in state-space modelling of animal movement. Auger-Méthé et al. (2015) conducted a comprehensive analysis and simulation study that showed that parameter bias and jagged, multimodal likelihood profiles can occur when analyzing animal movement with simple Gaussian linear state-space models, and that this problem can be exacerbated by a large amount of measurement error relative to process error. It is important to recognize that estimation problems such as these can impact statistical results, and therefore influence our interpretation of ecological processes. Auger-Méthé et al. (2015) demonstrated this by investigating the displacement of polar bears relative to sea ice drift, and showed that parameter estimation problems caused an overprediction of energy expenditure. In our grey seal results, we are confident in the state predictions because we show that both our state and location accuracy remains high even with larger amounts of measurement error. However, based on our results and those of (Auger-Méthé et al., 2015), future state-space modelling work for animal movement data may benefit from reparameterizing the model such that the ratio of the measurement to the process errors is estimated, rather than each of these parameters individually.

We calculated two standard errors: that from the observed Fisher information, and from a parametric bootstrap. The bootstrap estimates were most often larger than those from TMB (Table 4.2). It is better to use the more conservative bootstrap standard errors because for this hierarchical model it is not known what effective sample size is needed for the asymptotics of the observed Fisher information to be reliable.

4.6.3   Intraspecific Variability in Grey Seal Foraging Behaviour

Intraspecific foraging variability among breeding colonies has been documented in several pinniped species. For example, geographic separation of foraging habitat has been documented in the Antarctic fur seal (*Arctocephalus gazella*; Boyd et al. 2002) and the northern fur seal (*Callorhinus ursinus*; Robson et al. 2004), while variability in foraging tactics (e.g. distance/time/depth travelled) has been observed in South American fur seals (*Arcto cephalus australis*; Baylis et al. 2018) and Cape fur seals (*Arctocephalus pusillus pusillus*; Botha et al. 2020). In colonial breeding species with broad geographic distributions, some colonies may experience different environmental conditions and food availability compared to others, and movement patterns may reflect these discrepancies (Tremblay and Cherel, 2003). Furthermore, several studies on fur seal species and colonial breeding sea birds (Grémillet et al., 2004; Boyd et al., 2002; Baylis et al., 2018; Botha et al., 2020; Robson et al., 2004) suggest that colony-based separation of foraging habitat is a common strategy used to reduce competition for resources among colonies that occur in proximity.

We tested for differences in the post-breeding movement and foraging tactics of adult female grey seals from three geographically distinct colonies. During the post-breeding season, female grey seals focus their foraging effort on smaller fishes with higher energy densities, e.g., sandlance and redfish, presumably in order to quickly increase body lipid stores and thus increase probability of successful pregnancy (Beck et al., 2007). The importance of foraging during this season, as well as the relatively selective diet of females, makes post-breeding females an ideal demographic to study

for detecting intraspecific variability in foraging tactics. We detected this variability by using a novel iterative switching hierarchical model designed to predict behavioural states that we interpreted as apparent foraging (hereafter, foraging). Our results showed variability among colonies in the geographic distribution of foraging patches and significant differences in the parameters governing the movement processes as well as individual foraging tactics.

Evidence from diet, diving behaviour, and movement ecology indicate that intraspecific variability in grey seal foraging behaviour exists and is in part driven by age and sex (Breed et al., 2006; Beck et al., 2007; Breed et al., 2011, 2013). We attempted to control for such influences by studying only adult females at a time of their annual life cycle when they are likely feeding heavily to recover energy stores depleted during lactation. Three factors that we were unable to control are the difference in sampling years, difference in age distributions, and difference in sample size between the colonies. It is possible that the grey seals have altered their foraging tactics over the sampling period (from 2003-2018). Non-parametric tests did suggest that Sable females sampled in 2018 travelled further and spent a greater time foraging than Sable females tagged between 2003 and 2007 (p<0.001). Geographically, the later (2018) seals exploited an expanded range relative to the earlier (2003-2007) seals, i.e., the earlier seals largely remained on the Eastern Scotian Shelf, while the later seals travelled into the Gulf of St. Lawrence and down to Cape Cod. Second, it is possible that some of the intraspecific variability in foraging tactics is related to the age of the tagged animals. We might expect differences in adult foraging distributions among

animals that have recently matured (approximately ages 5-15), compared to those that are experienced breeders (ages 15-30), and older females (ages >30). However, age differences in diving behaviour have not been detected among adult females from Sable Island (Beck et al., 2003b) and we did not have the sample sizes to reliably test for these differences. For example, within the Southwest colonies, eight of the 10 tagged animals were <15 years old, whereas in the Sable colony only three animals were <15 years old (Table 4.1). Finally, it is also possible that the observed intraspecific variability, and specifically the larger distribution for the Sable colony relative to the other colonies, resulted from the larger sample size (43 at Sable vs 10 and 14 at Southwest and Hay, respectively). However, our sample sizes are roughly proportional to population size at these different colonies (in 2016, pup production was estimated at 87,485, 12,441, and 2107 individuals for the Sable, Gulf of St. Lawrence, and Southwest Nova Scotia components; den Heyer et al. 2020). Randomly selecting numbers of individuals from sub-groups proportional to the relative sizes of the sub-groups is a common statistical technique called stratified random sampling with proportional allocation (Lohr, 2010).

We documented a moderate amount of overlap in the ranging distributions between the Southwest and Sable colonies, and between the Hay and Sable colonies. No overlap was observed between the Southwest and Hay colonies. Although each colony shared between 45-65% of its ranging distribution, there was little overlap in the estimated foraging patches. The Sable and Hay colonies, separated by only 291

km, shared less than a quarter of their foraging habitat (20.0% of the Hay colony foraging distribution, and 8.3% of the Sable foraging distribution). Furthermore, neither the Sable nor Hay seals foraged in the same areas as the Southwest colony. Most of the shared distributions between the Hay and Sable colonies occurred on the Eastern Scotian shelf, which is known to be highly productive (King et al., 2016). By contrast, the Southwest seals avoided this area, despite the fact that they have the capacity to exploit these same foraging grounds.

The difference between the larger overlap of the ranging distribution and the reduced amount of foraging overlap may have resulted from a couple of factors. First, it could suggest that foraging is underestimated by the discrete behavioural states. Our model (via behavioural state classification) is designed to identify areas that marine predators intensively exploit, likely because they are highly productive (Scales et al., 2014; Nowak et al., 2020), and this presumably lowers the cost-benefit ratio of foraging. However, there is evidence that grey seals also forage opportunistically along routes of transit (Austin et al., 2006), which our model likely cannot identify. Second, it is possible that the kernel utilization distribution slightly overestimated the overlap in the ranging distribution, because this method necessarily smooths over the tracking data. Comparison of the track predictions with the ranging distribution suggest that any overestimation is minimal (Figs 4.6, 4.8). Third, female grey seals may travel along similar routes to reach geographically distinct foraging grounds. Although the grey seals share up to 65% of their total habitat, the fact that they share less than 25% of their foraging habitat illustrates that a significant degree of

separation exists to suggest colony-specific foraging habitat.

The pattern of shared foraging habitat coincides with the colony-specific distributions of movement parameters. That is, the parameters of the Southwest seals, which did not exploit similar foraging patches to either the Hay or Sable colonies, significantly differed from the other colonies. By contrast, the parameters of the Hay and Sable colonies did not significantly differ, and the foraging patches of these females did overlap. Unexpectedly, the behavioural state classification appeared to be more driven by the mean turning angles θ_1 and θ_2 and less driven by the autocorrelation parameters γ_1 and γ_2 compared to the other colonies. This suggests that changes in the movement persistence along the Southwest seals' tracks are not as prominent as they are within the other colonies.

Although females from the Southwest colony appear to be most different with respect to foraging habitat and movement parameters, females from the Hay Island colony are the most different with respect to the foraging tactics we calculated. Under optimal foraging theory of central-place foragers, individuals that travel farther to search for prey should increase their time spent actively foraging within patches (Charnov, 1976; Friedlaender et al., 2016). This behaviour has been observed in several marine predators, including baleen whales (Friedlaender et al., 2016; Doniol-Valcroze et al., 2011) and sea birds (Boyd et al., 2014). Sable and Southwest seals on average exploited non-overlapping grounds that were a similar distance away from their respective colonies, which could be an indication that profitable foraging areas exist at similar distances from each of these two colonies. By contrast, Hay seals

exploited foraging patches significantly farther away from the colony than either the Southwest or Sable seals (Fig 4.9). However, they did not appear to compensate for increased distance by increasing their time spent foraging. In fact, it was females from the Sable Island colony that spent a significantly larger amount of time foraging once they were within a patch compared to either of the other colonies. The least cost distance does not take into account distance travelled and haulout behaviour or resting at-sea along a track. Future research on concurrent diet, total distance travelled, haul-out, and resting at-sea would provide more information related to energy expenditure that could help elucidate these relationships.

Chapter 5

Predicting Aquatic Animal Movements and Behavioural States in Continuous-Time From Acoustic Detections

5.1   Introduction

Telemetry is a staple technology used to track aquatic animals and infer how movement relates to physiology, life history, oceanographic and environmental constraints, and anthropogenic actions (Hussey et al., 2015; Hays et al., 2016; Lennox et al., 2017a). Acoustic telemetry has been instrumental for monitoring the movements of taxonomic groups like teleost fishes, elasmobranchs, and crustaceans that do not frequently surface or that cannot accommodate a large tag burden (Hussey et al., 2015; Lennox et al., 2017a). With acoustic telemetry, we can now track both large scale movements of individuals over extensive periods of time (years) and across oceans (McAuley et al., 2017), as well as fine-scale, high resolution movements restricted to small study areas (e.g., 1.5 km^2; Cote et al. 2019).

Acoustic telemetry consists of a two-part system wherein receivers record ID codes that are transmitted from tags typically either surgically implanted or externally attached to the study animals. A transmission can only be recorded by a receiver if

it originates within the receiver's detection range. When a receiver array is designed such that detection ranges overlap and a transmission can be detected at multiple receivers, algorithms based on the differences among arrival times of a single transmission at several receivers can be used to calculate positions of the tagged animals on a spatially continuous scale (e.g., Espinoza et al. 2011; Trancart et al. 2020; Baktoft et al. 2017). Positioning algorithms are often closed-source (but see Trancart et al. 2020), expensive if implementation is carried out by the manufacturer, and the output can contain large amounts of error (Roy et al., 2014; Baktoft et al., 2017).

A recently developed alternative to manufacturer positioning systems is the `R` package Yet Another Positioning Solver, or `YAPS` (Baktoft et al., 2017). This open source software fits a hierarchical (state-space) model to spatially discrete detections with two levels: a measurement process that captures the variability in the transmission arrival times at different receivers relative to their expected arrival times, and an unobserved movement process that assumes the underlying animal track follows a Wiener process (i.e., exhibits Brownian motion; Baktoft et al. 2017). For model fitting, `YAPS` utilizes the R package Template Model Builder (`TMB`), a highly effective framework for fitting multi-dimensional hierarchical models with random effects to animal movement data (Albertsen et al., 2015; Auger-Méthé et al., 2017; Jonsen et al., 2019). By accounting for stochasticity in both the measurement and movement processes, `YAPS` achieves greater precision in the location predictions compared to the (usually deterministic) classic time-difference-of-arrival methods like those provided by manufacturers (Baktoft et al., 2017).

State-space models (SSMs), including `YAPS`, have become a popular tool in ecology (Auger-Méthé et al., 2020), and have proven particularly useful in movement ecology for predicting true locations from data observed with measurement error (Jonsen et al., 2005; Johnson et al., 2008; Patterson et al., 2008; Pedersen et al., 2008; McClintock et al., 2012; Auger-Méthé et al., 2017). Another methodology that has seen significant parallel development within movement ecology is the hidden Markov model (HMM), which enables researchers to classify multiple discrete states influencing the parameters governing the movement process, and these can be inferred to reflect animal behaviour (Auger-Méthé et al., 2020; McClintock et al., 2020). Behaviours of interest may include residency, foraging, migration, travelling, circum-topographical exploration, or spawning (Patterson et al., 2009; Michelot et al., 2016; Whoriskey et al., 2017). Behavioural states can be readily predicted from data sampled at regular temporal intervals via discrete-time HMMs (Michelot et al., 2016; Zucchini et al., 2016), however, most aquatic research can only record movements at opportunistic (irregularly sampled) times. Irregular sampling, if incorporated into animal movement models, has often been integrated into the movement process through the use of differential equations (e.g., Johnson et al. 2008), or into the measurement process via linear interpolation (e.g., Jonsen et al. 2005; McClintock et al. 2012). Fewer studies incorporate it directly into the behavioural process (but see Parton and Blackwell 2017; Michelot and Blackwell 2019). When it is incorporated, standard machinery for HMMs typically cannot be used because the movement of an animal no longer

only depends on the current (active) state; this is called the snapshot principle (Patterson et al., 2017). However, rigorous testing of the snapshot principle with respect to animal movement has not been documented.

A few methods exist for predicting both behavioural states and location states within a single statistical model (Jonsen et al. 2005; Pedersen et al. 2008; McClintock et al. 2012, and see Chapter 4 of this thesis), which we call switching hierarchical models (SHMs). These efforts have traditionally focused on developing methods for satellite telemetry, and few methods exist specifically for acoustic telemetry detections. One exception is that of Dorazio and Price (2019), who developed a Bayesian SHM for Gulf sturgeon (*Acipenser oxyrinchus desotoi*), but this method was designed for linear movement throughout a river and was therefore formulated in one-dimensional space. In the two-dimensional case, HMMs have been directly fitted to positional data (Whoriskey et al., 2017), and to location predictions from SSM-filtered positional data (Cote et al., 2020). These methods necessarily involve multiple separate modelling steps, e.g., a positioning algorithm to obtain an animal path from the detections, potentially followed by data cleaning or filtering via one or more SSMs, and finally an HMM to obtain behavioural states. A methodology that can simultaneously predict behavioural and location states specifically from acoustic detections would provide a more parsimonious solution.

Our research fills this gap by advancing the `YAPS` methodology to predict behavioural states along an animal path that is predicted from a set of acoustic telemetry detections. Because positions are sampled in continuous-time, we employ a

continuous-time Markov chain to model the behavioural state evolution. For model fitting, we follow the iterative framework outlined in Chapter 4, which takes advantage of maximum likelihood theory in both the HMM and SSM paradigms to efficiently and accurately fit SHMs to animal movement data. We relax the snapshot assumption such that we can adapt standard HMM computational tactics and use simulations to evaluate the accuracy of our implementation. Model efficacy is demonstrated by fitting both two- and three-state models to approximately six days' worth of acoustic detections collected on a female carnivorous fish, the northern pike (*Esox lucius*), throughout Hald Lake, Denmark.

5.2 Methods

In accordance with the original character of Baktoft et al. (2017), we name our behavioural `YAPS` methodology "Yet Another hidden Markov model Solver", or YAMS for short. YAMS has three goals: 1) predict a spatially and temporally continuous path from a series of spatially discrete animal detections that are measured with error; 2) predict the sequence of behavioural states, and 3) estimate the parameters governing the animal movement and detection processes.

5.2.1 Study System

Our study system is Hald Lake in Denmark, which covers an area of approximately 3.4 km^2 with a mean and max depth of 13.1 and 31 m, respectively (Jeppesen et al., 1999). From April 2019 to February, 2020, 70 Thelma TBR 700 receivers were deployed over

the entire range of Hald Lake. Three species were tagged as part of a broader ecological study, including brown trout (*Salmo trutta*), European eel (*Anguilla anguilla*), and northern pike. We limit our analysis to detections from a single adult (length = 93.2 cm) female pike which was tagged with a Thelma D-HP9 tag (30.5 mm long × 9 mm diameter, ∼ 9 month duration) that transmitted at 71 kHz. Acoustic transmissions were programmed to occur at random times within a fixed interval of 10-30s to reduce collisions. Our data include this random sequence of numbers, but other datasets do not, either because of manufacturing errors or because the sequence is not readily accessible by the consumer.

5.2.2   Data Notation

Detection data are structurally complex. They require a combination of three data types: tag and receiver metadata, and logs of detections at each receiver, such that a single observation consists of a time-stamp associated with a receiver location and a tag ID (Whoriskey et al., 2019). Detections are limited by predefined receiver locations, and are thus spatially discrete and biased based on the study design. The probability of detection varies based on a variety of factors including time, environmental condition, and distance between the receiver and the tag; thus, true animal absence cannot be measured, and the meaning of presence is dynamic because it is recorded within a changing detection range. When detection ranges overlap, a single data unit (transmission) leads to multiple observations (detections).

With these idiosyncracies in mind, we introduce the following indices and notation.

Throughout, the index i will be used for a variable ordered in time and range from 1 to N. The integer N therefore denotes the total number of data units (transmissions), but not the total number of observations (detections). When indexed with a colon, e.g., $1 : N$, this entails all values including and between 1 and N. The index c denotes the coordinate axes, which in our case will be Eastings or Northings. Two indices will be used for behavioural states: j, and k, and these each range from 1 to m total state values (in our case, m will equal either 2 or 3). In a minor abuse of notation but for concision and ease of interpretability, r will be used to both denote the location of a receiver (in which case it will be subscripted by c), and to index a variable at a receiver (in which case r will be the subscript); a misconduct that is only mildly offensive because, within our study, locations are unique among receivers. Finally, bold characters denote vectors and matrices.

5.2.3 Model Definition

YAMS is an SHM that takes advantage of both the SSM and HMM paradigms. The full model that we wish to consider is:

$$
\text{Measurement} \;=\;
\begin{cases}
e_{r,i} = \tau_{r,i} - \mu_{r,i} \sim T_3 \\[2ex]
\mu_{r,i} = t_i + d_{r,i}\upsilon^{-1} \\[2ex]
d_{r,i} = \left(\sum_{c=1}^{2} \left(r_c - x_{c,i} \right)^2 \right)^{0.5} \\[2ex]
t_i = t_{i-1} + \Delta_i + \delta_i \\[2ex]
\delta_i - \delta_{i-1} \mid \delta_{i-1}, \delta_{i-2} \sim N(\delta_{i-1} - \delta_{i-2}, \eta^2)
\end{cases}
\tag{5.1}
$$

$$
\text{Movement} \;=\;
\begin{cases}
x_{c,i} \mid x_{c,i-1} \sim N\left(x_{c,i-1}, \left(2 \cdot D_{b_i} \cdot (t_i - t_{i-1}) \right)^{0.5} \right)
\end{cases}
\tag{5.2}
$$

$$
\text{Behaviour} \;=\;
\begin{cases}
Pr(b_i = k \mid b_{i-1} = j) = A_{j,k}(t_{i-1}, t_i)
\end{cases}
\tag{5.3}
$$

For quick reference all terms in the equations above are described in Table 5.1. Equations 5.1-5.3 demonstrate how this model is hierarchical with three levels that relate to either the measurement process of detecting the tagged animals using acoustic telemetry (Eqn 5.1), the movement of the animal (Eqn 5.2), or the mathematical states that are assumed to drive the movement process and that are interpreted as behaviours (hereafter, behavioural states; Eqn 5.3).

Measurement We observe $\tau_{r,i}$, the time that a transmission arrives at receiver r. Critically, this is distinguished from the time that the transmission originated at the tag, which we denote t_i. We calculate the distance between the receiver location r_c and unknown tag location $x_{c,i}$, where c denotes the appropriate coordinate axis, and represent this with $d_{r,i}$. Then, the expected travel time of a transmission is calculated

Table 5.1: Parameter definitions for the YAMS formulation.

Term	Definition
i	Index of observations ordered in time.
t_i	Irregularly observed time of origin of a transmission.
m	Number of behavioural states.
j, k	Indices for behavioural states.
c	Coordinate axis.
r_c	Receiver location indexed by coordinate axis; because locations are unique amongst receivers, r is used synonymously with receiver ID.
b_i	Behavioural state at time t_i.
$x_{c,i}$	Location of animal at time t_i in coordinate axis c.
$\tau_{r,i}$	Observed time that a transmission arrives at a receiver.
$\mu_{r,i}$	Predicted time that a transmission arrives at a receiver.
$e_{r,i}$	Error between the observed and predicted time of arrival of an acoustic transmission at a receiver.
T_3	A t-distribution with three degrees of freedom.
ω	Estimated scale parameter of T_3.
$d_{r,i}$	The distance between receiver r and the unobserved true location of the animal at time t_i. This is computed for all receivers and all transmissions.
Δ_i	Random temporal interval between transmissions t_{i-1} and t_i.
δ_i	Tag internal clock drift at time t_i to account for variability with t_i and Δ_i.
η^2	Variance for the random walk modelling the tag drift.
υ	Speed of sound. We keep this constant at 1465ms^{-1}.
D_{b_i}	Diffusion parameter of the animal movement process.
$\mathbf{Q}$	Generator matrix of the continuous-time Markov process.
$\mathbf{A}(t_{i-1}, t_i)$	Continuous-time analogue to the transition probability matrix.

from $d_{r,i}$ and the speed of sound υ, and this is added to t_i to get the expected time, $\mu_{r,i}$, that a transmission arrives at a receiver. In some implementations of `YAPS`, υ is modelled as a Wiener process or included as data; here, we assume that it is constant, i.e., $\upsilon = 1465\text{ms}^{-1}$. The stochasticity of the transmission time t_i depends on whether the random transmission interval Δ_i is known or not. When known, as is the case in our implementation, t_i is a sum of the previous transmission time t_{i-1}, Δ_i, and an internal clock drift δ_i that is modelled with a random walk on its first differences with

variance η^2. Finally, errors in the expected vs. observed times of arrival can originate from multiple sources including, for example, varying aquatic conditions affecting the speed of sound or physical obstructions causing the transmissions to "bounce" before reaching a receiver. This measurement error is accounted for by modelling the difference between the observed and expected transmission arrival times, $e_{r,i}$, as a scaled t-distribution with three degrees of freedom (T_3) and scale parameter ω, as in (Baktoft et al., 2017).

Movement The locations are assumed to follow a Wiener process (Eqn 5.2) with diffusivity parameter D_{b_i}, which emulates discrete-time random walks in continuous-time.

Behaviour Because the locations are modelled at irregular time intervals, we choose to model the behavioural states with a continuous-time Markov process. This process is governed by the generator matrix $\mathbf{Q}$:

$$\mathbf{Q} = \begin{pmatrix} q_{11} & q_{12} & \cdots & q_{1m} \\ q_{21} & q_{22} & & q_{1m} \\ \vdots & & \ddots & \\ q_{m1} & q_{m2} & & q_{mm} \end{pmatrix}, \tag{5.4}$$

that has dimension $m \times m$, with $q_{ii} = -\sum_{i,j \neq i} q_{ij}$, and all $q_{ij} > 0$ for $i \neq j$. The negatives of the diagonal elements, $-q_{ii}$ describe the rate of transition out of state i, i.e., an animal will remain in state i for an amount of time that is exponentially distributed with rate parameter $-q_{ii}$ and mean $-q_{ii}^{-1}$ (Ross, 1996). The off-diagonal

elements denote the rate of transitioning from state i to state j. Given that an animal switches out of state i, it will switch into state $j \neq i$ with probability $-q_{ii}^{-1} \times q_{ij}$ (Ross, 1996).

Maximizing the likelihood of a hierarchical model of the sort formulated in Eqns 5.1-5.3 is difficult because of large numbers of mixed-scale random effects (Altman, 2007; McKellar et al., 2015). Rather than attempting to maximize the full likelihood directly, we employ the procedure outlined in Chapter 4 to estimate parameters and predict random effects via iterative optimization of an HMM and SSM likelihood. We now describe the SSM and HMM likelihoods below.

5.2.4   State-Space Model Likelihood

Given predicted values of $\mathbf{x}_{1:N}$ that we treat as known, Eqns 5.2-5.3 are efficiently maximized with the likelihood of a continuous-time HMM (see Section 5.2.5), which we denote by $L_{HMM}(\Theta \mid \hat{\mathbf{x}}_{1:N})$, where Θ denotes the full parameter set of this likelihood. Then, given a known (predicted) sequence of behavioural states, the joint likelihood for Eqns 5.1-5.2 is

$$L(\Psi, \ \mathbf{x}_{1:N}, \ \boldsymbol{\delta} \mid \hat{\mathbf{b}}) = \prod_{i=1}^{N} \left\{ \left(\prod_{r} f(e_{r,i}) \right) f(\delta_i | \delta_{i-1}, \delta_{i-1}) \left(\prod_{c=1}^{2} f(x_{c,i} | x_{c,i-1}, \hat{b}_i) \right) \right\},$$
(5.5)

where $f(\cdot)$ denotes the appropriate probability distribution based on Eqns 5.1-5.2. Importantly, the expression above denotes the joint likelihood (conditional on $\hat{\mathbf{b}}$) of all of the parameters $\Psi = \{\eta^2, \ D_{b_{t_i}}\}$ and random effects $\{\boldsymbol{\delta}, \ \mathbf{x}_{1:N}\}$, and these random

effects must be integrated over their respective state-spaces in order to obtain the marginal likelihood necessary for maximum likelihood estimation of the parameters. That is, we optimize:

$$L_{SSM}(\Psi \mid \hat{\mathbf{b}}) = \int\limits_{\{\mathbf{x}_{1:N},\ \delta_{1:N}\}} \prod_{i=1}^{N} \left\{ \left(\prod_{r} f(e_{r,i}) \right) f(\delta_i | \delta_{i-1}, \delta_{i-1}) \left(\prod_{c=1}^{2} f(x_{c,i} | x_{c,i-1}, b_i) \right) \right\} d\{\mathbf{x}_{1:N},\ \boldsymbol{\delta}\}.$$

(5.6)

Because this integral is analytically intractable, we approximate it using the Laplace approximation as implemented in `TMB`.

5.2.5 Hidden Markov Model Likelihood

Throughout this paper we interchange discrete-time and continuous-time to refer respectively to regular and irregular sampling, as is pervasively adopted within the literature. In reality, observing any biological or ecological process in continuous-time is near-impossible, or at the very least practically infeasible; to do so would require technology capable of recording infinite observations at infinitesimally small temporal intervals. In practice, all animal movement data represent discrete-time realizations of continuous-time behavioural processes. Consistent with this doctrine, we stress that the continuous-time processes that we utilize enable the user to predict locations and behavioural states at the temporal intervals of our choosing, which in our case are irregular. With this philosophy in mind, we describe our continuous-time implementation of the forward and Viterbi algorithms, as well as our calculation of pseudoresiduals.

As part of our model implementation, we fit a continuous-time HMM. In the classic HMM framework (without temporal covariates; see e.g., Li and Bolker 2017), the probability

of switching from state j from one time unit to the next is independent of the sampling time because all of the temporal intervals are the same, and this probability is contained in the jth row, kth column element of the transition probability matrix, which we represent with $\mathbf{A}$. For a Markov process, the probability of switching from b_{i-1} to b_i at some point within the observed interval $[t_{i-1}, t_i)$ is not independent of the sampling time, but it can be derived from the generator matrix $\mathbf{Q}$. The Kolmogorov differential equations give us the relationship between the transition probabilities from times t_{i-1} to time t_i, which we denote with $\mathbf{A}(t_{i-1}, t_i)$ (analogous to the discrete-time case), and $\mathbf{Q}$.

$$\mathbf{A}'(t_{i-1}, t_i) = \mathbf{A}(t_{i-1}, t_i)\mathbf{Q}. \tag{5.7}$$

This is the Kolmogorov forward equation in matrix form in continuous-time (Ross, 1996), which has the solution:

$$\mathbf{A}(t_{i-1}, t_i) = e^{\mathbf{Q} \times (t_i - t_{i-1})} \tag{5.8}$$

Thus, for an irregular time interval (t_i, t_{i-1}), we now have $Pr(b_i = k \mid b_{i-1} = j) = A_{j,k}(t_{i-1}, t_i)$. We directly substitute these probabilities into the calculations for the forward and Viterbi algorithms, as well as for the pseudoresiduals (Zucchini et al., 2016). That is, the $m \times 1$ vector of forward probabilities, $\boldsymbol{\alpha}_i$, that contains the joint probabilities of being in each state at time t_i and observing all data from time t_1 to t_i, is calculated recursively as

$$\boldsymbol{\alpha}_i = \boldsymbol{\alpha}_{i-1}\mathbf{A}(t_{i-1}, t_i)\mathbf{P}(\hat{\mathbf{x}}_i) \tag{5.9}$$

as in (Lu, 2017) where $\mathbf{P}(\hat{\mathbf{x}}_i)$ denotes the diagonal matrix with diagonal entries equal to

$f(\hat{\mathbf{x}}_i \mid \hat{\mathbf{x}}_{i-1}, b_i)$, determined by Eqn 5.2. We carry these calculations through to time t_N as

in the forward algorithm (Zucchini et al., 2016) to obtain the likelihood L_{HMM} as

$$L_{HMM}(\Theta \mid \hat{\mathbf{x}}) = \boldsymbol{\alpha}_N \mathbf{1} \tag{5.10}$$

$$= \boldsymbol{\pi}' \mathbf{A}(t_1, t_2)\mathbf{P}(\hat{\mathbf{x}}_2)\mathbf{A}(t_2, t_3)\mathbf{P}(\hat{\mathbf{x}}_3) \cdots \mathbf{A}(t_{N-1}, t_N)\mathbf{P}(\hat{\mathbf{x}}_N)\mathbf{1}, \tag{5.11}$$

where Θ denotes the full set of parameters governing the movement and behavioural pro-

cesses in Eqns 5.2 - 5.3, $\mathbf{1}$ is a column vector of size m with all elements $= 1$, and $\boldsymbol{\pi}$ is

the initial distribution, i.e., the kth element corresponds to $Pr(b_1 = k)$. We set $\boldsymbol{\pi}$ equal

to the stationary distribution of the continuous-time Markov chain which gives the limiting

proportion of time spent in each state (Cox and Miller, 1965), and can be interpreted as an

activity budget of the study animal (Lawler et al., 2019).

We implement the Viterbi algorithm in continuous-time in order to determine the most

likely sequence of hidden states given the model parameters by locally and recursively max-

imizing path segments from b_{i-1} to $b_i \forall i$ (Forney, 1973; Zucchini et al., 2016). Instead of

maximizing the posterior probability of the full path, $Pr(\mathbf{b} \mid \hat{\mathbf{x}}_{1:N})$, the algorithm equiva-

lently maximizes the joint probability of the observations and all possible behavioural state

sequences $Pr(\mathbf{b}, \hat{\mathbf{x}}_{1:N})$, which is more conveniently expressed by

$$Pr(\hat{\mathbf{x}}_{1:N} \mid \mathbf{b})Pr(\mathbf{b}) = Pr(b_1) \prod_{i=2}^{N} Pr(b_i \mid b_{i-1})Pr(\hat{\mathbf{x}}_i \mid b_i). \tag{5.12}$$

Maximizing this over all possible $\mathbf{b}$ would require m^N calculations; the Viterbi algorithm

reduces the computation time to be linear in N by recognizing that we need only maximize

$Pr(b_i \mid b_{i-1})Pr(\hat{\mathbf{x}}_i \mid b_i)$ for each i over all possible b_{i-1} (Forney, 1973; Zucchini et al., 2016). Because the transition probabilities of the Viterbi algorithm need not be time invariant (Forney, 1973), we again directly substitute the appropriate elements of $\mathbf{A}(t_{i-1}, t_i)$ wherever $Pr(b_i \mid b_{i-1})$ is required. Similarly to other continuous-time switching animal movement implementations (e.g., Parton and Blackwell 2017; Michelot and Blackwell 2019), our likelihood enables switches between states to occur outside of the discretely sampled observation times. Unlike these other approaches however, we do not concern ourselves with predicting the times that the switches occur, rather we focus our state predictions on the sampling times (i.e., the initiation times of the transmissions). Furthermore, our approach does not allow for multiple behavioural state switches between observation times.

Finally, we use forecast pseudoresiduals (z_i) to assess model validity. If the model is appropriate for the observed data, then $z_i = \Phi^{-1}\Big(Pr(\hat{\mathbf{X}}_i \leq \hat{\mathbf{x}}_i \mid \hat{\mathbf{X}}_{1:i-1} = \hat{\mathbf{x}}_{1:i-1})\Big)$, where Φ^{-1} is the inverse cumulative standard Normal distribution function, should be distributed as a standard Normal distribution (Zucchini et al., 2016). In order to calculate z_i, we require $Pr(b_i = k \mid b_{i-1} = j)$, which we obtain from $\mathbf{A}(t_{i-1}, t_i)$ and substitute directly into the standard pseudoresidual calculation (Zucchini et al., 2016):

$$z_i = \Phi^{-1}\left\{ \frac{\boldsymbol{\alpha}_{t-1}\mathbf{A}(t_{i-1}, t_i)\mathbf{F}(\hat{\mathbf{x}}_i)\mathbf{1}}{\boldsymbol{\alpha}_{t-1}\mathbf{1}} \right\}, \tag{5.13}$$

where $\mathbf{F}(\hat{\mathbf{x}}_i)$ is a diagonal matrix with entries equal to the cumulative distribution function of the observations given the current behavioural state. In practice, because each $\hat{\mathbf{x}}_i$ is multidimensional where the coordinate axes are assumed to be independent of each other, the pseudoresiduals are calculated for each coordinate axis separately. Importantly, these residuals are dependent on the accuracy of the location state predictions, $\hat{\mathbf{x}}$. As a result,

they can only be used to validate the model fit from Eqns 5.2-5.3, and cannot be used to assess validity of Eqn 5.1.

5.2.6   Model Fitting

In practice, we carry out the iteration as follows. To optimize the SSM step, we require a known sequence of behavioural states. To optimize the HMM step, reasonable location values are necessary. As a result, to initialize the optimization we could either treat a randomly generated sequence of behavioural states as known, or we need to obtain initial values of the locations in continuous space. We choose the latter option, and achieve this by fitting a one-behaviour SSM (`YAPS`) to the observed data. A HMM according to Eqn 5.11 (Section 5.2.5) is then fitted to these initial values, from which we obtain behavioural state predictions and estimates of Θ. The behavioural state predictions are then treated as known in the SSM step (Eqn 5.6). In Chapter 4 the movement parameters were also fixed during the SSM step; however, in this implementation we achieved better performance by treating the D_{b_i} as unknown during both the HMM and SSM steps. We run the iteration for a fixed number of steps, and following the implementation of Chapter 4, assume that the parameter estimates from the iteration with the maximum $L_{SSM}(\hat{\Psi}_{MLE} \mid \hat{\mathbf{b}})$ (the likelihood of the SSM step evaluated at the maximum likelihood estimates of the parameters) represent the global maximum because this theoretically corresponds to the parameter set that is most likely given the observed data. In practice, all calculations are performed on the negative log scale.

We additionally note that while we iterate between the two likelihoods in Eqns 5.11 and 5.6, two other optimizations occur in order to predict the random effects. For the location and drift states, the optimization is nested within the marginal likelihood calculations via

`TMB`; for the behavioural states, it is implemented via the Viterbi algorithm *ex post*. Eqns 5.11 and 5.6 show clearly that we are iterating between the maximization of two conditional likelihoods, which is a frequentist analogue to many Bayesian implementations of Markov Chain Monte Carlo simulations, where proposed samples are iteratively obtained from many conditional distributions (e.g., Parton and Blackwell 2017).

5.2.7   Analysis

We fitted YAMS to approximately six days' worth of data collected on an adult female pike tracked throughout Hald Lake in summer, 2019. Because many detections occur for a single transmission, and because the transmission interval is often small compared to the temporal scale of the study (in our case, 10-30 seconds), a relatively short study duration can yield a large dataset. For example, in our analysis approximately 6 days of monitoring a single pike resulted in 144,625 detections from 25,000 transmissions. Given that for N transmissions, there are $4N$ random effects in our model, analyzing a dataset of this magnitude is difficult. We therefore broke the dataset into groups of 5,000 transmissions, and fitted YAMS to each group, with both two and three behavioural states. For each group, we ran the model for 10 steps.

To carry out a proper simulation study (see below), we required an estimate of the detection efficiency. The terms detection efficiency and detection range are related, and in practice are often used interchangeably. Range and efficiency both describe the relationship between the probability of detection at a receiver and distance to the tag; we refer to a receiver's range when distance is the variable of interest, and its efficiency when the response is the probability of detection. We calculated the efficiency based on model results as follows: first, we computed all distances between each location of the predicted track

and all receivers. We then binned these into groups based on 5m intervals of distance, and calculated the proportion of receivers that registered a tag transmission. We fitted a binomial generalized additive model to these data to quantify the detection efficiency throughout the entire lake.

5.2.8 Simulation and the Snapshot Principle

When fitting continuous-time HMMs, it is necessary to consider whether the snapshot principle holds, which is the assumption that the observed movement of an animal is only dependent on the active behavioural state (Patterson et al., 2017). In our implementation, we relax the assumption of the snapshot principle in order to utilize computationally efficient machinery for approximating the likelihood and predicting the behavioural states. To assess the validity of our approximation, we designed the following simulation study.

We simulated 30 tracks using the estimated parameters of the first group of 5,000 transmissions. First, we simulated 4999 transmission intervals from a Uniform distribution with limits of 10 and 30 seconds, and 5000 tag drift times. Then, we simulated the embedded Markov chain, i.e., the discrete chains of holding times within states and jumps to the next state. With this embedded chain, we acquire the behavioural switching times, which determine the active behavioural state at each observation time, i.e., it simulates the 5000 behavioural states. To test our approximation, we combined the behavioural switching times with our observation times (and the corresponding states at switching with our behavioural state sequence), and simulated the animal locations based on these augmented sequences. Once the full movement path (of 5000+ locations) was simulated, we removed the locations and behavioural states corresponding to the exact switching times in order to simulate the effect of the unobserved and unaccounted for behavioural switches. From

Table 5.2: Three sets of results for the two- and three-state models fitted to each of the five groupings of the pike dataset. In the first set, the results for D_{b_i} estimated by the HMM are reported, which govern the movement of the animal. The second set depicts the activity budgets of the animal, as determined by the stationary distribution. The third set is the mean time spent within a state as determined by the diagonal entries of the generator matrix.

		Group 1	Group 2	Group 3	Group 4	Group 5
	Two-State Model					
	State 1	0.97	2.03	0.36	1.38	1.05
	State 2	20.76	18.51	11.45	13.63	14.02
D_{b_i}	**Three-State Model**					
	State 1	0.19	0.74	0.16	0.23	0.25
	State 2	3.69	11.88	1.42	1.39	3.59
	State 3	24.75	23.70	13.32	17.03	27.78
	Two-State Model					
	State 1	0.56	0.65	0.59	0.74	0.78
	State 2	0.44	0.35	0.41	0.26	0.22
π_i	**Three-State Model**					
	State 1	0.27	0.59	0.38	0.38	0.63
	State 2	0.41	0.20	0.29	0.38	0.26
	State 3	0.32	0.21	0.33	0.24	0.11
	Two-State Model					
	State 1	11.51	12.61	13.83	22.00	15.47
	State 2	9.15	6.78	9.67	7.85	4.47
$-q_{ii}^{-1}$	**Three-State Model**					
	State 1	4.91	8.39	8.28	13.85	15.20
	State 2	5.78	2.78	3.86	9.28	4.69
	State 3	11.68	60.95	8.95	8.27	8.20

here, we randomly placed the track within the lake and calculated the distances from every location to each hydrophone. In order to get a realistic representation of whether or not a receiver would have detected the animal or not, we used the detection efficiency model results to predict the probability that each receiver would have detected the simulated track based on these distances, and then we simulated a detection at each receiver with a Bernoulli trial. Finally, we fitted YAMS to each simulated dataset, and quantified the root mean squared error of the parameter estimates as well as the behavioural state accuracy as

the proportion of behavioural states correctly identified (see Chapter 4).

5.3   Results

5.3.1   Pike Dataset

We fitted models that assumed both two and three states to the pike dataset (Table 5.2). According to QQ plots of the pseudoresiduals, both models appeared to fit well (Fig B.1). Table 5.2 displays the estimated D_{b_i} for each model for the full pike dataset. Increasing state values correspond to increasing levels of dispersion, such that larger state values can be interpreted as "faster" movement relative to smaller state values. For comparison across groups, we will interpret any $D_{b_i} < 10$ as slow movement, $10 \leq D_{b_i} < 20$ as medium speed movement, and $20 \leq D_{b_i}$ as fast. The two-state model identified a slow state for all five groups. Fast movement was identified for the first group, while the other four groups included a medium speed state. For this model, the slow state was observed along most of the track (56-78% of the time), as determined by the activity budgets and the mean durations spent within a state (Table 5.2). The three-state model identified at least one slow state. Four of the five groups identified a second slow state, coupled with either a medium speed state (groups 3 and 4) or a fast state (groups 1 and 5). Group 2 identified both a medium speed state and a fast state. This model generally produced results consistent with the two-state model, e.g., it also suggested that the pike spent most of its time in a slow state (noting that multiple slow states were observed for most groups; Table 5.2).

Fig 5.1 reproduces the path of the pike coloured by behavioural state. For the duration of the analyzed data, the pike travelled throughout the Southwest portion of the lake. It appeared to exhibit higher speeds on the outer perimeter of the lake, and slower speeds
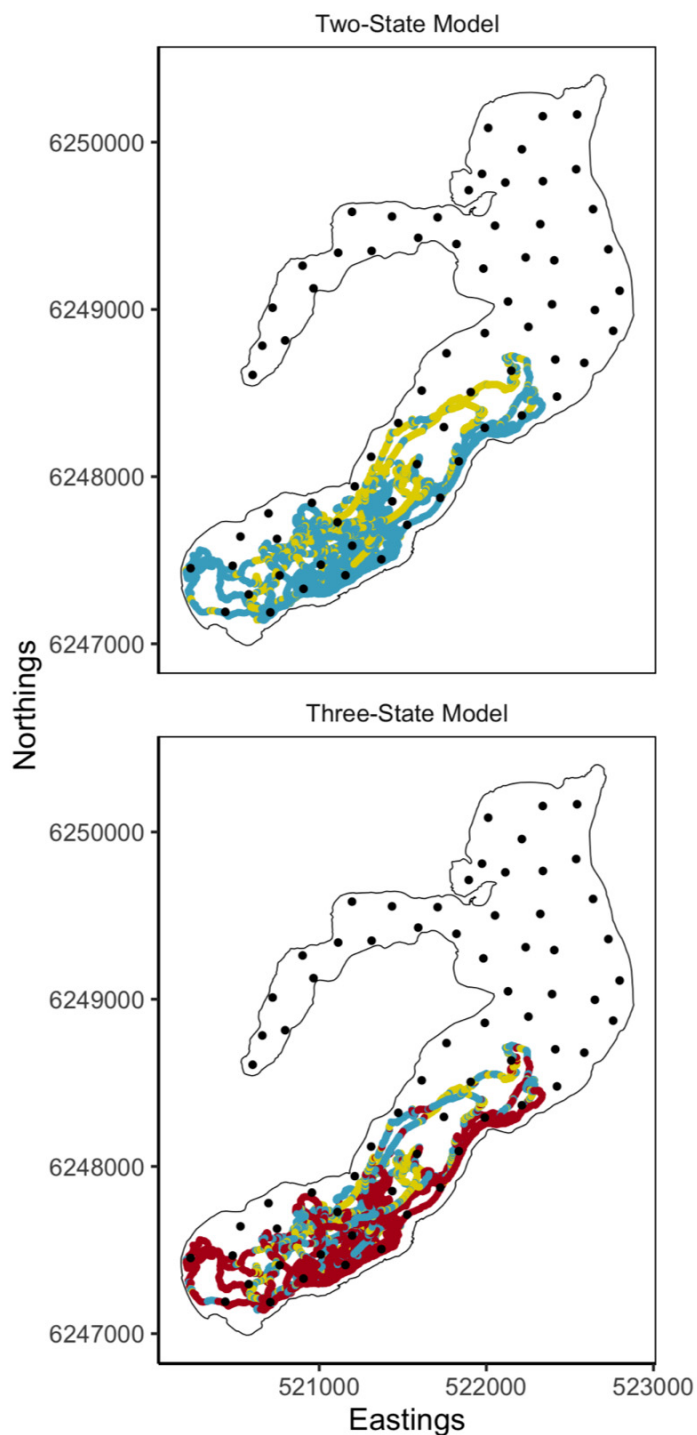
Figure 5.1: Compiled model track and behavioural state results from fitting YAMS to a set of acoustic detections collected on a female pike over six days in Hald Lake, Denmark, which covers an area of approximately 3.4 km². Top includes results from the two-state model, while bottom contains the results of the three-state model. Yellow, blue, and red colours denote behavioural states 1, 2, and 3, respectively. Within a model result, increasing values of the behavioural states denote increasing dispersion.

towards the interior.

The increasing values of D_{b_i} correspond well with the observed speeds of the animal (Fig 5.2, 5.3). The distribution of speeds changed over data group, which can be seen from the variability in the observed ranges of speeds in Figs 5.2 and 5.3. This also corresponds with the dynamic values of Table 5.2. Greater segregation was observed among states in the two-state model compared to the three-state model (Fig 5.2; Table 5.2).
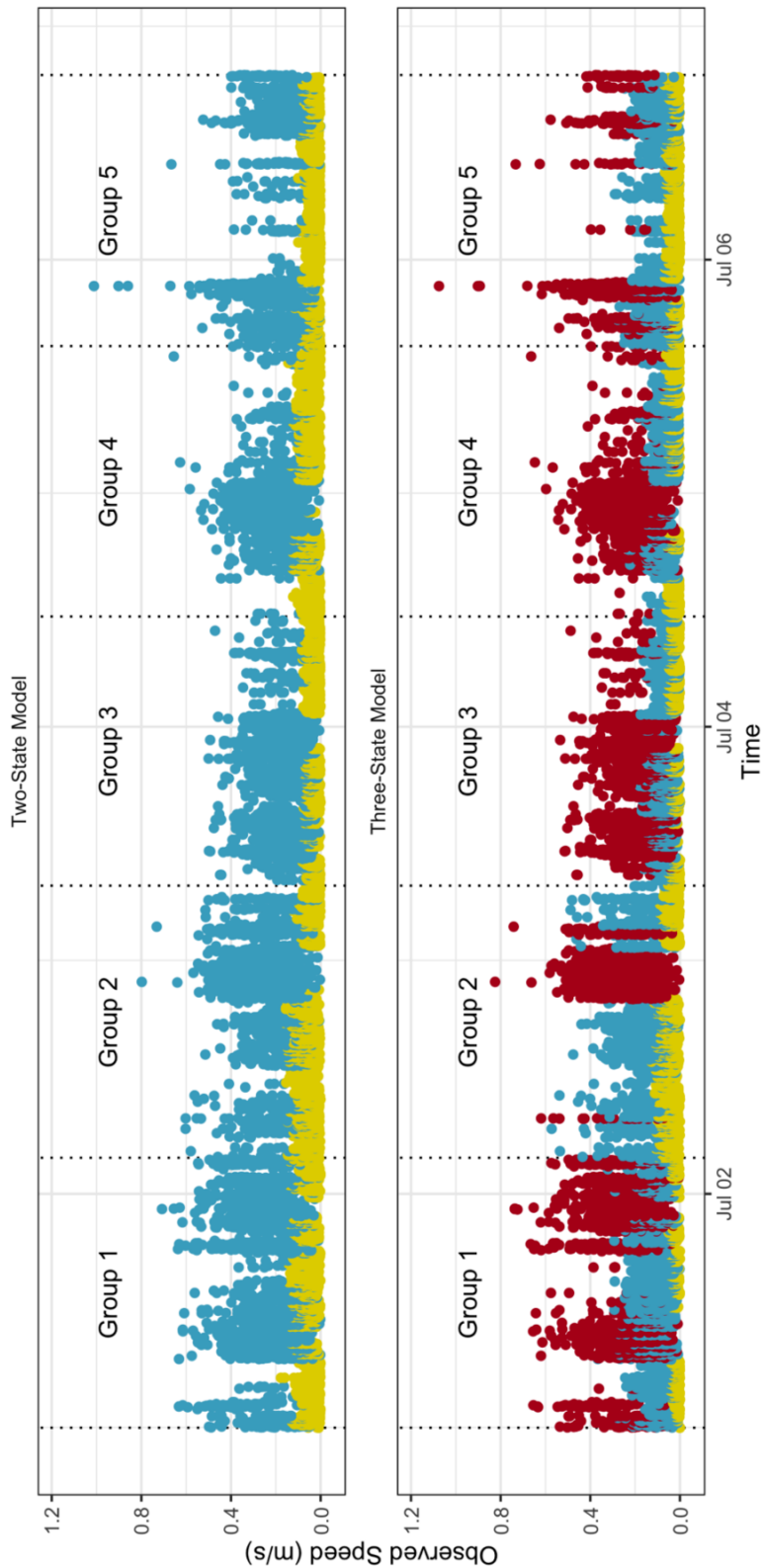
Figure 5.2: Observed pike speed over time calculated from location and time of transmission predictions for both the two-state (top) and three-state (bottom) models. Yellow, blue, and red colours denote behavioural states 1, 2, and 3, respectively. Within a model, increasing values of the behavioural states denote increasing dispersion. Dotted lines separate the time series by the data groups that were used to fit the models.
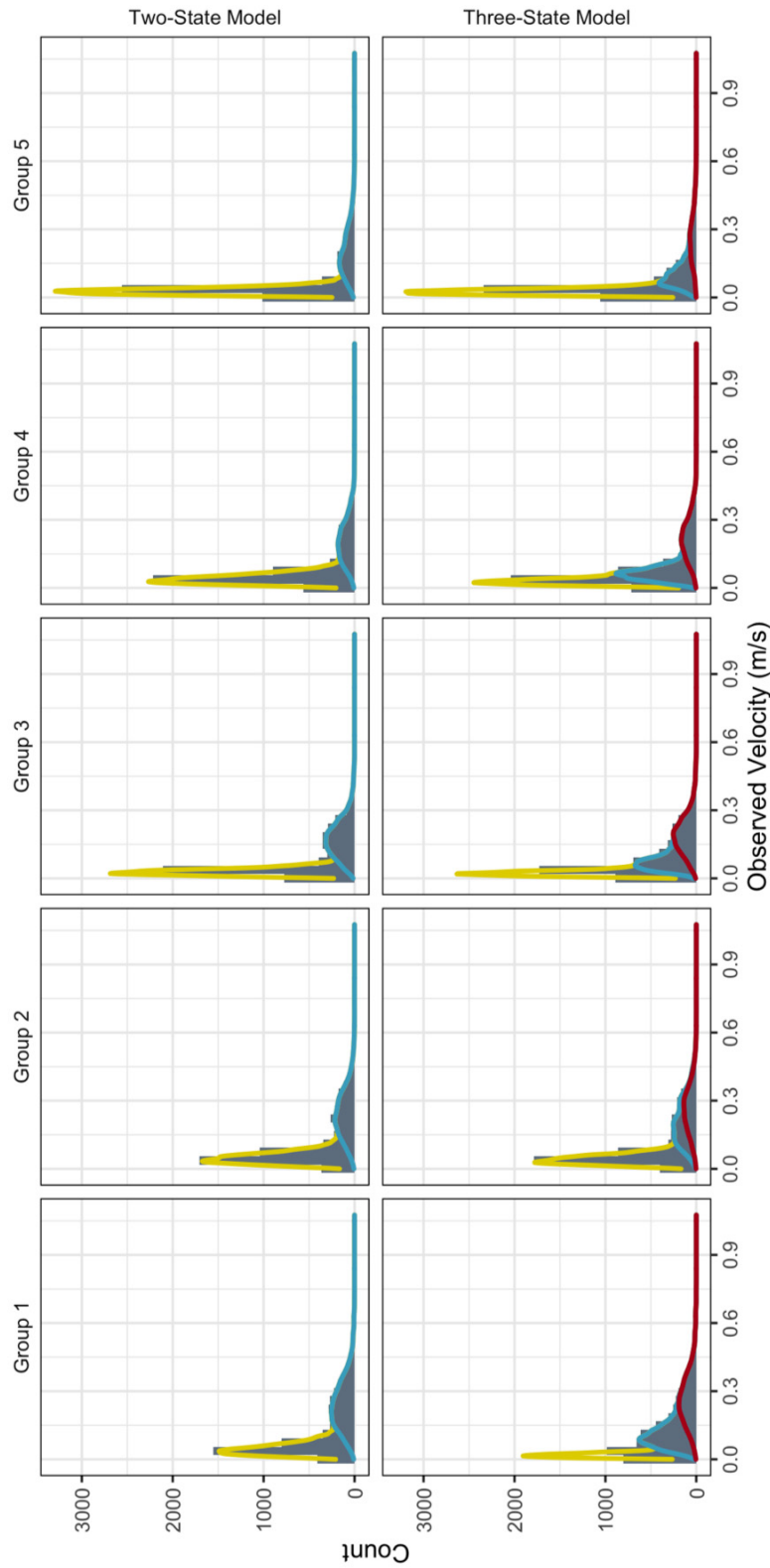
Figure 5.3: Histograms of the observed speeds of the pike calculated from the location and time of transmission predictions for both the two-state (top row) and three-state (bottom row) models. Overlaid stacked densities correspond to the density of the observed speeds within each behavioural state, and have been scaled to align appropriately with the histograms. Yellow, blue, and red colours denote behavioural states 1, 2, and 3, respectively. Within a model result, increasing values of the behavioural states denote increasing dispersion. Column facets separate the data by the groups that were used to fit the models.

5.3.2 Simulation Study

We used the GAM depicted in Fig 5.4 to simulate the detections of an animal throughout the lake given an underlying movement path. These results showed that detection efficiency dropped rapidly and non-linearly within the lake, with predicted detection probabilities of 0.74, 0.42, and 0.08 at distances of 100, 250, and 500 m from the receiver. Although other models were considered (e.g., mixed effects models to account for within-receiver variability), our model that considered the variability in detection efficiency to be constant throughout space was determined to fit the best based on cross-validation with 70% training and 30% testing datasets.

We fitted YAMS to 30 simulated tracks under both a two-state and three-state scenario. Within each simulation study, 12 of the models either exhibited false convergence, or did not converge at all. These results were removed from further analysis. The simulation study of the two-state model showed high levels of accuracy, with a mean behavioural state accuracy of 0.94 (Fig 5.5). Location state accuracy was also high, with an average RMSE of 1.29 and 1.34 m in the Eastings and Northings axes, respectively. The simulation study of the three-state model showed lower levels of accuracy than the two-state model in the behavioural state prediction, with an average proportion of 0.79 of the behavioural states being correctly classified. However, the three-state model achieved higher precision in the location state predictions, with average Easting and Northing RMSEs of 1.28 and 1.29 m (Fig 5.5). Parameter results were also precise, as documented by Tables C.1, C.2.
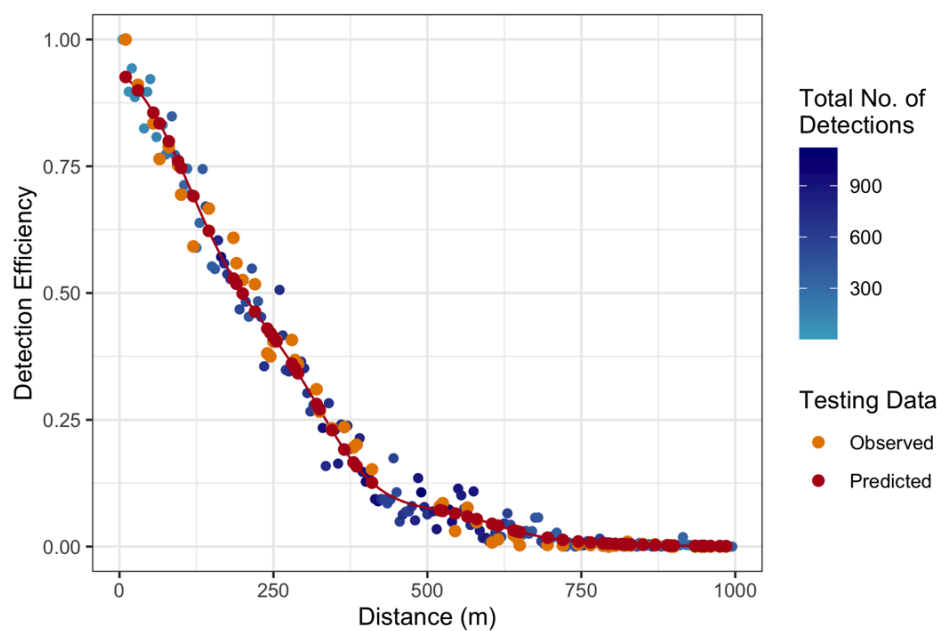
Figure 5.4: Results from a binomial-response generalized additive model fitted to detection efficiency data derived from the YAMS predicted pike locations. Efficiency was calculated for every 5m interval. Training data (70%) used to fit the model are depicted in blue where the shade of blue denotes the number of detections used in the calculation. The red line shows the fitted values from the model. Orange points are the data used in testing the model (30%), while the red points are the corresponding fitted values.
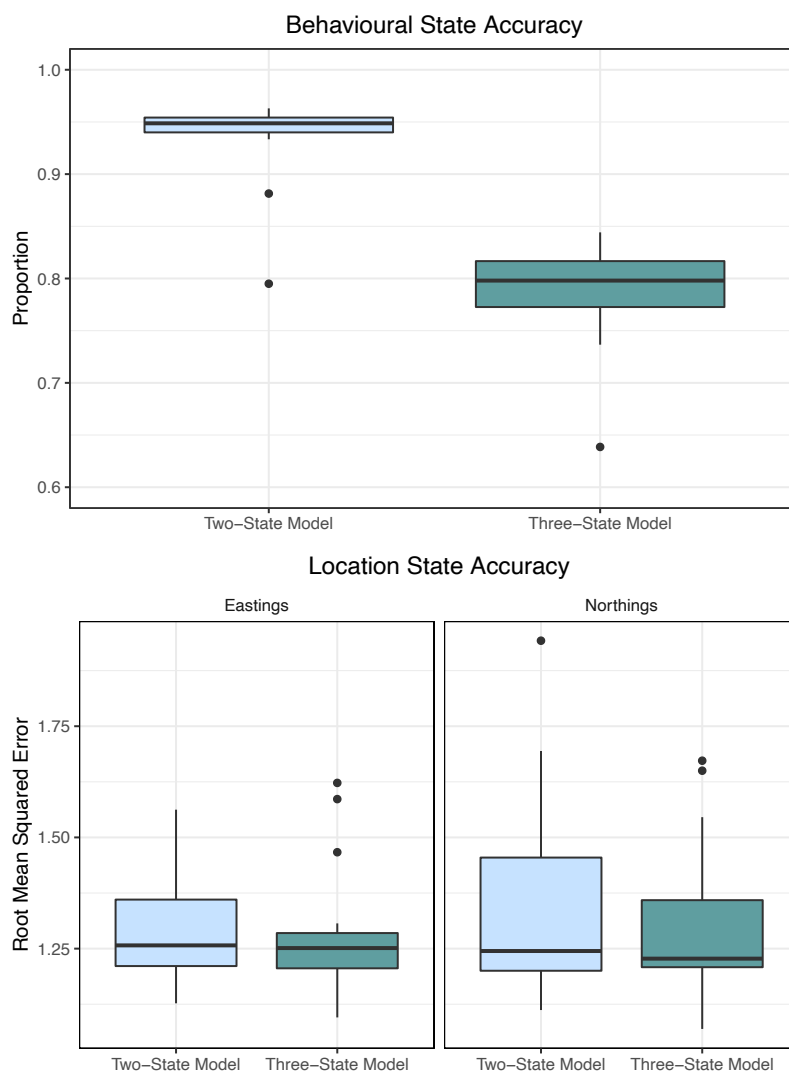
Figure 5.5: Results from fitting YAMS to 18 simulated animal tracks based on results from the first group of data. Top: behavioural state accuracy, calculated as the proportion of correctly identified states. Bottom: location state accuracy, calculated as the root mean squared error (RMSE; m) in both the Eastings and Northings axes. Blue and green results denote the two- and three-state models, respectively.

5.4 Discussion

This research combines the existing SSM of `YAPS` used to generate fine-scale positioning predictions with the iterative model fitting framework of Chapter 4 to develop a novel SHM designed specifically for acoustic detections. By incorporating a latent Markov chain into the existing `YAPS` formulation, a researcher need not depend on positioning algorithms from manufacturers, which can be expensive and contain larger amounts of error, and they can conveniently utilize the same model likelihood that predicts the location states to predict the behavioural states. We demonstrated the capabilities of this model to identify multiple behavioural states of a predatory fish, and tested its accuracy using simulation studies. Several decisions were made during model fitting that impacted the results.

To maintain consistency with `YAPS`, we chose a relatively simple process to model animal movement. The movement parameter D_{b_i} of the Wiener process governs the dispersion of an animal in any direction. More extensive information on how movement evolves through time might be determined by incorporating more complex models of movement. For example, using an Ornstein-Uhlenbeck process on the velocities, rather than a Wiener process on the locations, could allow for estimation of drift or home range tendencies and autocorrelation within the track (Johnson et al., 2008; Pedersen and Weng, 2013). Alternatively, modelling the step lengths and turning angles as separate continuous-time processes could provide more easily accessible interpretations of movement in continuous-time (Parton and Blackwell, 2017). In our pike analysis, we found that the relatively simplistic Wiener process was sufficient to accurately identify behavioural states that corresponded well to differences in the observed speed of the animal (Fig 5.3). Future research might benefit from investigating the utility of more complex movement models, however, other researchers have rationalized

the deliberate use of rather simplistic models in order to provide speedy and accurate results (Jonsen et al., 2020). The choice of a movement model will likely always depend on the interpretability and complexity of the mathematical equations used to describe the animal movement, as well as the ultimate ecological goal of the research.

When fine-scale positioning of acoustically tagged animals is a primary research goal, smaller transmission intervals and extensive receiver coverage over the entire study area will often result in extremely large datasets. In our case, approximately six days' worth of observation on a single pike resulted in 25,000 transmissions. We were unable to fit a single model to the full dataset because of computational limitations, therefore we split the dataset into five groups of 5,000 transmissions each for model fitting. Consequently, we obtained five different parameter sets for each of the two- and three-state models. Thus, the meanings of the movement parameters D_{b_i} were dynamic, and in some cases, resulted in different interpretations of the states across time. For example, the third state of the three-state model changed from a fast state in groups 1 and 2 to a medium speed state in groups 3 and 4 and then back to a fast state in group 5. For the two-state model, this effect appeared to be minimal, because the estimated D_{b_i} remained relatively constant over the five groups (Table 5.2). However, the dynamic effect on the three-state model was greater, for example as larger values of D_{b_i} were estimated for state 2 towards the beginning and end of the track (Table 5.2).

YAMS requires an ancillary stochastic step that we did not describe within this paper because it was not altered from the original implementation in YAPS. Both the receivers and tags of acoustic telemetry contain time keeping mechanisms, and these mechanisms experience drift. Small values of drift, even microseconds, can lead to error in position estimates on the order of meters because of the rate at which transmissions travel (speed

of sound). Although we account for drift in the tag clocks within the YAMS measurement process (Eqn 5.1), accounting for drift in the receiver clocks must also be achieved, and we did this prior to fitting the movement models by using an SSM (via YAPS) to synchronize the receiver clocks (Baktoft et al., 2019). Receiver synchronization, whether it is achieved by an SSM or other tactic, is typically required regardless of which method is used to generate positional estimates from acoustic detections (e.g., Smith 2013). Therefore, our model remains statistically more parsimonious compared to fitting an SSM to predict locations and then a separate HMM to predict behavioural states. The reader is referred to the guide of Baktoft et al. (2019) for further information on synchronizing the receiver clocks, and how to implement this step using YAPS.

In our continuous-time HMM formulation we are allowing the behavioural process to switch between sampling times. However, in our movement process, we specify that the location of an animal at time t_i is only dependent on the behavioural state at time t_i. For those occasions where the behavioural state switches between sampling times, the movement-behaviour dependence is not precise, because the movement of the animal depends on the behaviours at both the current and the previous sampling times ($b_{t_{i-1}}$ and b_{t_i}). This is called the snapshot principle (Patterson et al., 2017). To precisely model movement when the switches occur, the times of switches would have to be predicted. This has been done in Bayesian formulations (Parton et al., 2017; Michelot and Blackwell, 2019). Instead, we relaxed the snapshot assumption such that we could use HMM and SSM likelihood machinery available through TMB to approximate our likelihood around the times of switches, and take advantage of this platform's relative speed compared to sampling techniques (Auger-Méthé et al., 2015; Whoriskey et al., 2017). However, we specifically designed our simulation studies to measure the error in our model fitting procedure incurred in part by this approximation.

The results of our studies showed high levels of accuracy for the behavioural and location states, suggesting that our model is accurate despite relaxing the snapshot assumption. This is likely because the temporal resolution of our data (observations occurring randomly every 10-30s) is fine relative to the scale of the behavioural states that we are predicting. Longer transmission intervals (e.g., 60-120s is frequently used) might incur larger amounts of error, therefore future researchers endeavouring to use this implementation should carefully consider the temporal scales of their inferred behaviours relative to their observations and re-evaluate the snapshot principle with simulation studies when necessary.

The simulation studies showed a high level of accuracy attained by both the two- and three-state models. We did have to omit approximately one third of the simulated tracks based on false or lack of convergence. This was surprising because we encountered this very infrequently during model fitting on the real data (we had false convergence for one out of ten iterations when fitting the two-state model to the first group, and for two out of ten iterations when fitting the three-state model to the fourth group), but may be explained by the fact that sometimes simulations cannot fully capture the variability inherent to real-life scenarios. When it is not possible to eliminate problematic tracks (e.g., when analyzing real data), researchers may successfully fit models with TMB if they change starting values either by adding a small amount of random noise or by selecting an entirely new set.

Interestingly, the three-state model more accurately predicted the location states, but less accurately predicted the behavioural states compared to the two-state model. Contrasting estimates of behavioural state accuracy under different numbers of assumed states exist in the literature. For example, Lawler et al. (2019) compared the ability of two different HMMs (one with autocorrelation in the step lengths, the other without) to accurately

predict states under both a two- and three-state scenario. Although the model with auto-correlation performed worse with three states, the model without performed better (Table 3; Lawler et al. 2019). Our case might be explained by the fact that the three-state model did involve considerably more switches (136-209; numbers varied because of the five groups of data) among behavioural states than the two-state model (92-136). Although it does not seem unreasonable that more states and more switches could result in larger amounts of error, it is also possible that this error resulted from our approximation in likelihood around the times of switches. However, we are unable to answer this question because our simulation studies were unable to separate error inherent to the behavioural state prediction from error specifically incurred by relaxing the snapshot assumption. Increasing error could also be explained by the fact that the three-state model most often predicted two slow states for each group, thus reducing the separation in D_{b_i} that drives the state classification. Regardless of the causes, our simulation studies illustrate an interesting trade-off between location and behavioural state accuracy when deciding which model to use for ecological interpretation. Although this result is specific to YAMS, future studies may want to investigate whether a trade-off in accuracy occurs while fitting other SHMs to animal movement data.

We now offer interpretations of the two-state rather than the three-state model with respect to pike ecology. We base this decision on 1) the average increase of 15% behavioural state accuracy in the two-state model, 2) the relatively increased segregation of the two-state movement parameters and observed speeds among groups compared to the three-state model, and 3) the dynamic nature of the behavioural states among groups.

Pike are commonly referred to as sit-and-wait predators (Eklöv, 1997). Lab experiments have shown that pike often remain stationary, watching and then ambushing prey

when they come within range (Savino and Stein, 1989; Harper and Blake, 1991). They additionally suggest that pike will often track their prey slowly with an elongated posture before attacking (Harper and Blake, 1991). During prey capture attempts, acceleration can reach up to 96 ms^{-1} (Harper and Blake, 1991). During escape, acceleration can be even higher (120 ms^{-1}; Harper and Blake 1991), thus, both behaviours are energetically costly (Frith and Blake, 1995). In this study, we were able to classify slow, medium, and fast rates of movement of our single northern pike. It is unlikely that our fast state identified acute hunting or predator avoidance for three reasons. First, these events are nearly instantaneous, and our observed speeds did not reach those that have been previously documented for these behaviours. Here, our maximum observed speed was ~ 1.15 ms^{-1}, compared to maximum speeds of ~ 3 and ~ 4 ms^{-1} for predatory and escape behaviours, respectively (Harper and Blake, 1991). Second, the fast behaviour had a large variability in observed speed, including values that might suggest stationary movement (Fig 5.2). Third, the fast behaviour was persistent, i.e., the pike was observed to remain within this behaviour for an extended period of time ($\sim$ 5-10 mins; Table 5.2), therefore it is unlikely that this animal was consistently hunting or avoiding predators during these time periods given the energetic cost (Frith and Blake, 1995). Rather, it is more likely that the fast behaviour is documenting exploratory travel throughout the lake, which could include either of the above rapid response behaviours.

We offer two explanations for the slow behaviour. This state did not identify stationary behaviour by itself, which is made evident by the fact that speeds within this state were observed to be >0 ms^{-1}, and the pike was observed to still be covering distance while within this state (Fig 5.1). However, it is possible that this state identifies a composite of stationary behaviour and slow tracking of prey items before prey capture attempts as

was documented in (Harper and Blake, 1991). Alternatively, it is possible that this pike adopts a slow, steady speed at regular intervals and for a majority of its time (Table 5.2) to conserve energy that may be needed for rapid acceleration at later, opportunistic times. This has been proposed to explain an observed high proportion of low activity in another ambush predator, the great barracuda *Sphyraena barracuda* (O'Toole et al., 2010). Fine scale accelerometry data would help to distinguish between these two possible behaviours, by correlating the timing of slow movement with fast-starts and transmission speeds.

Chapter 6

Conclusion

6.1 Summary of Research

This thesis demonstrates that combining the Laplace approximation and Automatic Differentiation as made available by Template Model Builder (`TMB`) offers a powerful approach to modelling animal movement. This combination is appealing because it can incorporate non-Gaussian measurement errors and high numbers of random effects, and is computationally efficient compared to likelihood sampling methods. Throughout my research, I used `TMB` to fit a hidden Markov model (HMM), a Gaussian Random Field (GRF), and two separate switching hierarchical models (SHMs). Model fitting encompassed a variety of data types, including GPS, filtered light level data, Argos, and acoustic telemetry detection data, that are sampled in both discrete and continuous space, and which I modelled in both discrete and continuous time. By developing parallel methods for both satellite and telemetry data, my research draws a powerful and timely link between the statistical regimes typically used to analyze these data.

As with other model fitting platforms, assumptions should be carefully considered. Specifically, the Laplace approximation is only accurate when the marginal likelihood is approximately Gaussian, or at least unimodal. This can sometimes be checked by examining

the profile likelihood (as in Auger-Méthé et al. 2017), or by utilizing the **checkConsis-tency** function of `TMB`. In addition, whether the data agree with the model family being used can be checked with one step ahead prediction residuals (including pseudoresiduals; Zucchini et al. 2016; Thygesen et al. 2017). Computationally efficient algorithms exist for calculating residuals while fitting HMMs (Zucchini et al., 2016). However, the existing strategy for computing residuals for state-space models (SSMs) within `TMB` requires cumulative optimizations over the random effects. I investigated this strategy for a seal track of ∼2000 locations. Because it required 4000 optimizations, this computation took several hours. For an acoustic telemetry dataset with 5000 locations and 5000 random tag drifts, 15000 optimizations would be required. Because I make use of the HMM framework when fitting the SHMs, I chose to utilize solely the HMM implementation of the residuals, which are calculated assuming that the locations states have been accurately predicted. Some research suggests that SSMs of animal movement may not fit the data as accurately as is assumed within the literature (Thygesen et al., 2017); future research would benefit from rigorously testing the suite of models currently being used.

When fitting models that include behavioural states, additional assumptions are made to interpret the states as individual behaviours. Avoiding the inclusion of too many states to ensure feasible biological interpretation of results has been frequently discussed (e.g., Li and Bolker 2017; Pohle et al. 2017). However, current research is largely incapable of validating the interpretations themselves. For example, although we can interpret the behavioural states of the grey seals in Chapters 2 and 4 as travelling and foraging based on classifying the movement into two states representative of area-restricted search patterns, we cannot be certain of the frequency that the individuals actually use this search tactic to forage. Most studies generate predictions of *apparent* behaviour, and would benefit from being able

to collect independent secondary evidence that can justify the interpretations. Although more certainty in the state interpretations can perhaps be generated by utilizing further data streams not included in this thesis, for example depth (deRuiter et al., 2017) and fine-scale accelerometry data (Wang, 2019), true validation is rare. Promising research suggests great future potential for validation from field observations (Farhadinia et al., 2020) and animal-borne cameras (Volpov et al., 2015).

This thesis concerned itself with the movement of aquatic animals. As a result, I initially focused efforts on creating a faster, frequentist implementation of the first-Difference Correlated Random Walk with Switching (DCRWS) originally implemented in the package `bsam` (Jonsen et al., 2005). For many years, this was the tool of choice for fitting SHMs to aquatic telemetry data because it incorporated measurement error distributions specifically designed for Argos telemetry. An alternative option that has become popular for analyzing animal telemetry data with error is the R package `momentuHMM`, which combines the continuous-time SSM of `crawl` (Johnson et al., 2008) with the discrete-time HMM on the distributions of step lengths and turning angles available through `moveHMM` (Michelot et al., 2016). In Chapter 2 I showed that the two movement processes under a negligible measurement error scenario can provide different results. Specifically, the DCRWS movement process appears to be most applicable when the behaviours to be identified consist of directed travelling and tortuous movement indicative of area-restricted search (Whoriskey et al. 2017).

In practice, the `moveHMM` process often provides more accessible interpretations of animal behaviour, for example, by directly modelling the mean step length of an animal, whereas the DCRWS models the autocorrelation in step length. In addition, it allows for more freedom in the state-dependent distributions in two ways. First, it contains two parameters

(location and scale) that model each of the turning angles and step lengths along a track, whereas the DCRWS only contains one autocorrelation parameter that acts on both the step lengths and turning angles, and one location parameter that governs the turning angles. Second, and directly following from the first point, the `moveHMM` process assumes that the step lengths and turning angles are independent (McClintock et al., 2014), whereas they are implicitly correlated in the DCRWS. This makes it more difficult to define and interpret more than two states in the DCRWS, although significant research has cautioned against the overfitting of models via the inclusion of too many states (Li and Bolker, 2017; Pohle et al., 2017). My attempts to fit a step length and turning angle model (*sensu* Lawler et al. 2019) in `TMB` were unsuccessful. Such a model includes an intermediate multivariate, non-linear, non-stochastic equation to recreate an animal path from the unknown random step lengths and turning angles, i.e., the link

$$\mathbf{x}_t = \mathbf{x}_{t-1} + \frac{\mathbf{d}_t}{\mathbf{d}_{t-1}} \begin{pmatrix} \cos(\theta_t) & -\sin(\theta_t) \\ \sin(\theta_t) & \cos(\theta_t) \end{pmatrix} (\mathbf{x}_{t-1} - \mathbf{x}_{t-2}), \tag{6.1}$$

where $\mathbf{d}_t$ denotes the step length between locations $\mathbf{x}_{t-1}$ and $\mathbf{x}_t$, and θ_t the turn angle between $\mathbf{x}_{t-2}$, $\mathbf{x}_{t-1}$, and $\mathbf{x}_t$ (Lawler et al., 2019). This step is necessary to provide an appropriate link between the measurement error and the movement process. However, it involves non-normal random effects, including a wrapped distribution, that require transformation through copulas to establish normality. The combination of this link, coupled with these transformations, unfortunately made estimation very slow and unreliable. Compared to the step length and turning angle model, the DCRWS is relatively easy to fit, and provides reliable results for those animals that consistently exhibit area-restricted search.

This thesis concerned data collected by many devices that can be broadly classified

into two kinds: spatially continuous animal paths collected by satellite telemetry, and spatially discrete detections of animal presence like those often registered by acoustic receivers. Although state-space and hidden Markov modelling have become enormously popular for analyzing animal paths, uptake within the acoustic telemetry world has lagged behind, likely because the discrete nature of acoustic telemetry precludes these data from being analyzed as a time series in the traditional sense. For example, a single tag transmission can be registered at multiple receivers, yielding multiple locations for an individual at a single moment in time. One early exception includes the work of Pedersen and Weng (2013), who discretized the location state-space and used the likelihood of an HMM developed in continuous-time to predict locations of a humphead wrasse (*Cheilinus undulatus*). This implementation was subsequently reformulated with a continuous location state-space for estimation via Markov Chain Monte Carlo sampling in Alós et al. (2016). These examples did not incorporate state-switching to predict underlying behaviours. Now, fine-scale positioning methods have reconciled some of the differences between satellite and acoustic telemetry data by producing paths from detection data, and as a result there is increasing enthusiasm for predicting discrete behavioural states, which has become evident within the literature (Whoriskey et al., 2017; Bacheler et al., 2019; Cote et al., 2020), at conferences (e.g., International Statistical Ecology Conference 2020), and through my personal interactions at various workshops (e.g., ideasOTN 2020 Telemetry Workshop Series). This development highlights two secondary results: 1) despite inherent differences, it is possible for the satellite and acoustic telemetry disciplines to adapt statistical techniques developed by the other; and 2) there remains a discrepancy between satellite and acoustic telemetry movement data that makes comparison of results from the two challenging unless paths can be reconstructed from detections.

6.2 Future Directions

This thesis has shown that significant knowledge can be gained by adapting methods for data collected by one kind of technology that were originally developed (within the context of animal movement) for another. For example, Chapter 3 adapted a GRF for detection data that had previously been used to model at-sea seal encounters detected by Vemco Mobile Transceivers (Carson and Mills Flemming, 2014) or dive behaviour determined by archival data loggers (Carson, 2018). Furthermore, Chapter 5 developed an SHM for acoustic detections using a framework that was previously developed for satellite telemetry locations in Chapter 4. Future research for analyzing acoustic detections could benefit from studying the ability to incorporate and account for measurement error in satellite telemetry statistical techniques.

Many researchers measure the effect of various factors on receiver detection efficiency, typically through the use of stationary tags deployed throughout the study duration to measure temporal variability within specific habitats (Pedersen and Weng, 2013), mobile tags towed throughout the study location (typically from a boat) to measure spatial variability, or tags placed on/within different mediums (Dance et al., 2016). Most researchers recognize the importance of accounting for variability in detection efficiency (Payne et al., 2010; Dance et al., 2016; Reubens et al., 2019; Swadling et al., 2020) because it affects the quality of data collection. However, statistical resources to accomplish this are limited. Researchers may inflate their datasets based on standardized detection rates measured from stationary (deployed) reference tags (Payne et al., 2010). Although this can be useful, stochastic methods would likely provide a greater ability to capture uncertainty in the detection process. Those who do account for variable detection efficiency using stochastic methods typically do so

in order to produce fine scale position predictions (e.g., Pedersen and Weng 2013; Winton et al. 2018; Hostetter and Royle 2020). Although fine-scale positioning is important and increasing in popularity, many researchers are not capable of conducting one of these studies either because of monetary restrictions or because it is not conducive to their study animal or ecological question (e.g., wide ranging or burrowing animals). Stochastic methods that can be used to account for statistical detection efficiency on detections without producing positions are lacking in the literature and would provide an important contribution. One technique that is very commonly used to analyze acoustic telemetry data is the generalized mixed model (Whoriskey et al., 2019). By continuing to develop methods of quantifying measurement error distributions as is commonly done in satellite telemetry analyses, and by recognizing that it might be possible to re-express SSMs like those frequently used to analyze satellite telemetry data as mixed models (Piepho and Ogutu, 2007), researchers may be able to harness currently available and widely understood statistical machinery to more accurately model animal detections.

This thesis was primarily concerned with the movement of individuals. Considerable effort by others has focused on collective movement, e.g., by modelling the tracks of several individuals simultaneously with individual random effects (deRuiter et al., 2017) or hyper-priors (Jonsen et al., 2006). However, these analyses are typically limited to single species and paths of animal movement. Multi-species studies are often of interest, for example to examine niche overlap (Villegas-Amtmann et al., 2013), interspecific interactions and competition (Heupel et al., 2019), and predator-prey relationships (Moxley et al., 2020). These ecological processes can be more difficult to investigate when the different species of interest have been tagged with contrasting technologies because the data to compare have inherently different structures. Moxley et al. (2020) did investigate how the movement of

satellite-tagged grey seals (*Halichoerus grypus*) varied with increasing predation pressure from aerial and acoustically tracked white sharks *Carcharodon carcharias*), but they relied more on visual comparisons of derived measurements rather than formally incorporating statistical links between the two data structures. Instead, spatial statistics might provide a convenient framework that can model movement from multiple individuals as well as standardize information across different data collection strategies. Prior research documents the use of spatial models to analyze animal movement data. For example, spatial point process models have been used to study habitat selection of northern fur seals (*Callorhinus ursinus*; Johnson et al. 2013), and to recreate animal paths from acoustic detections (Winton et al., 2018). GRFs have been used to model the movement of killer whales (*Orcinus orca*) influenced by social dynamics of conspecifics (Scharf et al., 2016), the distribution of interspecific interactions in grey seals (Carson and Mills Flemming, 2014), and the distribution of bull trout (*Salvelinus confluentus*) in relation to an anthropogenic structure (Whoriskey et al., 2019). One benefit of the GRF is that the locations of the response variable are determined prior to model fitting, thereby providing a potential solution to reconciling the spatial scale differences between satellite and acoustic telemetry data. Furthermore, equations can be incorporated to account for sampling error (Thorson et al., 2015) or covariates (Whoriskey et al. 2019; see Chapter 3), and multiple GRFs can be integrated into one hierarchical model, for example to relate foraging behaviour of grey seals to distribution of prey (Chapter 7 of Carson 2018). Spatial models, and specifically GRFs, have great potential for modelling animal movement at a collective level, from multiple data sources, and across species and trophic regimes.

6.3 Concluding Remarks

Throughout my studies, I have been fortunate to be included in several fieldwork operations, as well as tasked with the co-organization of various workshops. These opportunities have yielded valuable lessons with great benefits towards my applied statistical research. First, I have found that fieldwork opportunities can be hugely beneficial to an applied statistician. By participating in the data collection itself, I have obtained a thorough understanding of animal tracking data, and this has helped me to catch errors in my analysis, comprehensively interpret the results, understand the limitations of the statistical methods used, and provide suggestions on future work. Fieldwork experiences have additionally provided me with an extraordinary appreciation for the physical and mental labor put forth by both the scientists and the study animals in order to collect data. For example, it can take a team of four to five scientists 20-60 minutes to safely capture a single grey seal and obtain simple but important measurements of the animal (e.g., length, weight). I will also never forget the feeling (pain) in my hands from holding an anaesthetized adult salmon in a trough of 5°C ocean water for $\sim$ 10 minutes during tagging and bloodwork sampling. For me, these kinds of experiences have highlighted the need to safeguard collected data and to include as much of it as possible in an analysis (e.g., through the modelling of measurement error).

The zenith of my experience co-organizing workshops was the ideasOTN (integrate, describe, explain, and synthesize Ocean Tracking Network) Telemetry Workshop Series (TWS), hosted over four days, that focused on designing, analyzing, and communicating the results of telemetry studies. This workshop, hosted February 17-20, 2020, brought together over 50 international early career researchers (ECRs) in person, and was additionally

live-streamed to allow those unable to travel to participate. Given that the COVID-19 pandemic erupted shortly after completion of the TWS, other workshops and even conferences primarily adopted online platforms in 2020, and these experiences have highlighted that there is a tremendous ability to connect with distant researchers and share educational resources globally through the Internet. If possible, hosting workshop resources online indefinitely, e.g., through GitHub and/or YouTube as was done with the TWS, can provide huge benefits, including enabling the materials to persist, allowing other researchers to use them as building blocks, and providing metrics of utility for grant applications/reports (e.g., number of accesses or views). However, in my experience, it is hard to recreate the full benefits of in-person networking with online interaction. At the TWS, we put a huge amount of effort into planning social activities to facilitate connections on both a professional and personal level, and to help the ECRs learn from each other (through a panel discussion) and teach each other (through a research rodeo that crowd-sourced solutions to research questions). For me, these ancillary events help to foster an inclusive community within academia and can facilitate the discussions that spark ideas for future research.

Over the last decade, collaborative groups have grown in popularity for providing platforms under which marine science can be effectively conducted. These networks have actuated the collection of massive datasets through the sharing of resources and infrastructure, and have stimulated connections across disciplines including ecology, oceanography, statistics, and sociology. The methods presented here are a direct result of two such groups, the Canadian Statistical Sciences Institute Project "Advancements to state-space models for fisheries science" and the Ocean Tracking Network. With their guidance and support, I developed highly versatile frameworks that can quickly analyze large datasets and account

for the autocorrelation and error pervasive in aquatic animal movement data. My experience as a graduate student, from collaborative research to workshops, has therefore helped to advance statistical tools as well as translate them to ecologists, thus contributing to the growth and momentum of the movement ecology discipline (Lennox et al., 2017a).

Bibliography

Adam, T., Griffiths, C., Leos-Barajas, V., Meese, E., Lowe, C., Blackwell, P., Righton, D., and Langrock, R. (2019). Joint modelling of multi-scale animal movement data using hierarchical hidden Markov models. *Methods in Ecology and Evolution*, 10:1536–1550.

Albertsen, C., Whoriskey, K., Yurkowski, D., Nielsen, A., and Mills Flemming, J. (2015). Fast fitting of non-Gaussian state-space models to animal movement data via Template Model Builder. *Ecology*, 96(10):2598–2604.

Alós, J., Palmer, M., Balle, S., and Arlinghaus, R. (2016). Bayesian state-space modelling of conventional acoustic tracking providess accurate descriptors of home range behaviour in a small-bodied coastal fish species. *PLoS One*, 11(4):e0154089.

Altman, R. (2007). Mixed hidden Markov models: An extension of the hidden Markov model to the longitudinal data setting. *Journal of the American Statistical Association*, 102(477):201–210.

Amstrup, S., McDonald, T., and Manly, B. (2005). *Handbook of capture-recapture analysis*. Princeton, NJ: Princeton University Press.

Andersen, P. and Gill, R. (2005). Cox's regression model for counting processes, a large sample study. *Tha Annals of Statistics*, 10:1100–1120.

Arthur, B., Hindell, M., Bester, M., Trathan, P., Jonsen, I., Staniland, I., Oosthuizen, C., Wege, M., and Lea, M.-A. (2015). Return customers: Foraging site fidelity and the effect of environmental variability in wide-ranging Antarctic fur seals. *PLoS One*, 10(3):e0120888.

Auger-Méthé, M., Albertsen, C., Jonsen, I., Derocher, A., Lidgard, D., Studholme, K., Bowen, W., Crossin, G., and Mills Flemming, J. (2017). Spatiotemporal modelling of marine movement data using Template Model Builder (TMB). *Marine Ecology Progress Series*, 565:237–249.

Auger-Méthé, M., Field, C., Albertsen, C., Derocher, A., Lewis, M., Jonsen, I., and Mills Flemming, J. (2015). State-space models' dirty little secrets: even simple linear Gaussian models can have estimation problems. *Scientific Reports*, 6:26677.

Auger-Méthé, M., Newman, K., Cole, D., Empacher, F., Gryba, R., King, A., Leos-Barajas, V., Mills Flemming, J., Nielsen, A., Petris, G., and Thomas, L. (2020). An introduction to state-space modeling of ecological time series. *arXiv*, page 2002.02001v1.

Austin, D., Bowen, W., McMillan, J., and Iverson, S. (2006). Linking movement, diving, and habitat to foraging success in a large marine predator. *Ecology*, 87(12):3095–3108.

Austin, D., McMillan, J., and Bowen, W. (2003). A three-stage algorithm for filtering erroneous Argos satellite locations. *Marine Mammal Science*, 19(2):371–383.

Avgar, T., Potts, J., Lewis, M., and Boyce, M. (2016). Integrated step selection analysis: bridging the gap between resource selection and animal movement. *Methods in Ecology and Evolution*, 7:619–630.

Bacheler, N., Michelot, T., Cheshire, R., and Shertzer, K. (2019). Fine-scale movement patterns and behavioral states of gray triggerfish *balistes capriscus* determined from acoustic telemetry and hidden markov models. *Fisheries Research*, 215:76–89.

Bailey, H., Mate, B., Palacios, D., Irvine, L., Bograd, S., and Costa, D. (2009). Behavioural estimation of blue whale movements in the Northeast Pacific from state-space model analysis of satellite tracks. *Endangered Species Research*, 10:93–106.

Baker, J. (1975). The DRAGON system - an overview. *IEEE Transactions on acoustics, speech, and signal processing*, ASSP-23(1):24–29.

Baker, L., Jonsen, I., Mills Flemming, J., Lidgard, D., Bowen, W., Iverson, S., and Webber, D. (2014). Probability of detecting marine predator-prey and species interactions using novel hybrid acoustic transmitter-receiver tags. *PLoS One*, 9(6):e98117.

Baktoft, H., Gjelland, K., Økland, F., Rehage, J., Rodemann, J., Santos Corujo, R., Viadero, N., and Thygesen, U. (2019). Opening the black box of high resolution fish tracking using yaps. *bioRxiv*, (https://doi.org/10.1101/2019.12.16.877688).

Baktoft, H., Gjelland, K., Økland, F., and Thygesen, U. (2017). Positioning of aquatic animals based on time-of-arrival and random walk models using YAPS (Yet Another Positioning Solver). *Scientific Reports*, 7:14294.

Barbour, A., Boucek, R., and Adams, A. (2012). Effect of pulsed gastric lavage on apparent survival of a juvenile fish in a natural system. *Journal of Experimental Marine Biology and Ecology*, 422-423(107-113).

Barker, R. (1997). Joint modeling of live-recapture, tag-resight, and tag-recovery data. *Biometrics*, 53:666–677.

Baum, L. and Petrie, T. (1966). Statistical inference for probabilistic functions of finite state Markov chains. *The Annals of Mathematical Statistics*, 37(6):1554–1563.

Baylis, A.M.M. annd Tierney, M., Orben, R., Staniland, I., and Brickle, P. (2018). Geographic variation in the foraging behaviour of South American fur seals. *Marine Ecology Progress Series*, 596:233–245.

Beck, C., Bowen, W., and Iverson, S. (2003a). Sex differences in the seasonal patterns of energy storage and expenditure in a phocid seal. *Journal of Animal Ecology*, 72:280–291.

Beck, C. A., Bowen, W. D., McMillan, J., and Iverson, S. J. (2003b). Sex differences in the diving behaviour of a size-dimorphic capital breeder: the grey seal. *Animal Behaviour*, 66:777–789.

Beck, C. A., Iverson, S. J., Bowen, W. D., and Blanchard, W. (2007). Sex differences in grey seal diet reflect seasonal variation in foraging behaviour and reproductive expenditure: evidence from quantitative fatty acid signature analysis. *Journal of Animal Ecology*, 76:490–502.

Benoît, H., Capizzano, C., Knotek, R., Rudders, D., Sulikowski, J., Dean, M., Hoffman, W., Zemeckis, D., and Mandelman, J. (2015). A generalized model for longitudinal short- and long-term mortality data for commercial fishery discards and recreational fishery catch-and-releases. *ICES Journal of Marine Science*, 72(6):1834–1847.

Bestley, S., Jonsen, I., Hindell, M., Guinet, C., and Charrassin, J.-B. (2013). Integrative modelling of animal movement: incorporating *in situ* habitat and behavioural information for a migratory marine predator. *Proceedings of the Royal Society B*, 280(1750):20122262.

Binder, T., Thompson, H., Muir, A., Riley, S., Marsden, J., Bronte, C., and Krueger, C. (2015). New insight into the spawning behavior of lake trout, *Salvelinus namaycush*, from a recovering population in the Laurentian Great Lakes. *Environmental Biology of Fishes*, 98:173–181.

Block, B., Jonsen, I., Jorgensen, S., Winship, A., Shaffer, S., Bograd, S., Hazen, E., Foley, D., Breed, G., Harrison, A.-L., Ganong, J., Swithenbank, A., Castleton, M., Dewar, H., Mate, B., Shillinger, G., Schaefer, K., Benson, S., Weise, M., Henry, R., and Costa, D. (2011). Tracking apex marine predator movements in a dynamic ocean. *Nature*, 475(86-90).

Bodey, T., Cleasby, I., Bell, F., Parr, N., Schultz, A., Votier, S., and Bearhop, S. (2018). A phylogenetically controlled meta-analysis of biologging device effects on birds: Deleterious effects and a call for more standardized reporting of study data. *Methods in Ecology and Evolution*, 9:946–955.

Bolker, B., Brooks, M., Clark, C., Geange, S., Poulsen, J., Stevens, M., and White, J.-S. (2009). Generalized linear mixed models: A practical guide for ecology and evolution. *Trends in Ecology and Evolution*, 24:127–135.

Börger, L., Franconi, N., Ferretti, F., Meschi, F., De Michele, G., Gantz, A., and Coulson, T. (2006). An integrated approach to identify spatiotemporal and individual-level determinants of animal home range size. *The American Naturalist*, 168:471–485.

Botha, J., Kirkman, S., Arnould, J., Lombard, A., Hofmeyr, G., Meÿer, M., Kotze, P., and Pistorius, P. (2020). Geographic variation in at-sea movements, habitat use, and diving behaviour of female cape fur seals. *Marine Ecology Progress Series*, 649:201–218.

Bowen, W. and Harrison, G. (2006). Seasonal and interannual variability in grey seal diets on sable island, eastern scotian shelf. *NAMMCO Scientific Publications*, 6:123–134.

Bowen, W., Lawson, J., and Beck, B. (1993). Seasonal and geographic variation in the species composition and size of prey consumed by grey seals (halichoerus grypus) on the scoitan shelf. *Canadian Journal of Fisheries and Aquatic Sciences*, 50:1768–1778.

Boyd, C., Punt, A., Weimerskirch, H., and Bertrand, S. (2014). Movement models provide insights into variation in the foraging effort of central place foragers. *Ecological Modelling*, 286:13–25.

Boyd, I., Staniland, I., and Martin, A. (2002). Distribution of foraging by female antarctic fur seals. *Marine Ecology Progress Series*, 242:285–294.

Braun, C., Skomal, G., Thorrold, S., and Berumen, M. (2015). Movements of the reef manta ray (*Manta alfredi*) in the Red Sea using satellite and acoustic telemetry. *Marine Biology*, 162:2351–2362.

Breed, G., Bowen, W., and Leonard, M. (2011). Development of foraging strategies with age in a long-lived marine predator. *Marine Ecology Progress Series*, 431:267–279.

Breed, G., Bowen, W., and Leonard, M. (2013). Behavioral signature of intraspecific competition and density dependence in colony-breeding marine predators. *Ecology and Evolution*, 3:3838–3854.

Breed, G., Bowen, W., McMillan, J., and Leonard, M. (2006). Sexual segregation of seasonal foraging habitats in a non-migratory marine mammal. *Proceedings of the Royal Society B*, 273:2319–2326.

Breed, G., Costa, D., Jonsen, I., Robinson, P., and Mills Flemming, J. (2012). State-space methods for more completely capturing behavioral dynamics from animal tracks. *Ecological Modelling*, 235-236:49–58.

Breed, G., Jonsen, I., Myers, R., Bowen, W., and Leonard, M. (2009). Sex-specific, seasonal foraging tactics of adult grey seals (halichoerus grypus) revealed by state–space analysis. *Ecology*, 273:3209–3221.

Brousseau, L., Sclafani, M., Smith, D., and Carter, D. (2004). Acoustic-tracking and radio-tracking of horseshoe crabs to assess spawning behavior and subtidal habitat use in Delaware Bay. *North American Journal of Fisheries Management*, 24(4):1376–1384.

Brownscombe, J., Lédée, E., Raby, G., Struthers, D., Gutowsky, L., Nguyen, V., Young, N., Stokesbury, M., Holbrook, C., Brenden, T., Vandergoot, C., Murchie, K., Whoriskey, K., Mills Flemming, J., Kessel, S., Krueger, C., and Cooke, S. (2019). Conducting and interpreting fish telemetry studies: considerations for researchers and resource managers. *Reviews in Fish Biology and Fisheries*, 29:369–400.

Bunck, C., Chen, C., and Pollock, K. (1995). Robustness of survival estimates from radio-telemetry studies with uncertain relocation of individuals. *The Journal of Wildlife Management*, 59:790–794.

Burnham, K. (1993). *Marked Individuals in the study of bird populations*, chapter A theory for commbined analysis of ring recovery and recapture data. Basel, Switzerland: Birkháuser Verlag.

Cagua, E., Berumen, M., and Tyler, E. (2013). Topography and biological noise determine acoustic detectability on coral reefs. *Coral Reefs*, 32:1123–1134.

Calenge, C. (2006). The package "adehabitat" for the r software: A tool for the analysis of space and habitat use by animals. *Ecological Modelling*, 197(3-4):516–519.

Campbell, H., Watts, M., Dwyer, R., and Franklin, C. (2012). V-Track: Software for analysing and visualising animal movement from acoustic telemetry detections. *Marine and Freshwater Research*, 63:815–820.

Cappé, O., Moulines, E., and Rydén, T. (2005). *Inference in Hidden Markov Models*. Springer Science + Business Media, Inc., New York, NY.

Carson, S. (2018). *Spatial and spatio-temporal models for use in the marine environment with applications to the Scotian Shelf*. PhD thesis, Dalhousie University.

Carson, S. and Mills Flemming, J. (2014). Seal encounters at sea: A contemporary spatial approach using R-INLA. *Ecological Modelling*, 291:175–181.

Carson, S., Shackell, N., and Mills Flemming, J. (2017). Local overfishing may be avoided by examining parameters of a spatio-temporal model. *PLoS One*, 12:e0184427.

Carter, M., McClintock, B., Embling, C., Bennett, K., Thompson, D., and Russel, D. (2020). From pup to predator: generalized hidden Markov models reveal rapid development of movement strategiees in a naïve long-lived vertebrate. *Oikos*, 129:630–642.

Castro-Santos, T. and Haro, A. (2003). Quantifying migratory delay: A new application of survival analysis methods. *Canadian Journal of Fisheries and Aquatic Sciences*, 60(986-996).

Charnov, E. (1976). Optimal foraging: The marginal value theorem. *Theoretical Population Biology*, 9:129–136.

Cooke, S., Hinch, S., Lucas, M., and Lutcavage, M. (2012). *Fisheries techniques*, chapter Chapter 18 - Biotelemetry and biologging. Bethesda, MD: American Fisheries Society.

Cosandey-Godin, A., Krainski, E., Worm, B., and Mills Flemming, J. (2015). Applying bayesian spatiotemporal models to fisheries bycatch in the canadian arctic. *Canadian Journal of Fisheries and Aquatic Sciences*, 72:186–197.

Costa, D., Breed, G., and Robinson, P. (2012). New insights into pelagic migrations: Implications for ecology and conservation. *Annual Review of Ecology, Evolution, and Systematics*, 43:73–96.

Cote, D., Morris, C., Regular, P., and Piersiak, M. (2020). Effects of 2D seismic on snow crab movement behaviour. *Fisheries Research*, 230:105661.

Cote, D., Nicolas, J.-M., Whoriskey, F., Cook, A., Broome, J., Regular, P., and Baker, D. (2019). Characterizing snow crab (*Chionoecetes opilio*) movements in the Sydney Bight (Nova Scotia, Canada): a collaborative approach using multiscale acoustic telemetry. *Canadian Journal of Fisheries an Aquatic Sciences*, 76(2):334–346.

Cox, D. and Miller, H. (1965). *The Theory of Stochastic Processes*. Methuen & Co Ltd, London, Great Britain.

Csárdi, G. and Nepusz, T. (2006). The igraph software package for complex network research. *InterJournal, Complex Systems*, 1695.

Curtis, J., Johnson, M., Diamond, S., and Stunz, G. (2015). Quantifying delayed mortality from barotrauma impairment in discarded red snapper using acoustic telemetry. *Marine and Coastal Fisheries*, 7:434–449.

Dale, M. and Fortin, M.-J. (2010). From graphs to spatial graphs. *Annual Review of Ecology, Evolution, and Systematics*, 41:21–38.

Dance, M., Moulton, D., Furey, N., and Rooker, J. (2016). Does transmitter placement or species affect detection efficiency of tagged animals in biotelemetry research? *Fisheries Research*, 183:80–85.

Danylchuk, S., Danylchuk, A., Cooke, S., Goldberg, T., Koppelman, J., and Philipp, D. (2007). Effects of recreational angling on the post-release behavior and predation of bonefish (*Albula vulpes*): The role of equilibrium status at the time of release. *Journal of Experimental Marine Biology and Ecology*, 346:127–133.

Davison, A. and Hinkley, D. (1997). *Bootstrap Methods and their Application*. Cambridge University Press.

den Heyer, C., Bowen, W., Dale, J., Gosselin, J.-F., Hammill, M., Johnston, D., Lang, S., Murray, K., Stenson, G., and Wood, S. (2020). Contrasting trends in gray seal (*Halichoerus grypus*) pup production throughout the increasing northwest Atlantic metapopulation. *Marine Mammal Science*, pages 1–20.

deRuiter, S., Langrock, R., Skirbutas, T., Goldbogen, J., Calambokidis, J., Friedlaender, A., and Southall, B. (2017). A multivariate mixed hidden Markov model for blue whale behaviour and responses to sound exposure. *The Annals of Applied Statistics*, 11(1):362–392.

Dmitrieva, l., Jüssi, M., Jüssi, I., Kasymbekov, Y., Verevkin, M., Baimukanov, M., Wilson, S., and Goodman, S. (2016). Individual variation in seasonal movements and foraging strategies of a land-locked, ice-breeding pinniped. *Marine Ecology Progress Series*, 554:241–256.

Donaldson, M., Hinch, S., Suski, C., Fisk, A., Heupel, M., and Cooke, S. (2014). Making connections in aquatic ecosystems with acoustic telemetry monitoring. *Frontiers in Ecology and the Environment*, 12:565–573.

Doniol-Valcroze, T., Lesage, V., Giard, J., and Michaud, R. (2011). Optimal foraging theory predicts diving and feeding strategies of the largest marine predator. *Behavioural Ecology*, 22(4):880–888.

Dorazio, R. and Price, M. (2019). State-space models to infer movements and behavior of fish detected in a spatial array of acoustic receivers. *Canadian Journal of Fisheries and Aquatic Sciences*, 76(4):543–550.

Dowd, M. and Joy, R. (2011). Estimating behavioral parameters in animal movement models using a state-augmented particle filter. *Ecology*, 92(3):568–575.

Dudgeon, C., Lanyon, J., and Semmens, J. (2013). Seasonality and site fidelity of the zebra shark, *stegostoma fasciatum*, in southeast queensland, australia. *Animal Behaviour*, 85:471–481.

Dudgeon, C., Pollock, K., Braccini, J., Semmens, J., and Barnett, A. (2015). Integrating acoustic telemetry into mark–recapture models to improve the precision of apparent survival and abundance estimates. *Oecologia*, 178:761–772.

Dwyer, R., Brooking, C., Brimblecombe, W., Campbell, H., Hunter, J., Watts, M., and Franklin, C. (2015). An open Web-based system for the analysis and sharing of animal tracking data. *Animal Biotelemetry*, 3:1.

Dwyer, R., Campbell, H., Cramp, R., Burke, C., Micheli-Campbell, M., Pillans, R., Lyon, B., and Franklin, C. (2020). Niche partitioning between river shark species is driven by seasonal fluctuations in environmental salinity. *Functional Ecology*, doi:10.1111/1365-2435.13626.

Eckert, S., Moore, J., Dunn, D., Sagarminaga van Buiten, R., Eckert, K., and Halpin, P. (2008). Modeling loggerhead turtle movement in the Mediterranean: importance of body size and oceanography. *Ecological Applications*, 18(2):290–308.

Efford, M. and Fewster, R. (2013). Estimating population size by spatially explicit capture–recapture. *Oikos*, 122:918–928.

Eklöv, P. (1997). Effects of habitat complexity and prey abundance on the spatial and temporal distributions of perch (*Perca fluviatilis*) and pike (*Esox lucius*). *Canadian Journal of Fisheries and Aquatic Sciences"*, 54:1520–1531.

Ellis, A., Burchett, W., Harrar, S., and Bathke, A. (2017). Nonparametric inference for multivariate data: The **R** package **npmv**. *Journal of Statistical Software*, 76(4):1–18.

Espinoza, M., Farrugia, T., Webber, D., Smith, F., and Lowe, C. (2011). Testing a new acoustic telemetry technique to quantify long-term, fine-scale movements of aquatic animals. *Fisheries Research*, 108(2-3):364–371.

Espinoza, M., Lédée, E., Simpfendorfer, C., Tobin, A., and Heupel, M. (2015). Contrasting movements and connectivity of reef-associated sharks using acoustic telemetry: Implications for management. *Ecological Applications*, 25:2101–2118.

Farhadinia, M., Michelot, T., Johnson, P., Hunter, L., and Macdonald, D. (2020). Understanding decision making in a food-caching predator using hidden markov models. *Movement Ecology*, 8:9.

Farine, D. and Whitehead, H. (2015). Constructing, conducting, and interpreting animal social network analysis. *Journal of Animal Ecology*, 84:1144–1163.

Field, I., Bradshaw, C., Burton, H., Sumner, M., and Hindell, M. (2005). Resource partitioning through oceanic segregation of foraging juvenile southern elephant seals (*Mirounga leonina*). *Oecologia*, 142:127–135.

Finn, J., Brownscombe, J., Haak, C., Cooke, S., Cormier, R., Gagne, T., and Danylchuk, A. (2014). Applying network methods to acoustic telemetry data: Modeling the movements of tropical marine fishes. *Ecological Modelling*, 293:139–149.

Fitzpatrick, R., Thums, M., Bell, I., Meekan, M., Stevens, J., and Barnett, A. (2012). A comparison of the seasonal movements of tiger sharks and green turtles provides insight into their predator-prey relationship. *PLoS One*, 7(12):e51927.

Forney, G. (1973). The viterbi algorithm. *Proceedings of the IEEE*, 61(3):268–278.

Fouchet, D., Santin Janin, H., Sauvage, F., Yoccoz, N., and Pontier, D. (2016). An R package for analysing survival using continuous-time open capture–recapture models. *Methods in Ecology and Evolution*, 7:518–528.

Fournier, D., Skaug, H., Ancheta, J., Ianelli, J., Magnusson, A., Maunder, M., Nielsen, A., and Sibert, J. (2012). AD Model Builder: using automatic differentiation for statistical inference of highly parameterized complex nonlinear models. *Optimization Methods & Software*, 27(2):233–249.

Fox, R. and Bellwood, D. (2014). Herbivores in a small world: Network theory highlights vulnerability in the function of herbivory on coral reefs. *Functional Ecology*, 28:642–651.

Frair, J., Fieberg, J., Hebblewhite, M., Cagnacci, F., DeCesare, N., and Pedrotti, L. (2010). Ressolving issues of imprecise and habitat-biased locations in ecological analyses using GPS telemetry data. *Philisophical Transactions of the Royal Society B*, 365:2187–2200.

Freitas, C., Lydersen, C., Fedak, M., and Kovacs, K. (2008). A simple new algorithm to filter marine mammal Argos locations. *Marinen Mammal Science*, 24(2):315–325.

Friedlaender, A., Johnston, D., Tyson, R., Kaltenberg, A., Goldbogen, J., Stimpert, A., Curtice, C., Hazen, E., Halpin, P., Read, A., and Nowacek, D. (2016). Multiple-stage decisions in a marine central-place forager. *Royal Society Open Science*, 3:160043.

Frith, H. and Blake, R. (1995). The mechanical power output and hydromechanical efficiency of northern pike (*esox lucius*) fast-starts. *The Journal of Experimental Biology*, 198:1863–1873.

Furey, N., Hinch, S., Bass, A., Middleton, C., Minke Martin, V., and Lotto, A. (2016). Predator swamping reduces predation risk during nocturnal migration of juvenile salmon in a high-mortality landscape. *Journal of Animal Ecology*, 85:948–959.

Gallon, S., Sparling, C., Georges, J.-Y., Fedak, M., Biuw, M., and Thompson, D. (2007). How fast does a seal swim? Variations in swimming behaviour under differing foraging conditions. *The Journal of Experimental Biology*, 210:3285–3294.

González Carman, V., Falabella, V., Maxwell, S., Albareda, D., Campagna, C., and Mianzan, H. (2012). Revisiting the ontogenetic shift paradigm: The case of juvenile green turtles in the SW Atlantic. *Journal of Experimental Marine Biology and Ecology*, 429:64–72.

Goulet, A.-M., Hammill, M., and Barrette, C. (2001). Movements and diving of grey seal females (*Halichoerus grypus*) in nthe Gulf of St. Lawrence, Canada. *Polar Biology*, 24:432–439.

Graham, R., Witt, M., Castellanos, D., Remolina, F., Maxwell, S., Godley, B., and Hawkes, L. (2012). Satellite tracking of manta rays highlights challenges to their conservation. *PLoS One*, 7(5):e36834.

Grémillet, D., Dell'Omo, G., Ryan, P., Peters, G., Ropert-Coudert, Y., and Weeks, S. (2004). Offshore diplomacy, or how seabirds mitigate intra-specific competition: a case study based on GPS tracking of Cape gannets from neighbouring colonies. *Marine Ecology Progress Series*, 268:265–279.

Gutowsky, L., Harrison, P., Martins, E., Leake, A., Patterson, D., Power, M., and Cooke, S. (2016). Interactive effects of sex and body size on the movement ecology of adfluvial bull trout (*Salvelinus confluentus*). *Canadian Journal of Zoology*, 94:31–40.

Hammill, M., den Heyer, C., Bowen, W., and Lang, S. (2017). Grey seal population trends in canadian waters, 1960-2016 and harvest advice. *DFO Can. Sci. Advis. Sec. Res. Doc.*, 2017/052. v + 30 p.

Harper, D. and Blake, R. (1991). Prey capture and the fast-start performance of northern pike *esox lucius*. *Journal of Experimental Biology*, 155:175–192.

Harrell, F. (2015). *Regression modeling strategies: With applications to linear models, logistic and ordinal regression, and survival analysis*. Berlin: Springer.

Hart, K., Lamont, M., Fujisaki, I., Tucker, A., and Carthy, R. (2012). Common coastal foraging areas for loggerheads in the Gulf of Mexico: Opportunities for marine conservation. *Biological Conservation*, 145(1):185–194.

Harvey, V., Hammill, M., Swain, D., Breed, G., Lydersen, C., and Kovacs, K. (2012). Winter foraging by a top predator, the grey seal *Halichoerus grypus*, in relation to the distribution of prey. *Marine Ecology Progress Series*, 462:273–286.

Harwood, L., Smith, T., Auld, J., Melling, H., and Yurkowski, D. (2015). Seasonal movements and diving of ringed seals, *Pusa hispida*, in the Western Canadian Arctic, 1999-2001 and 2010-11. *Arctic*, 68(2):193–209.

Hayden, T., Holbrook, C., Fielder, D., Vandergoot, C., Bergstedt, R., Dettmers, J., Krueger, C., and Cooke, S. (2014). Acoustic telemetry reveals large-scale migration patterns of walleye in lake huron. *PLoS One*, (9):e114833.

Hays, G., Ferreira, L., Sequeira, A., Meekan, M., Duarte, C., Bailey, H., Bailleul, F., Bowen, W., Caley, M., Costa, D., Eguíluz, V., Fossette, S., Friedlaender, A., Gales, N., Gleiss, A., Gunn, J., Harcourt, R., Hazen, E., Heithaus, M., Heupel, M., Holland, K., Horning, M., Jonsen, I., Kooyman, G., Lowe, C., Madsen, P.,

Marsh, H., Phillips, R., Righton, D., Ropert-Coudert, Y., Sato, K., Shaffer, S., Simpfendorfer, C., Sims, D., Skomal, G., Takahashi, A., Trathan, P., Wikelski, M., Womble, J., and Thums, M. (2016). Key questions in marine megafauna movement ecology. *Trends in Ecology & Evolution*, 31(6):463–475.

Hays, G., Åkesson, S., Godley, B., Luschi, P., and Santidrian, P. (2001). The implications of location accuracy for the interpretation of satellite-tracking data. *Animal Behaviour*, 61:1035–1040.

Hazen, E., Jorgensen, S., Rykaczewski, R., Bograd, S., Foley, D., Jonsen, I., Shaffer, S., Dunne, J., Costa, D., Crowder, L., and Block, B. (2013). Predicted habitat shifts of Pacific top predators in a changing climate. *Nature Climate Change*, 3:234–238.

Heerah, K., Hindell, M., Andrew-Goff, V., Field, I., McMahon, C., and Charrassin, J.-B. (2017). Contrasting behavior between two populations of an ice-obligate predator in East Antarctica. *Ecology and Evolution*, 7:606–618.

Heupel, M., Munroe, S., Lédée, E., Chin, A., and Simpfendorfer, C. (2019). Interspecific interactions, movement patterns and habitat use in a diverse coastal shark assemblage. *Marine Biology*, 166:68.

Heupel, M., Semmens, J., and Hobday, A. (2006). Automated acoustic tracking of aquatic animals: Scales, design and deployment of listening station arrays. *Marine and Freshwater Research*, 57:1–13.

Hoenner, X., Huveneers, C., Steckenreuter, A., Simpfendorfer, C., Tattersall, K., Jaine, F., Atkins, N., Babcock, R., Brodie, S., Burgess, J., Campbell, H., Heupel, M., Pasquer, B., Proctor, R., Taylor, M., Udyawer, V., and Harcourt, R. (2018). Australia's continental-scale acoustic tracking database and its automated quality control process. *Scientific Data*, 5:170206.

Hoenner, X., Whiting, S., Hindell, M., and McMahon, C. (2012). Enhancing the use of Argos satellite data for home range and long distance migration studies of marine animals. *PLoS One*, 7(7):e40713.

Holbrook, C., Hayden, T., and Binder, T. (2017). glatos: A package for the great lakes acoustic telemetry observation system. *R package version 0.1.3*, page Retrieved from https://gitlab.oceantrack.org/GreatLakes/glatos.

Holbrook, C., Kinnison, M., and Zydlewski, J. (2011). Survival of migrating Atlantic salmon smolts through the Penobscot River, Maine: A prerestoration assessment. *Transactions of the American Fisheries Society*, 140:1255–1268.

Holbrook, C., Perry, R., Brandes, P., and Adams, N. (2013). Adjusting survival estimates for premature transmitter failure: A case study from the Sacramento-San Joaquin Delta. *Environmental Biology of Fishes*, 96:165–173.

Hostetter, N. and Royle, J. (2020). Movement-assisted localization from acoustic telemetry data. *Movement Ecology*, 8:15.

Huserbråten, M., Moland, E., Knutsen, h., Olsen, E., André, C., and Stenseth, N. (2013). Conservation, spillover and gene flow within a network of Northern European marine protected areas. *PLoS One*, 8:e73388.

Hussey, N., Kessel, S., Aearestrup, K., Cooke, S., Cowley, P., Fisk, A., Harcourt, R., Holland, K., Iverson, S., Kocik, J., Mills Flemming, J., and Whoriskey, F. (2015). Aquatic animal telemetry: A panoramic window into the underwater world. *Science*, 348(6240):1255642–1.

Illian, J., Søorbye, S., and Rue, H. (2012). A toolbox for fitting complex spatial point process models using integrated nested Laplace approx- imation (INLA). *The Annals of Applied Statistics*, 6:1499–1530.

Ironside, K., Mattson, D., Arundel, T., and Hansen, J. (2017). Is GPS telemmetry location error screening beneficial? *Wildlife Biology*, 17:wlb.00229.

Irvine, L., Mate, B., Winsor, M., Palacios, D., Bograd, S., Costa, D., and Bailey, H. (2014). Spatial and temeporal occurrence of blue whales off the U.S. West coast, with implications for management. *PLoS One*, 9(7):e102959.

Iverson, S., Bowen, W., Boness, D., and Oftedal, O. (1993). The effect of maternal size and milk energy output on pup growth in grey seals (*Halichoerus grypus*). *Physiological and Biochemical Zoology*, 66(1):61–88.

Jacoby, D., Brooks, E., Croft, D., and Sims, D. (2012). Developing a deeper understanding of animal movements and spatial dynamics through novel application of network analysis. *Methods in Ecology and Evolution*, 3:574–583.

Jazwinski, A. (1970). *Stochastic Processes and Filtering Theory*. Dover Publications, Inc., Mineola, NY.

Jeppesen, E., Søndergaard, M., Kronvang, B., Jensen, J., Svendsen, L., and Lauridsen, T. (1999). Lake and catchment management in denmark. *Hydrobiologia*, 395/396:419–432.

Jepsen, N., Thorstad, E., Havn, T., and Lucas, M. (2015). The use of external electronic tags on fish: An evaluation of tag retention and tagging effects. *Animal Biotelemetry*, 3:49.

Johnson, C., Boyce, M., Schwartz, C., and Haroldson, M. (2004). Modeling survival: Application of the Andersen-Gill model to Yellowstone grizzly bears. *Journal of Wildlife Management*, 68:966–978.

Johnson, D., Hooten, M., and Kuhn, C. (2013). Estimating animal resource selection from telemetry data using point process models. *Journal of Animal Ecology*, 82(6):1155–1164.

Johnson, D., London, J., Lea, M.-A., and Durban, J. (2008). Continuous-time correlated random walk model for animal telemetry data. *Ecology*, 89(5):1208–1215.

Jonsen, I. (2016). Joint estimation over multiple individuals improves behavioural state inference from animal movement data. *Scientific Reports*, 6:20625.

Jonsen, i., McMahon, C., Patterson, T., Auger-Méthé, M., Harcourt, R., Hindell, M., and Bestley, S. (2019). Movement responses to environment: fast inference of variation among southern elephant seals with a mixed effects model. *Ecology*, 100(1):e02566.

Jonsen, I., Mills Flemming, J., and Myers, R. (2005). Robust state-space modeling of animal movement data. *Ecology*, 86(11):2874–2880.

Jonsen, I., Myers, R., and James, M. (2006). Robust hierarchical state-space models reveal diel variation in travel rates of migrating leatherback turtles. *Journal of Animal Ecology*, 75(5):1046–1057.

Jonsen, I., Myers, R., and Mills Flemming, J. (2003). Meta-analyssis of animal movement using state-space models. *Ecology*, 84(11):3055–3063.

Jonsen, I., Patterson, T., Costa, D., Doherty, P., Godley, B., Grecian, W., Guinet, C., Hoenner, X., Kienle, S., Robison, P., Votier, S., Witt, M., Hindell, M., Harcourt, R., and McMahon, C. (2020). A continuous-time state-space model for rapid quality-control of argos locations from animal-borne tags. *Movement Ecology*, 8:31.

Kalman, R. (1960). A new approach to linear filtering and prediction problems. *ASME Journal of Basic Engineering*, 82:35–45.

Kalman, R. and Bucy, R. (1961). New results in linear filtering and prediction theory. *Journal of Basic Engineering*, 83(1):95–108.

Kays, R., Crofoot, M., Jetz, W., and Wikelski, M. (2015). Terrestrial animal tracking as an eye on life and planet. *Science*, 348(6240):aaa2478.

Kessel, S., Chapman, D., Franks, B., Gedamke, T., Gruber, S., Newman, J., White, E., and Perkins, R. (2014a). Predictable temperature-regulated residency, movement and migration in a large, highly mobile marine predator (*Negaprion brevirostris*). *Marine Ecology Progress Series*, 514:175–190.

Kessel, S., Cooke, S., Heupel, M., Hussey, N., C.A., S., S., V., and A.T., F. (2014b). A review of detection range testing in aquatic passive acoustic telemetry studies. *Reviews in Fish Biology and Fisheries*, 24:199–218.

Ketchum, J., Hearn, A., Klimley, A., Peñaherrera, C., Espinoza, E., Bessudo, S., Soler, G., and Arauz, R. (2014). Inter-island movements of scalloped hammerhead sharks (*Sphyrna lewini*) and seasonal connectivity in a marine protected area of the eastern tropical Pacific. *Marine Biology*, 161:939–951.

King, M., Fenton, D., Aker, J., and Serdynska, A. (2016). Offshore ecologically and biologically significant areas in the Scotian Shelf bioregion. *DFO Can. Sci. Advis. Sec. Res. Doc.*, 2016/007:viii + 02 p.

Klein, J. and Moeschberger, M. (2003). *Survival analysis: Techniques for censored and truncated data.* New York, NY: Springer Science & Business Media Inc.

Kristensen, K., Nielsen, A., Berg, C., and Skaug, H. (2016). TMB: automatic differentiation and Laplace approximation. *Journal of Statistical Software*, 70(5):1–21.

Laake, J. (2013). RMark: An R interface for analysis of capture–re- capture data with MARK. Technical report, AFSC Processed Report 2013-01. Alaska Fisheries Science Centre, NOAA, National Marine Fisheries Service, Seattle, WA.

Langrock, R., King, R., Matthiopoulos, J., Thomas, L., Fortin, D., and Morales, J. (2012). Flexible and practical modeling of animal telemetry data: hidden markov models and extensions. *Ecology*, 93(11):2336–2342.

Lawler, E., Whoriskey, K., Aeberhard, W., Field, C., and Mills Flemming, J. (2019). The conditionnally autoregressive hidden Markov model (CarHMM): Inferring behavioural states from animal tracking data exhibiting conditional autocorrelation. *Journal of Agricultural, Biological, and Environmental Statistics*, 24:651–668.

Leenders, R. (2002). Modeling social influence through network autocorrelation: Constructing the weight matrix. *Social Networks*, 24:21–47.

Lennox, R., Aarestrup, K., Cooke, S., Cowley, P., Deng, Z., Fisk, A., Harcourt, R., Heupel, M., Hinch, S., Holland, K., Hussey, N., Iverson, S., Kessel, S., Kocik, J., Lucas, M., Mills Flemming, J., Nguyen, V., Stokesbury, M., Vagle, S., Vanderzwaag, D., Whoriskey, F., and Young, N. (2017a). Envisioning the future of aquatic animal tracking: Technology, science, and application. *Bioscience*, 67(20):884–896.

Lennox, R., Filous, A., Danylchuk, S., Cooke, S., Brownscombe, J., Friedlander, A., and Danylchuk, A. (2017b). Factors influencing postrelease predation for a catch-and-release tropical flats fishery with a high predator burden. *North American Journal of Fisheries Management*, 37:1045–1053.

Leos-Barajas, V., Gangloff, E., Adam, T., Langrock, R., van Beest, F., Nabe-Nielsen, J., and Morales, J. (2017). Multi-scale modeling of animal movement and general behaviour data using hidden Markov models with hierarchical structures. *Journal of Agricultural, Biological, and Environmental Statistics*, 22:232–248.

Li, M. and Bolker, B. (2017). Incorporating periodic variability in hidden Markov models for animal movement. *Movement Ecolog*, 5:1.

Lindberg, M. (2012). A review of designs for capture–mark–recapture studies in discrete time. *Journal of Ornithology*, 152:355–370.

Lohr, S. (2010). *Sampling: Design and Analysis.* Boston, MA: Brooks/Cole, Cengage Learning.

Lopez, R., Malardé, J.-P., Royer, F., and Gaspar, P. (2014). Improving Argos doppler location using multiple-model Kalman filtering. *IEEE Transactions on Geoscience and Remote Sensing*, 52(8):4744–4755.

Lu, S. (2017). A continuous-time HMM approach to modeling the magnitude-frequency distribution of earthquakes. *Journal of Applied Statistics*, 44(1):71–88.

Lucas, M. and Baras, E. (2000). Methods for studying spatial behaviour of freshwater fishes in the natural environment. *Fish and Fisheries*, 1:283–316.

Marins, E., Gutowsky, L., Harrison, P., Mills Flemming, J., Jonsen, I., Zhu, D., Leake, A., Patterson, D., Power, M., and Cooke, S. (2014). Behavioral attributes of turbine entrainment risk for adult resident fish revealed by acoustic telemetry and state-space modeling. *Animal Biotelemetry*, 2:13.

Marshell, A., Mills, J., Rhodes, K., and McIlwain, J. (2011). Passive acoustic telemetry reveals highly variable home range and movement patterns among unicornfish within a marine reserve. *Coral Reefs*, 30:631–642.

Martins, E., Gutowsky, L., Harrison, P., Patterson, D., Power, M., Zhu, D., Leake, A., and Cooke, S. (2013). Forebay use and entrainment rates of resident adult fish in a large hydropower reservoir. *Aquatic Biology*, 19:253–263.

Martins, E., Hinch, S., Patterson, D., Hague, M., Cooke, S., Miller, K., Lapointe, M., English, K., and Farrell, A. (2011). Effects of river temperature and climate warming on stock-specific survival of adult migrating Fraser River sockeye salmon (*Oncorhynchus nerka*). *Global Change Biology*, 17(1):99–114.

Matich, P. and Heithaus, M. (2014). Multi-tissue stable isotope analysis and acoustic telemetry reveal seasonal variability in the trophic interactions of juvenile bull sharks in a coastal estuary. *Journal of Animal Ecology*, 83:199–213.

Maxwell, S., Breed, G., Nickel, B., Makanga-Bahouna, J., Pemo-Makaya, E., Parnell, R., Formia, A., Ngouessono, S., Godley, B., Costa, D., Witt, M., and Coyne, M. (2011). Using satellite tracking to optimize protection of long- lived marine species: Olive ridley sea turtle conservation in central Africa. *PLoS One*, 6(5):e19905.

McAuley, R., Bruce, B., Keay, I., Mountford, S., Pinnell, T., and Whoriskey, F. (2017). Broad-scale coastal movements of white sharks off western australia described by passive acoustic telemetry data. *Marine and Freshwater Research*, 68:1518–1531.

McClintock, B., Johnson, D., Hooten, M., Ver Hoef, J., and Morales, J. (2014). When to be discrete: the importance of time formulation in understanding animal movement. *Movement Ecology*, 2:21.

McClintock, B., King, R., Thomas, L., Matthiopoulos, J., McConnell, B., and Morales, J. (2012). A general discrete-time modeling framework for animal movement using multistate random walks. *Ecological Monographs*, 82:335–349.

McClintock, B., Langrock, R., Gimenez, O., Cam, E., Borchers, D., Glennie, R., and Patterson, T. (2020). Uncovering ecological state dynamics with hidden markov models. *arXiv*, page arXiv:2002.10497.

McClintock, B., London, J., Cameron, M., and Boveng, P. (2015). Modelling animal movement using the Argos satellite telemetry location error ellipse. *Methods in Ecology and Evolution*, 6:266–277.

McClintock, B., London, J., Cameron, M., and Boveng, P. (2017). Bridging the gaps in animal movement: hidden behaviors and ecological relationships revealed by integrated data streams. *Ecosphere*, 8(3):e01751.

McClintock, B. and Michelot, T. (2018). momentuhmm: R package for generalized hidden markov models of animal movement. *Methods in Ecology and Evolution*, 9(6):1518–1530.

McKellar, A., Langrock, R., Walters, J., and Kesler, D. (2015). Using mixed hidden Markov models to examine behavioural states in a cooperatively breeding bird. *Behavioural Ecology*, 26(1):148–157.

Meckley, T., Holbrook, C., Wagner, C., and Binder, T. (2014). An approach for filtering hyperbolically positioned underwater acoustic telemetry data with position precision estimates. *Animal Biotelemetry*, 2(7).

Meekan, M., Duarte, C., Fernández-Gracia, J., Thums, M., Sequeira, A., Harcourt, R., and Eguíluz, V. (2017). The ecology of human mobility. *Trends in Ecology and Evolution*, 32:198–210.

Mellish, J.-A., Iverson, S., and Bowen, W. (1999). Variation in milk production and lactation performance in grey seals and consequences for pup growth and weaning characteristics. *Physiological and Biochemical Zoology*, 72(6):677–690.

Michelot, T. and Blackwell, P. (2019). State-switching continuous-time correlated random walks. *Methods in Ecology and Evolution*, 10:637–649.

Michelot, T., Langrock, R., and Patterson, T. (2016). moveHMM: an R package for the statistical modelling of animal movement data using hidden Markov models. *Methods in Ecology and Evolution*, 7(11):1308–1315.

Moore, M., Berejikian, B., Goetz, F., Berger, A., Hodgson, S., Connor, E., and Quinn, T. (2015). Multi-population analysis of Puget Sound steelhead survival and migration behavior. *Marine Ecology Progress Series*, 537:217–232.

Morales, J., Haydon, D., Frair, J., Holsinger, K., and Fryxell, J. (2004). Extracting more out of relocation data: Building movement models as mixtures of random walks. *Ecology*, 85(9):2436–2445.

Moxley, J., Skomal, G., Chisholm, J., Halpin, P., and Johnston, D. (2020). Daily and seasonal movement of Cape Cod gray seals vary with predation risk. *Marine Ecology Progress Series*, 644:215–228.

Muir, A., Blackie, C., Marsden, J., and Krueger, C. (2012). Lake charr *Salvelinus namaycush* spawning behaviour: new field observations and a review of current knowledge. *Reviews in Fish Biology and Fisheries*, 22:575–593.

Murray, D. (2006). On improving telemetry-based survival estimation. *Journal of Wildlife Management*, 70(6):1530–1543.

Nathan, R., Getz, W., Revilla, E., Holyoak, M., Kadmon, R., Saltz, D., and Smouse, P. (2008). A movement ecology paradigm for unifying organismal movement research. *Proceedings of the National Academy of Sciences of the United States of America*, 105(49):19052–19059.

Naughton, G., Caudill, C., Keefer, M., Bjornn, T., Stuehrenberg, L., and Peery, C. (2005). Late-season mortality during migration of radio-tagged adult sockeye salmon (*Oncorhynchus nerka*) in the Columbia River. *Canadian Journal of Fisheries and Aquatic Sciences*, 62:30–47.

Newland, C., Field, I., Nichols, P., Bradshaw, C., and Hindell, M. (2009). Blubber fatty acid profiles indicate dietary resource partitioning between adult and juvenile southern elephant seals. *Marine Ecology Progress Series*, 384:303–312.

Niezgoda, G., Benfield, M., Sisak, M., and Anson, P. (2002). Tracking acoustic transmitters by code division multiple access (CDMA)-based telemetry. *Hydrobiologia*, 483:275–286.

Nowak, B., Bowen, W., Whoriskey, K., Lidgard, D., Mills Flemming, J., and Iverson, S. (2020). Foraging behaviour of a continental shelf marine predator, the grey seal (*Halichoerus grypus*), is associated with *in situ* subsurface oceanographic conditions. *Movement Ecology*, 8:41.

O'Toole, A., Murchie, K., Pullen, C., Hanson, K., Suski, C., Danylchuk, A., and Cooke, S. (2010). Locomotory activity and depth distribution of adult great barracuda (*Sphyraena barracuda*) in Bahamian coastal habitats determined using acceleration and pressure biotelemetry transmitters. *Marine and Freshwater Research*, 61:1446–1456.

Parton, A. and Blackwell, P. (2017). Bayesian inference for multistate 'step and turn' animal movement in continuous time. *Journal of Agricultural, biological, and environmental statistics*, 22(3):373–392.

Parton, A., Blackwell, P., and Skarin, A. (2017). Bayesian inference for continuous time animal movement based on steps and turns. In Argiento, R., Lanzarone, E., Antoniano Villalobos, I., and Mattei, A., editors, *Bayesian Statistics in Action. BAYSM 2016. Springer Proceedings in Mathematics & Statistics*, volume 194. Springer, Cham.

Patefield, W. (1977). On the maximized likelihood function. *Sankhya: The Indian Journal of Statistics*, 39:92–96.

Patterson, T., Basson, M., Bravington, M., and Gunn, J. (2009). Classifying movement behaviour in relation to environmental conditions using hidden Markov models. *Journal of Animal Ecology*, 78(6):1113–1123.

Patterson, T., Parton, A., Langrock, R., Blackwell, P., Thomas, L., and King, R. (2017). Statistical modelling of individual animal movement: an overview of key methods and a discussion of practical challenges. *Advances in Statistical Analysis*, 101:399–438.

Patterson, T., Thomas, L., Wilcox, C., Ovaskainen, O., and Matthiopoulos, J. (2008). State-space models of individual animal movemen. *Trends in Ecology and Evolution*, 23:87–94.

Payne, N., Gillanders, B., Webber, D., and Semmens, J. (2010). Interpreting diel activity patterns from acoustic telemetry: the need for controls. *Marine Ecology Progress Series*, 419:295–301.

Pedersen, M., Burgess, G., and Weng, K. (2014). A quantitative approach to static sensor network design. *Methods in Ecology and Evolution*, 5:1043–1051.

Pedersen, M., Righton, D., Thygesen, U., Andersen, K., and H., M. (2008). Geolocation of North Sea cod (Gadus morhua) using hidden Markov models and behavioural switching. *Canadian Journal of Fisheries and Aquatic Sciences*, 65(11):2367–2377.

Pedersen, M. and Weng, K. (2013). Estimating individual animal movement from observation networks. *Methods in Ecology and Evolution*, 4:920–929.

Pedersen, M. W., Patterson, T., Thygesen, U., and H., M. (2011). Estimating animal behavior and residency from movement data. *Oikos*, 120:1281–1290.

Piepho, H.-P. and Ogutu, J. (2007). Simple state-space models in a mixed model framework. *The American Statistician*, 61(3):224–232.

Plummer, M. (2015). rjags: Bayesian graphical models using mcmc. *R package version 3-15.*

Pohle, J., Langrock, R., van Beest, F., and Schmidt, N. (2017). Selecting the number of states in hidden Markov models: pragmatic solutions illustrated using animal movement. *Journal of Agricultural, Biological, and Environmental Statistics*, 22(3):270–293.

Pollock, K., Winterstein, S., Bunck, C., and Curtis, P. (1989a). Survival analysis in telemetry studies: The staggered entry design. *Journal of Wildlife Management*, 53:7–15.

Pollock, K., Winterstein, S., and Conroy, M. (1989b). Estimation and analysis of survival distributions for radio-tagged animals. *Biometrics*, 45:99–109.

Prieto, R., Silva, M., Waring, G., and Gonçalves, J. (2014). Sei whale movements and behaviour in the North Atlantic inferred from satellite telemetry. *Endangered Species Research*, 26:103–113.

R Core Team (2018). *R: A language and environment for statistical computing*. R Foundation for Statistical Computing, Vienna, Austria.

Raabe, J., Gardner, B., and Hightower, J. (2014). A spatial capture–recapture model to estimate fish survival and location from linear continuous monitoring arrays. *Canadian Journal of Fisheries and Aquatic Sciences*, 71:120–130.

Rabiner, L. R. (1989). A tutorial on hidden Markov models and selected applications in speech recognition. *Proceedings of the IEEE*, 77(2):257–286.

Reid, T., Ronconi, R., Cuthbert, R., and Ryan, P. (2014). The summer foraging ranges of adult spectacled petrels *Procellaria conspicillata*. *Antarctic Science*, 26(1):23–32.

Reubens, J., Verhelst, P. van der Knaap, I., Deneudt, K., Moens, T., and Hernandez, F. (2019). Environmental factors influence the detection probability in acoustic telemetry in a marine environment: results from a new setup. *Hydrobiologia*, 845:81–94.

Richard, A., Bernatchez, L. Valiquette, E., and Dionne, M. (2014). Telemetry reveals how catch and release affects prespawning migration in Atlantic salmon (*Salmo salar*). *Canadian Journal of Fisheries and Aquatic Sciences*, 71:1730–1739.

Riley, S., Binder, T., Wattrus, N., Faust, M., Janssen, J., Menzies, J., Marsden, J., Ebener, M., Bronte, C., He, J., Tucker, T., Hansen, M., Thompson, H., Muir, A., and Krueger, C. (2014). Lake trout in northern Lake Huron spawn on submerged drumlins. *Journal of Great Lakes Research*, 40(2):415–420.

Robson, B., Goebel, M., Baker, J., Ream, R., Loughlin, T., Francis, R., Antonelis, G., and Costa, D. (2004). Separation of foraging habitat among breeding sites of a colonial marine predator, the northern fur seal (*Callorhinus ursinus*). *Canadian Journal of Zoology*, 82:20–29.

Ross, S. (1996). *Stochastic Processes*. John Wiley & Sons, Inc, 2 edition.

Roy, R., Beguin, J., Argillier, C., Tissot, L., Smith, F., Smedbol, S., and De-Oliveira, E. (2014). Testing the VEMCO Positioning System: spatial distribution of the probability of location and the positioning error in a reservoir. *Animal Biotelemetry*, 2:1.

Royle, J., Chandler, R., Sollmann, R., and Gardner, B. (2014). *Spatial capture-recapture*. Waltham, MA: Academic Press.

Savino, J. and Stein, R. (1989). Behavioural interactions between fish predators and their prey: effects of plant density. *Animal Behaviour*, 37:311–321.

Scales, K., Miller, P., Hawkes, L., Ingram, S., Sims, D., and Votier, S. (2014). On the Front Line: frontal zones as priority at-sea conservation areas for mobile marine vertebrates. *Journal of Applied Ecology*, 51:1575–1583.

Scharf, H., Hooten, M., Fosdick, B., Johnson, D., London, J., and Durban, J. (2016). Dynamic social networks based on movement. *Annals of Applied Statistics*, 10(4):2182–2202.

Schliehe-Diecks, S., Kappeler, P., and Langrock, R. (2012). On the application of mixed hidden Markov models to multiple behavioural time series. *Interface Focus*, 2(2):180–189.

Schwarz, C., Schweigert, J., and Arnason, A. (1993). Estimating migration rates using tag-recovery data. *Biometrics*, 49:177–193.

Simpfendorfer, C., , Heupel, M., and Hueter, R. (2002). Estimation of short-term centers of activity from an array of omnidirectional hydrophoness and its use in studying animal movements. *Canadian Journal of Fisheries and Aquatic Sciences*, 59:23–32.

Simpfendorfer, C., Heupel, M., and Collins, A. (2008). Variation in the performance of acoustic receivers and its implication for positioning algorithms in a riverine setting. *Canadian Journal of Fisheries and Aquatic Sciences*, 65:482–492.

Skaug, H. and Fournier, D. (2006). Automatic approximation of the marginal likelihood in non-Gaussian hierarchical models. *Computational Statistics & Data Analysis*, 51:699–709.

Smith, F. (2013). Understanding hpe in the vemco positioning system (vps). *VEMCO Document #: DOC-005457-01.*

Sollmann, R., Furtado, M., Jácomo, A., Tôrres, N., and Silveira, L. (2010). Maned wolf survival rate in central Brazil. *Journal of Zoology*, 282:207–213.

Stehfast, K., Patterson, T., Barnett, A., and Semmens, J. (2015). Markov models and network analysis reveal sex-specific differences in the space-use of a coastal apex predator. *Oikos*, 124:307–318.

Stehfast, K., Patterson, T., Dagorn, L., Holland, K., Itano, D., and Semmens, J. (2013). Network analysis of acoustic tracking data reveals the structure and stability of fish aggregations in the ocean. *Animal Behaviour*, 85:839–848.

Stich, D., Kinnison, M., Kocik, J., and Zydlewski, J. (2015). Initiation of migration and movement rates of Atlantic salmon smolts in fresh water. *Canadian Journal of Fisheries and Aquatic Sciences*, 72:1339–1351.

Swadling, D., Knott, N., Rees, M., Pederson, H., Adams, K., Taylor, M., and Davis, A. (2020). Seagrass canopiess and the performance of acoustic telemetry: implications for the interpretation of fish movements. *Animal Biotelemetry*, 8:8.

Teo, S., Boustany, A., Blackwell, S., Walli, A. Weng, K., and Block, B. (2004). Validation of geolocation estimates based on light level and sea surface temperature from electronic tags. *Marine Ecology Progress Series*, 283:81–98.

Thorley, J., Youngson, A., and Laughton, R. (2007). Seasonal variation in rod recapture rates indicates differential exploitation of Atlantic salmon, *Salmo salar*, stock components. *Fisheries Management and Ecology*, 14:191–198.

Thorson, J. and Minto, C. (2015). Mixed effects: A unifying framework for statistical modelling in fisheries biology. *ICES Journal of Marine Science*, 72:1245–1256.

Thorson, J., Skaug, H., Kristensen, K., Shelton, A., Ward, E., Harms, J., and Benante, J. (2015). The importance of spatial models for estimating the strength of density dependence. *Ecology*, 96:1202–1212.

Thums, M., Fernández-Gracia, J., Sequeira, A., Eguíluz, V., Duarte, C., and Meekan, M. (2018). How big data fast tracked human mobility research and the lessons for animal movement ecology. *Frontiers in Marine Science*, 5:21.

Thygesen, U., Albertsen, C., Berg, C., Kristensen, K., and Nielsen, A. (2017). Validation of ecological state space models using the laplace approximation. *Environmental and Ecological Statistics*, 24(317-339).

Topping, D. and Szedlmayer, S. (2011). Site fidelity, residence time and movements of red snapper *Lutjanus campechanus* estimated with long-term acoustic monitoring. *Marine Ecology Progress Series*, 437:183–200.

Trancart, T., Carpentier, A., Acou, A., Danet, V., Elliott, S., and Feunteun, E. (2020). Behaviour of endangered Euroopean eels in proximity to a dam during downstream migration: Novel insights using high accuracy 3D acoustic telemetry. *Ecology of Freshwater Fish*, 29(2):266–279.

Tremblay, Y. and Cherel, Y. (2003). Geographic variation in the foraging behaviour, diet and chick growth of rockhoppere penguins. *Marine Ecology Progress Series*, 251:279–297.

Tukey, J. (1962). The future of data analysis. *The Annals of Mathematical Statistics*, 33(1):1–67.

Udyawer, V., Read, M., Hamann, M., Simpfendorfer, C., and Heupel, M. (2015). Effects of environmental variables on the movement and space use of coastal sea snakes over multiple temporal scales. *Journal of Experimental Marine Biology and Ecology*, 473:26–34.

Urban, D., Minor, E., Treml, E., and Schick, R. (2009). Graph models of habitat mosaics. *Ecology Letters*, 12:260–273.

van Etten, J. (2018). *gdistance: Distances and Routes on Geographical Grids*, R package version 1.2-2 edition.

Villegas-Amtmann, S., Jeglinski, J., Costa, D., Robinson, P., and Trillmich, F. (2013). Individual foraging strategies reveal niche overlap between endangered Galapagos pinnipeds. *PLoS One*, 8(8):e70748.

Villepique, J., Bleich, V., Pierce, B., Stephenson, T., Botta, R., and Bowyer, R. (2008). Evaluating GPS collar error: a critical evaluation of Televilt POSREC-Science (TM) collars and a method for screening location data. *California Fish and Game*, 94(4):155–168.

Vincent, C., McConnell, B., Ridoux, V., and Fedak, M. (2002). Assessment of argos location accuracy from satellite tags deployed on captive grey seals. *Marine Mammal Science*, 18(1):156–166.

Volpov, B., Hoskins, A., Battaile, B., Viviant, M., Wheatley, K., Marshall, G., Abernathy, K., and Arnould, J. (2015). Identification of prey captures in Australian fur seals (*Arctocephalus pusillus doriferus*) using head-mounted accelerometers: Field validation with animal-borne video cameras. *PLoS ONE*, 10(6):e0128789.

Wang, G. (2019). Machine learning for inferring animal behavior from location and movement data. *Ecological Informatics*, 49:69–76.

Welch, D., Melnychuk, M., Rechisky, E., Porter, A., Jacobs, M., Ladouceur, A., McKinley, R., and Jackson, G. (2009). Freshwater and marine migration and survival of endangered Cultus Lake sockeye salmon (*Oncorhynchus nerka*) smolts using POST, a large-scale acoustic telemetry array. *Canadian Journal of Fisheries and Aquatic Sciences*, 66:736–750.

White, G. and Burnham, K. (1999). Program MARK: Survival estimation from populations of marked animals. *Bird Study*, 46(sup1):S120–S139.

White, G. and Garrott, R. (1990). *Analysis of wildlife radio-tracking data.* San Diego, CA: Academic Press.

Whoriskey, K., Auger-Méthé, M., Albertsen, C., Whoriskey, F., Binder, T., Krueger, C., and Mills Flemming, J. (2017). A hidden Markov movement model for rapidly identifying behavioral states from animal tracks. *Ecology and Evolution*, 7:2112–2121.

Whoriskey, K., Martins, E., Auger-Méthé, M., Gutowsky, L., Lennox, R., Cooke, S., Power, M., and Mills Flemming, J. (2019). Current and emerging statistical techniques for aquatic telemetry data: A guide to analysing spatially discrete animal detections. *Methods in Ecology and Evolution*, 10(7):935–948.

Williams, B., Nichols, J., and Conroy, M. (2001). *Analysis and management of animal populations: Modeling, estimation, and decision making.* San Diego, CA: Academic Press.

Wilson, R., Liebsch, N., Gómez-Laich, A., Kay, W., Bone, A., Hobson, V., and Siebert, U. (2015). Options for modulating intra-specific competition in colonial pinnipeds: the case of harbour seals (*Phoca vitulina*) in the Wadden Sea. *PeerJ*, 3:e957.

Winship, A., Jorgensen, S., Shaffer, S., Jonsen, I., Robinson, P., Costa, D., and Block, B. (2012). State-space framework for estimating measurement error from double-tagging telemetry experiments. *Methods in Ecology and Evolution*, 3:291–302.

Winton, M., Kneebone, J., Zemeckis, D., and Fay, G. (2018). A spatial point process model to estimate individual centres of activity from passive acoustic telemetry data. *Methods in Ecology and Evolution*, 9:2262–2272.

Witt, M., Åkesson, S., Broderick, A., Coyne, M., Ellick, J., Formia, A., Hays, G., Luschi, P., Stroud, S., and Godley, B. (2010). Assessing accuracy and utility of sattelite-tracking data using Argos-linked Fastloc-GPS. *Animal Behaviour*, 80:571–581.

Wood, S. (2006). *Generalized additive models: An introduction with R.* Boca Raton, FL: Taylor & Francis Group, LLC.

Zhang, Y., Xu, Q., Al'os, J., Liu, H., Xu, Q., and Yang, H. (2015). Short-term fidelity, habitat use and vertical movement behavior of the black rockfish *Sebastes schlegelii* as determined by acoustic telemetry. *PLoS One*, 10:e0134381.

Zollner, P. and Lima, S. (1999). Search strategies for landscape-level interpatch movements. *Ecology*, 80(3):1019–1030.

Zucchini, W., Macdonald, I., and Langrock, R. (2016). *Hidden Markov models for time series: An introduction using R.* Chapman and Hall/CRC Press, 2 edition.

Zuur, A., Ieno, E., and Saveliev, A. (2017). *Beginner's guide to spatial, temporal, and spatial-temporal ecological data analysis with R-INLA. Volume 1: Using GLM and GLMM.* Newburgh, UK: Highland Statistics Ltd.

Zuur, A., Ieno, E., Walker, N., Saveliev, A., and Smith, G. (2009). *Mixed effects models and extensions in ecology with R.* New York, NY: Springer Science + Business Media.

Appendix A

Identifiability of Measurement and Process Error

For each bootstrap, we plotted the estimates of ψ^{-1} against the estimates of σ_{lon} and σ_{lat}. We chose to plot ψ^{-1} because as ψ^{-1} increases, so does the magnitude of measurement error. We additionally fitted a linear model to single combinations of the measurement error vs. each of the process error parameters, i.e., for each bootstrap, we fitted

$$\psi_i^{-1} \sim \beta_0 + \beta_1\sigma_{lon,i} \quad \text{and} \quad \psi_i \sim \beta_0 + \beta_1\sigma_{lat,i}, \tag{A.1}$$

where β_0 and β_1 are the standard regression coefficients. In Figs A.1 and A.2, we plot each of these regressions, and display the p-value for β_1. We chose these simpler models over multiple regression with interactions for ease of interpretability. All R-squared values were low (< 0.1), therefore we chose to display the β_1 p-values for each regression. However, these are meant for illustrative purposes only, and should not be interpreted as the results of rigorous testing for identifiability.
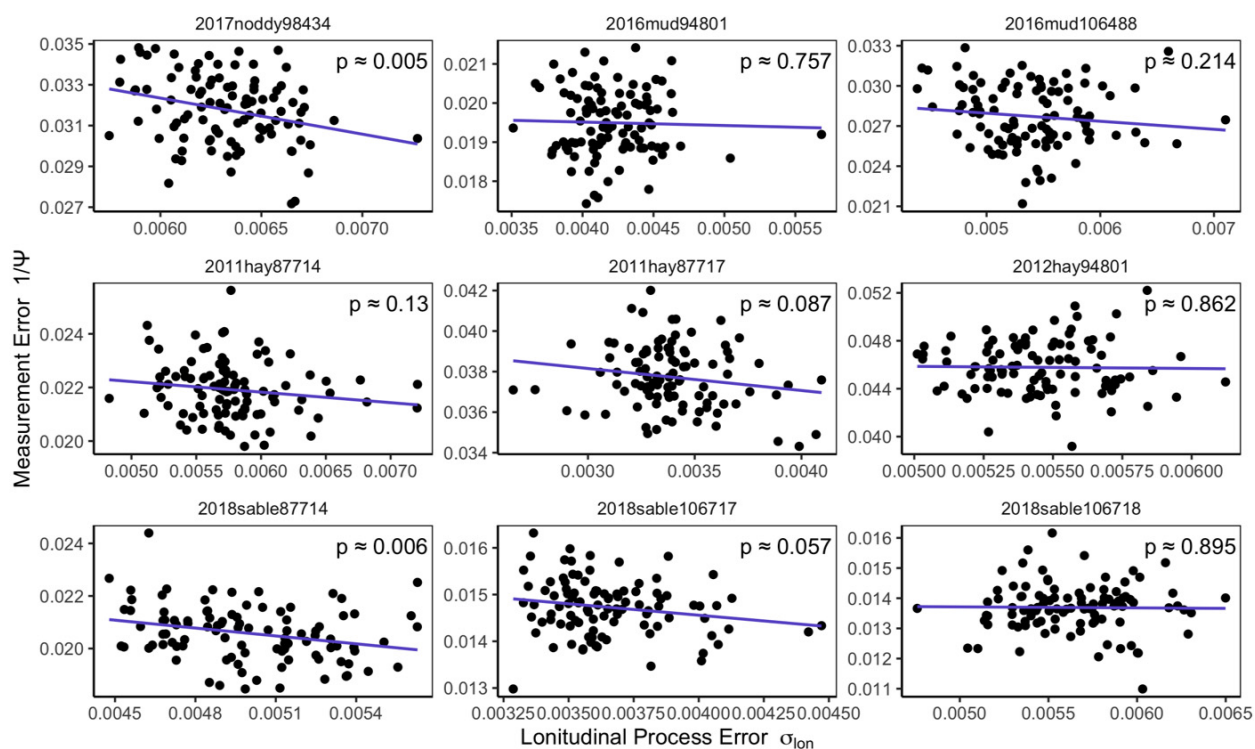
Figure A.1: Estimates of the longitudinal process error plotted against the inverse of the estimated measurement parameter, ψ for nine separate bootstraps based off of parameters from fitted switching hierarchical models. Increasing ψ^{-1} causes increasing measurement error. Each facet is unique to a bootstrap, with the name containing an alphanumeric denoting the sampling year, tagging island, and tag PTT of the seal track that formed the basis for the bootstrap. The purple line is the line of best fit, and the p-value corresponds to the slope.
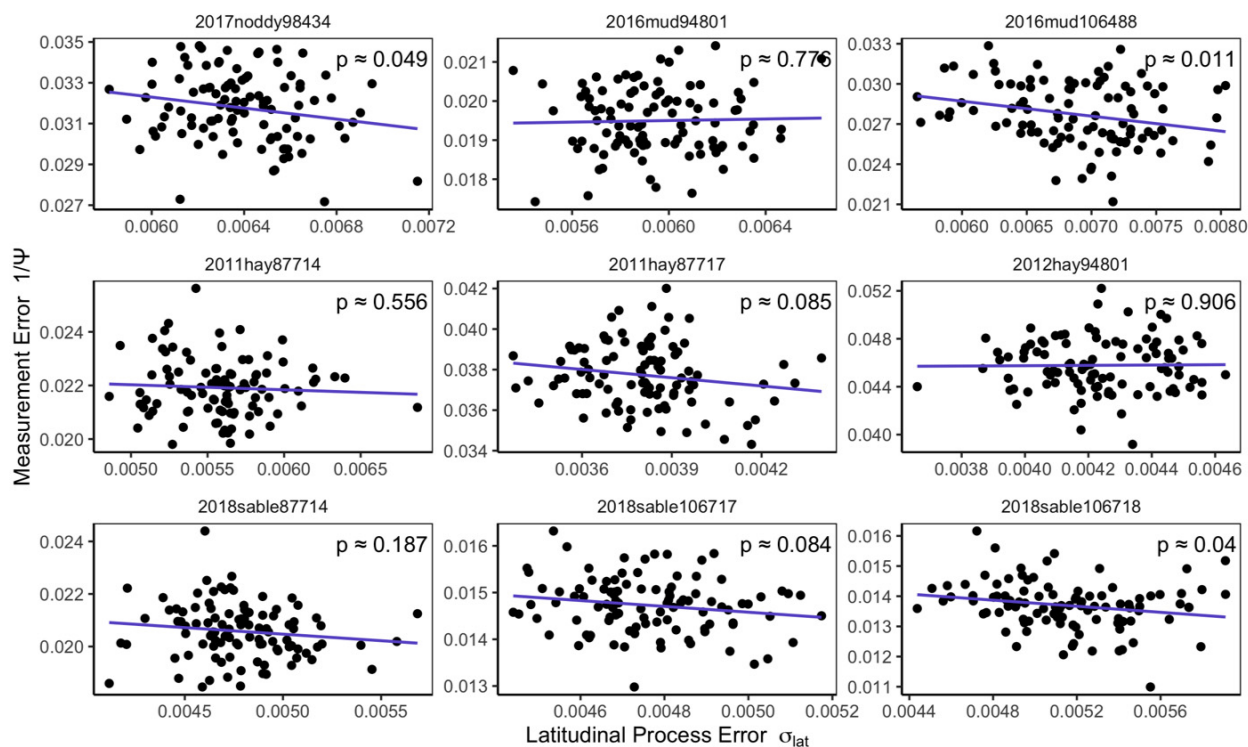
Figure A.2: Estimates of the longitudinal process error plotted against the inverse of the estimated measurement parameter, ψ for nine separate bootstraps based off of parameters from fitted switching hierarchical models. Increasing ψ^{-1} causes increasing measurement error. Each facet is unique to a bootstrap, with the name containing an alphanumeric denoting the sampling year, tagging island, and tag PTT of the seal track that formed the basis for the bootstrap. The purple line is the line of best fit, and the p-value corresponds to the slope.

Appendix B

YAMS Model Validation

The pseudoresiduals are presented for both the two- and three-state models fitted to the pike dataset. Because all residuals should follow a $N(0,1)$ distribution, we pooled the residuals from all five groups into one plot each for the Eastings and Northings axes. These residuals assume that the location predictions are accurate, and can therefore not be used to validate the measurement equation of YAMS.
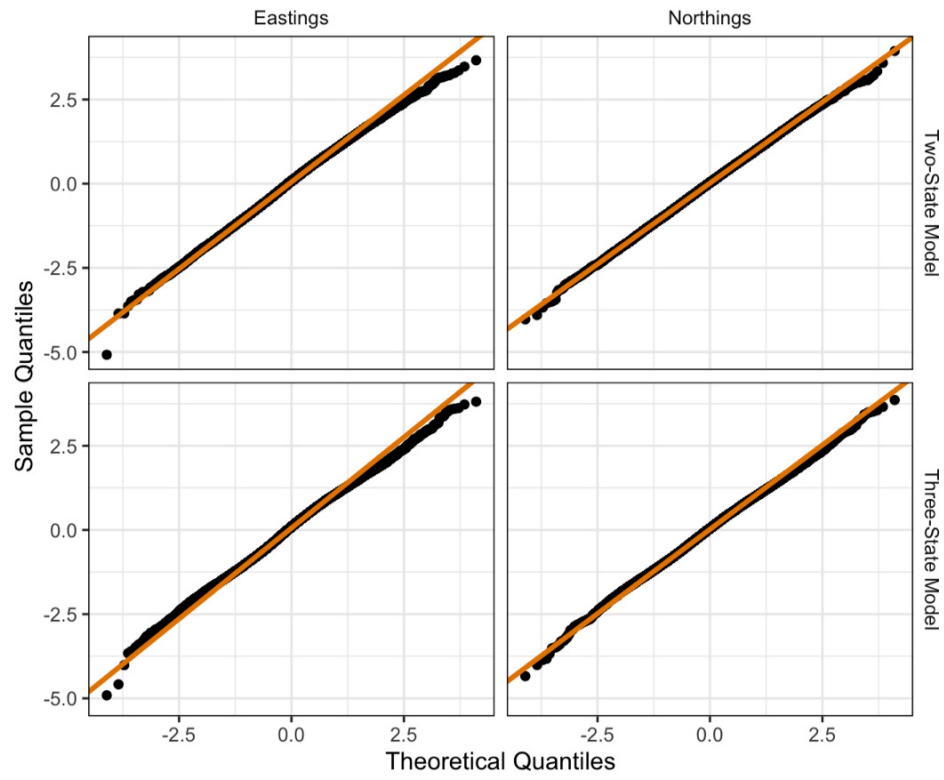
Figure B.1: QQ plots of the pseudoresiduals for the two-state (top) and three-state (bottom) models fitted to the pike dataset. Residuals are calculated for each of the coordinate axes, with Eastings on the left and Northings on the right.

Appendix C

YAMS Simulation Study Parameter Results

The accuracy of YAMS is demonstrated by its ability to recover parameter values during simulation studies. We fitted the two- and three-state models to tracks simulated based on the parameter values from the first group of 5,000 transmissions in our pike dataset.

Table C.1: Parameter estimates from a simulation study of the two-state model.

Parameter	True	Mean	Median	SD	2.5% Quantile	97.5% Quantile
D_1 (HMM)	0.974	0.468	0.267	0.472	0.225	1.661
D_2 (HMM)	20.763	14.408	15.308	2.814	7.229	16.746
q_{11}	-0.087	-0.086	-0.077	0.042	-0.197	-0.056
q_{21}	0.109	0.106	0.091	0.050	0.071	0.227
q_{12}	0.087	0.086	0.077	0.042	0.056	0.197
q_{22}	-0.109	-0.106	-0.091	0.050	-0.227	-0.071
D_1 (SSM)	0.974	0.976	0.966	0.135	0.830	1.306
D_2 (SSM)	20.763	18.666	18.666	0.964	16.816	20.021
σ	0.000	0.000	0.000	0.000	0.000	0.000
ω	0.001	0.001	0.001	0.000	0.001	0.001

Table C.2: Parameter estimates from a simulation study of the three-state model.

Parameter	True	Mean	Median	SD	2.5% Quantile	97.5% Quantile
D_1 (HMM)	0.188	0.101	0.085	0.058	0.032	0.224
D_2 (HMM)	3.692	1.728	1.617	0.607	1.074	3.166
D_3 (HMM)	24.751	18.974	19.051	1.628	15.969	21.947
q_{11}	-0.204	-0.144	-0.139	0.029	-0.210	-0.110
q_{21}	0.125	0.088	0.086	0.033	0.038	0.161
q_{31}	0.011	0.019	0.013	0.017	0.000	0.055
q_{12}	0.174	0.118	0.101	0.035	0.083	0.192
q_{22}	-0.173	-0.127	-0.116	0.047	-0.234	-0.074
q_{32}	0.075	0.066	0.061	0.028	0.029	0.123
q_{13}	0.029	0.027	0.026	0.018	0.000	0.055
q_{23}	0.048	0.039	0.036	0.022	0.012	0.082
q_{33}	-0.086	-0.084	-0.076	0.027	-0.152	-0.057
D_1 (SSM)	0.188	0.355	0.303	0.149	0.203	0.664
D_2 (SSM)	3.692	3.540	3.396	0.933	2.469	5.732
D_3 (SSM)	24.751	22.758	22.628	1.540	20.432	26.262
σ	0.000	0.000	0.000	0.000	0.000	0.000
ω	0.001	0.001	0.001	0.000	0.001	0.001

Appendix D

Copyright Release

The following two chapters were fully published under the following citations.

Chapter 2: A Hidden Markov Movement Model for rapidly identifying behavioural states from animal tracks

Whoriskey, K., Auger-Méthé, M., Albertsen, C., Whoriskey, F., Binder, T., Krueger, C., and Mills Flemming, J. (2017). A hidden Markov movement model for rapidly identifying behavioural states from animal tracks. Ecology and Evolution, 7:2112-2121.

Chapter 3: Current and emerging statistical techniques for aquatic telemetry data: A guide to analysing spatially discrete animal detections

Whoriskey, K., Martins, E. Auger-Méthé, M. Gutowsky, L. Lennox, R. Cooke, S., Power, M. and Mills Flemming, J. (2019). Current and emerging statistical techniques for aquatic telemetry data: A guide to analysing spatially discrete animal detections. *Methods in Ecology and Evolution*, 10(7):935-948.

The author of published Wiley articles retains the right to publish their articles within their dissertation. In this case, letters of permission are not required. (https://www.wiley.com/network/researchers/latest-content/how-to-clear-permissions-for-a-thesis-or-dissertation)